UNIVERSITY OF SOUTHAMPTON

WIND STRESS OVER THE OPEN OCEAN

Margaret J. Yelland

Thesis submitted for the degree of Doctor of Philosophy at the
University of Southampton Department of Oceanography.

March 1997

UNIVERSITY OF SOUTHAMPTON

ABSTRACT

FACULTY OF SCIENCE

OCEANOGRAPHY

Doctor of Philosophy

WIND STRESS OVER THE OPEN OCEAN

by Margaret J. Yelland

An automatic inertial dissipation system was used during three cruises of the RRS Discovery in the Southern Ocean to obtain a large data set of open-ocean wind stress estimates. The wind speed varied from near-calm to 26 m/s, and the sea-air temperature differences ranged from -8 to +4°C. It is shown that, under unstable atmospheric conditions, the assumption of a balance between local production and dissipation of turbulent kinetic energy is false, and that the sign and magnitude of the imbalance, Φ_D, depends critically on both stability, z/L, and wind speed, U_{10N}:

$$\Phi_D = \frac{z}{L}\left(0.5 - \frac{U_{10N}}{6.5}\right) \qquad z/L < 0$$

Application of this empirical term increased the wind stress values obtained under unstable conditions, and brought them into agreement with the data obtained under neutral conditions.

The flow of air around the RRS Discovery was simulated in three dimensions using a computational fluid dynamics model. The vertical displacement and the acceleration of the air flow reaching the anemometer site were quantified. The results were used to correct the measured drag coefficient, C_{D10N}, and wind speed estimates. The resulting mean wind stress to wind speed relationship:

$$1000\, C_{D10N} = 0.53 + 0.064\, U_{10N} \qquad 6 \le U_{10N} \le 26 \ \ m/s$$

confirmed those obtained by Smith (1980) and Large and Pond (1981).

Wave measurement suggested that the sea state was not, on average, fully developed for wind speeds above 12 m/s. However, contrary to findings from other studies, no persistent anomalies in the drag coefficient were detected despite the range of conditions and sea states encountered. It is shown that the wave-age dependent wind stress formulae, derived by previous authors from data obtained over shallow water, do not apply to open ocean conditions.

TABLE OF CONTENTS

LIST OF FIGURES

LIST OF TABLES

ACKNOWLEDGEMENTS

I would particularly like to thank Peter K. Taylor (JRD) for providing impetus, and Ben Moat (JRD) for his invaluable work on the CFD simulations. Vic Cornell of NCS provided much needed support. The work of Robin Pascal and Charles Clayson (both of COTD) in preparing the meteorological instruments and software is much appreciated. Neil Wells (Southampton University Department of Oceanography) was my supervisor. Thanks are of course due to the scientists and ship's staff on the various cruises. This research was partly funded by the Ministry of Agriculture, Fisheries and Food.

This work is dedicated to my grandmother, Edna Yelland.

1 INTRODUCTION

The sea surface wind stress represents the vertical transfer of horizontal momentum between the atmosphere and the ocean surface. The air-sea fluxes of heat and water vapour also depend on the wind stress, or momentum flux, as do the fluxes of trace gases such as CO_2. Improved understanding of these fluxes is of critical importance to studies of climate (OOSDP, 1995). Knowledge of the fluxes are required to determine the atmospheric forcing of the ocean's circulation, and as boundary conditions in atmospheric or ocean models. In coupled ocean-atmosphere models, the air-sea fluxes provide the physical description of the interface between the two thermodynamic systems. The return signal received by scatterometers is strongly dependent on the wind stress and can be used to infer the wind field over the oceans if the wind stress to wind speed relationship can be determined. The growth and spectra of surface waves are determined by the wind stress, as are surface drift currents, aerosol generation and whitecap coverage.

In most applications the wind stress is not directly available since it is difficult to measure, especially over the open ocean where fixed platforms are rarely available. In such cases, the wind stress is estimated from the wind speed using an empirical relationship. The variation of the stress with the wind speed is usually parameterised via a drag coefficient, which in turn has a wind speed dependence. The aim of this study is to determine the mean drag coefficient to wind speed relationship over the open ocean.

In recent years it has been suggested that the drag coefficient has a strong dependence on the sea state, as well as on the wind speed, and evidence for this has previously been found over coastal waters and lakes. The influence of the sea state on the wind stress over the open ocean is investigated in this study.

Section 2 outlines the theory relating the wind stress to the wind speed and describes the inertial dissipation method used in this study to obtain estimates of the

wind stress. Section 3 describes the validation of the dissipation method by previous authors, and discusses the advantages and disadvantages of both this technique and the more direct eddy correlation method.

The majority of the data used in this study were obtained using a sonic anemometer during three cruises of the RRS Discovery in the Southern Ocean. It is the largest published open-ocean data set to date, and was obtained under a wide range of atmospheric conditions. The wind speed varied from near-calm to 26 m/s, and the air-sea temperature ranged from -8º to +4ºC. Data collection and processing are described in Section 4.

In many previous studies which employed the inertial dissipation method, the assumption of a balance between local production and dissipation of turbulent kinetic energy was made. This assumption is shown to be false for the unstable atmospheric conditions which predominate over the oceans. An empirical formulation for the imbalance between production and dissipation is determined from the Discovery data in Section 5.

Once the wind stress has been measured, by whatever method, it has to be related to the true wind speed. However, the measurement of the wind speed can be severely affected by the distortion of the flow of air around the measurement platform. In previous studies these effects have, at best, been discussed qualitatively. In this study (Section 6), a computational fluid dynamics model is used to produce three dimensional simulations of the air flow around various research ships, including the RRS Discovery. The results of the model are used to quantify, and correct for, the effects of the flow distortion on the wind stress and wind speed measurements.

The use of a) the imbalance term, and b) the air flow distortion corrections effectively removes the two main sources of systematic error which have affected other wind stress data. The data from the Discovery cruises enable the mean

relationship between the drag coefficient and the wind speed to be accurately determined for open ocean conditions (Section 7).

For any given wind speed the scatter of the drag coefficient estimates is large. It has previously been suggested that much of this scatter is due to the dependence of the drag coefficient on the changing sea-state. This hypothesis is investigated in Section 8. The results of this study are summarised and discussed in Section 9, where suggestions for future work are also made.

2 MEASUREMENT OF THE WIND STRESS.

The wind stress is defined and related to the turbulent kinetic energy budget in Section 2.1, where the theory of the dissipation method of estimating the stress is also described. The practical application of this method is discussed in Section 2.2. The sensitivity of the stress estimates to measurement error is investigated in Section 2.3.

2.1 Wind stress and the turbulent kinetic energy budget.

Wind stress is the vertical transfer of horizontal momentum between the atmosphere and ocean. It is defined as;

$$\tau = -\rho\langle u' w' \rangle \qquad (2.1)$$

where ρ is the density of air, and the brackets denote a time average of the product of u' and w', the along wind and vertical wind speed fluctuations. The stress is positive for a net transfer of momentum into the ocean. The direction of the stress is commonly assumed to be the same as that of the mean horizontal wind, although observations described by Geernaert (1990) show differences of the order of 10 degrees. In the surface layer the stress is assumed to be constant with height and equal to the surface value (Section 2.3.d). The friction velocity, u_*, can then be defined as;

$$u_*^2 = \frac{|\tau|}{\rho} \qquad (2.2)$$

Wind stress is related to the wind speed, U, via the drag coefficient, C_D, which is defined as;

$$C_{D10N} = \frac{u_*^2}{U_{10N}^2} \qquad (2.3)$$

where the subscripts 10 and N refer to a height above the sea surface of 10 m, and neutral stability conditions respectively. An equivalent parameterisation is via the

roughness length, z_0. For neutral conditions, mixing length theory (e.g. Stull, 1988) gives;

$$\frac{dU_N}{dz} = \frac{u_*}{zk_v} \tag{2.4}$$

which, when integrated from a height z_0 at which U is zero relative to the water surface, gives;

$$U_{zN} = \frac{u_*}{k_v} \ln\left(\frac{z}{z_0}\right) \tag{2.5}$$

where k_v is the von Kármán constant, and z is the height above the sea surface. Combining Eqns. (2.3) and (2.5) gives the relationship between the drag coefficient and the roughness length;

$$\sqrt{C_{D10N}} = \frac{k_v}{\ln\left(10/z_0\right)} \tag{2.6}$$

The drag coefficient also has a dependence on wind speed. For wind speeds above 5 m/s or more, this dependence is commonly represented by a linear relationship;

$$1000 * C_{D10N} = a + b\, U_{10N} \tag{2.7}$$

where a and b are constants, the values of which are determined experimentally. It is worth noting that this relationship describes data corrected to an arbitrary height of 10 m: the logarithmic wind profile (Eqn. (2.5)) implies that, at any other height, the relationship would be non-linear. However, most data are too scattered to suggest a more universal form for the relationship.

The various methods of determining the wind stress are reviewed by Kraus and Businger (1994). A brief summary of the eddy correlation method is given here since it is the most direct method. The inertial dissipation technique is described in more detail as it is the method employed in this study.

In the eddy correlation technique, all three components of the wind speed are measured and the stress is calculated from Eqn. (2.1). The stress is then related to

the measured wind speed via Eqn. (2.3) or (2.5). However, Eqn. (2.1) must be integrated over a wide range of frequencies, necessitating a sampling period of 30 minutes or more, depending on wind speed and measurement height (Wyngaard, 1973), during which conditions must be stationary. In addition, the eddy correlation method is very sensitive to flow distortion caused by the measurement platform (Oost et al., 1994), and is difficult to use on moving platforms such as ships or buoys (Section 3.3). Previous wind stress results obtained using the eddy correlation method have generally been restricted to relatively shallow, coastal waters where a fixed platform could be used.

The inertial dissipation technique is a less direct method of determining the wind stress, but one that is more practical for use on a moving measurement platform in the open ocean. This method (Weiler and Burling, 1967; Hicks and Dyer,1972) relates the friction velocity, or wind stress, to the dissipation rate, ε, using the turbulent kinetic energy (TKE) budget (Busch, 1972). Turbulence is produced at low frequencies (less than about 0.1 Hz) and dissipated at high frequencies (of the order 1000 Hz), with no significant production or dissipation occurring in the region between (McBean and Elliott, 1975). In this middle region, or inertial subrange, the TKE is merely transported from the low to the high frequencies. In the inertial subrange, the Kolmogoroff hypothesis suggests that the dissipation rate is related to the power spectral density, $S(n)$, of the longitudinal wind component, by;

$$S(n) = K\varepsilon^{2/3} n^{-5/3} \qquad (2.8)$$

where n is the wavenumber, and K is the one-dimensional Kolmogorov constant. The Kolmogoroff hypothesis is based on the assumption of isotropy in the inertial subrange ("local" isotropy), which may not always be justified over the ocean. The implications of this are discussed in Section 2.2.b and Section 3.

Taylor's hypothesis, or the assumption of "frozen" turbulence, allows the conversion of $S(n)$ to $S(f)$, where f is the frequency, via;

$$S(f) = \frac{n}{f} S(n) \qquad (2.9)$$

where;

$$\frac{n}{f} = \frac{2\pi}{U_{rel}} \tag{2.10}$$

and U_{rel} is the wind speed as measured by the anemometer. Hence Eqn. (2.8) becomes;

$$S(f) = K\varepsilon^{2/3} f^{-5/3} \left(U_{rel} / 2\pi\right)^{2/3} \tag{2.11}$$

The dissipation rate can thus be obtained by calculating the mean value of $f^{5/3}S(f)$ over an appropriate frequency range.

For steady state, horizontally homogeneous turbulence, the TKE budget can be written;

$$u_*^2 \frac{\partial}{\partial z}\langle U \rangle + g\frac{\langle w'TV' \rangle}{TV} - \frac{\partial}{\partial z}\langle w'e' \rangle - \frac{1}{\rho}\frac{\partial}{\partial z}\langle w'p' \rangle = \varepsilon \tag{2.12}$$

or

$$P \quad + \quad B \quad - \quad D_t \quad - \quad D_p \quad = \quad \varepsilon$$

where primes indicate fluctuations, brackets indicate mean quantities, U is in the longitudinal wind direction and w the vertical, and TV is the virtual potential temperature. Term P is the mechanical or shear production of turbulent kinetic energy, e. B represents the buoyant production (under unstable conditions) or loss term. D_t and D_p are the vertical divergences of the TKE flux and the pressure transport term respectively. ε represents the rate of loss of TKE at small scales to molecular dissipation. Eqn. (2.12) is made dimensionless by multiplying by the Monin-Obukhov surface layer scaling parameter $k_v z / u_*^3$;

$$\phi_m - \frac{z}{L} - \phi_t - \phi_p = \frac{k_v z \varepsilon}{u_*^3} = \phi_\varepsilon \tag{2.13}$$

where the Monin-Obukhov similarity argument suggests that the dimensionless profiles, ϕ_i, are unique functions of z/L. The Obukhov length, L, is defined;

$$L = \frac{-u_*^3 TV}{g k_v \langle TV' w' \rangle} \tag{2.14}$$

Yelland, M. J., 1997: Wind stress over the open ocean. *PhD thesis*, University of Southampton, U.K.,

Thus if the terms on the left-hand side of Eqn. (2.13) are known, the friction velocity can be evaluated from an estimate of the dissipation.

Eqn. (2.13) defines the dimensionless dissipation function, ϕ_ε. The forms of the other dimensionless profiles are not well known (Fairall and Larsen, 1986), and the form of $\phi_m(z/L)$ is critically dependent on the assumed value for the von Kármán constant, k_v (Frenzen and Vogel, 1994). Taking k_v = 0.4, Edson et al. (1991) reviewed several formulations for $\phi_m(z/L)$. The best performing formulae could be summarised by:

$$\phi_m(z/L) = \left(1 - \alpha(z/L)\right)^{-1/4} \qquad z/L < 0 \qquad (2.15)$$

$$\phi_m(z/L) = 1 + \Gamma(z/L) \qquad z/L > 0 \qquad (2.16)$$

Values of α ranging from 16 to 28 all fitted the data to a similar degree and Edson et al. (1991) chose a value α = 20 which gave the best overall fit with Γ = 8. However, Eqs (2.15) and (2.16) still require further verification over the open ocean. Values k_v = 0.4 and α = 20 were also used in this study, but Γ = 5 was chosen in order that $\partial\phi_m / \partial(z/L)$ should be continuous across $z/L = 0$.

With regard to the vertical divergence terms, Large (1979) argued that the available evidence suggested that;

$$-\phi_t \approx \phi_p \qquad (2.17)$$

which leads to a balance between dissipation and the sum of mechanical and buoyant production;

$$\phi_\varepsilon = \left(\phi_m - \frac{z}{L}\right) \qquad (2.18a)$$

However, both the results of this study (Section 5.2) and those reported by other authors (Section 5.3) suggest an imbalance between production and dissipation;

$$\phi_\varepsilon = \left(\phi_m - \frac{z}{L} - \phi_D\right) \qquad (2.18b)$$

where the imbalance term, $\phi_D = (\phi_t + \phi_p)$, is significantly larger than the uncertainty in the formula for ϕ_m (Section 2.3).

2.2 The application of the dissipation technique.

The process of estimating the wind stress and the 10 m neutral wind speed, with an assumed balance between production and dissipation, is described in Section 2.2.a. Section 2.2.b discusses the effective Kolmogoroff constant and the implications for an imbalance between production and dissipation.

2.2.a Calculation of u_*, U_{10N} *and* C_{D10N} *values.*

The neutral 10 m drag coefficient and wind speed values are calculated from a set of parameters obtained from a particular measurement height. The power spectral density estimate, $S(f)$, and relative wind speed, U_{rel}, were measured at a height z_u. The air temperature, T, and the wet bulb temperature, T_w, were measured at a height z_t. Measurements of the air pressure, P, and sea surface temperature, T_s, are also required, as is a value for the true wind speed, U_{true}, which is obtained from the relative wind speed and the ship speed (Section 4.8). The temperatures are in Kelvin.

The calculations were performed first at the measurement height, and were then corrected to a height of 10 m and neutral stability. Reversing the order of the corrections would simplify the iterative procedure, but was found to produce more cases of non-convergence (Taylor, 1995). The iterative calculation of the 10m neutral values was performed using a FORTRAN program "bfdissY.F" which was an adaptation of a similar program "bform.F". Taylor (1995) gives a complete description of the calculations, which will be summarised here in the order in which they are performed.

1) The specific humidity, q_t (kg/kg), at the height z_t, is calculated from the air temperatures and pressure. The specific humidity at the sea surface, q_s, is calculated from the sea temperature and the air pressure assuming a relative humidity of 98% at the sea surface.

2) The air temperature, T, is converted to a potential temperature at the measurement height by;

$$TA_{zt} = T + 0.00976\, z_t \qquad (2.19)$$

where 0.00976 (K/m) is the negative of the dry adiabatic lapse rate.

3) The dissipation rate, ε, is calculated from the power spectral density estimate and the relative wind speed using Eqn. (2.11). The first estimate of the friction velocity is made from Eqn. (2.13), assuming neutral stability ($z/L = 0$, $\phi_m = 1$) and a balance between production and dissipation, i.e.;

$$u_*^3 = k_v z_u \varepsilon \qquad (2.20)$$

Likewise, the first estimate of the drag coefficient at the measurement height is obtained from

$$C_D = \frac{u_*^2}{U_{true}^2} \qquad (2.21)$$

4) The iterative process begins at this point. Initially, neutral stability is assumed, so that z/L and the stratification functions, Ψ, are zero, and the dimensionless profile $\phi_m = 1$.

5) The true wind speed is corrected to 10m and neutral conditions using the profile formula;

$$U_{10N} = U_{true} - \frac{u_*}{k_v}\left(\ln\left(\frac{z_u}{10}\right) - \Psi_m\right) \qquad (2.22)$$

Where the stratification function for momentum, Ψ_m, is defined (Paulson 1970);

$$\Psi_m = 2\ln\left(\frac{1+\phi_m^{-1}}{2}\right) + \ln\left(\frac{1+\phi_m^{-2}}{2}\right) - 2\tan^{-1}\phi_m^{-1} + \frac{\pi}{2} \qquad (z/L < 0) \qquad (2.23a)$$

$$\Psi_m = 1 - \phi_m \qquad (z/L > 0) \qquad (2.23b)$$

6) A new estimate of the friction velocity is made;

$$\phi_m - \frac{z}{L} = \frac{k_v z \varepsilon}{u_*^3} \qquad (2.24)$$

and the drag coefficient is recalculated using the U_{10N} value;

$$C_{D10N} = \frac{u_*^2}{U_{10N}^2} \qquad (2.25)$$

The value of the drag coefficient at the measurement height is necessary for the following calculation of the stability parameter, z/L, and is obtained from (Large 1979);

$$C_D = C_{D10N}\left\{ 1 + \frac{(C_{D10N})^{1/2}}{k_v}\left(\ln\left(\frac{z_u}{10}\right) - \Psi_m\right)\right\}^{-2} \qquad (2.26)$$

7) The Smith (1988) values of the 10 m neutral transfer coefficients for sensible and latent heat are;

$$C_{T10N} = 1.0 \times 10^{-3} \qquad (2.27)$$

$$C_{q10N} = 1.2 \times 10^{-3} \qquad (2.28)$$

Again, these are adjusted to the measurement height;

$$C_T = \frac{C_{T10N}(\frac{C_D}{C_{D10N}})^{1/2}}{(1 + \left(\frac{C_{T10N}}{k_v C_{D10N}^{1/2}}\right)\left(\ln\left(\frac{z_T}{10}\right) - \Psi_t\right)} \qquad (2.29)$$

and similarly for C_q, where (Paulson, 1970);

$$\Psi_t = \Psi_q = 2\ln\left(\frac{1+\phi_m^{-2}}{2}\right) \qquad (z/L < 0) \qquad (2.30a)$$

$$\Psi_t = \Psi_q = 1 - \phi_m \qquad (z/L > 0) \qquad (2.30b)$$

8) The temperature and humidity scales are then evaluated from the bulk formulae;

$$T_* = C_T U_{true}(TA_{zt} - T_s)/u_* \qquad (2.31)$$

$$q_* = C_q U_{true}(q_t - q_s)/u_* \qquad (2.32)$$

9) The potential temperature is then corrected to 10 m and neutral stability using the profile formula;

$$TA_{10N} = TA_{zt} - \frac{T_*}{k_v}\left(\ln\left(\frac{z_t}{10}\right) - \Psi_t\right) \qquad (2.33)$$

Yelland, M. J., 1997: Wind stress over the open ocean. *PhD thesis*, University of Southampton, U.K.,

and similarly for the specific humidity. These values are then used to calculate the virtual potential temperature at 10 m and neutral stability (Stull, 1988);

$$TV_{10N} = TA_{10N}(1 + 0.61q_{10N}) \tag{2.34}$$

and similarly, the virtual temperature scale;

$$T_{v*} = T_* + 0.61TA_{10N}q_* \tag{2.35}$$

10) Finally, the stability parameter is calculated using the definition of the Obukhov length (Eqn (2.14));

$$\frac{z}{L} = \frac{z(gkT_{v*})}{(TV_{10N}u_*^2)} \tag{2.36}$$

since, by definition;

$$T_{v*} = -\frac{\langle TV'w' \rangle}{u_*} \tag{2.37}$$

11) The iterative process then returns to step 5), and the calculations are repeated using the z/L value calculated in the last stage. Iteration is repeated until the parameters have converged: the limits of convergence were set at 0.01 m/s for U_{10N} and 0.005 m/s for u_* (Taylor, 1995). The parameters are set to absent if the value of the neutral 10 m wind speed becomes negative or if the iteration has been performed 30 times without convergence.

2.2.b The Kolmogoroff constant.

A value of 0.55 for the Kolmogoroff constant has previously been found to give good agreement between dissipation-derived stress estimates with estimates obtained using the eddy correlation technique (Large and Pond, 1981; Edson et al., 1991), as discussed in Section 3.2. A value of 0.55 was therefore used in this study. However, Frenzen and Vogel (1992) suggested a true value of 0.52, and Edson et al. (1991) suggested that the true value was 0.51, with the value 0.55 representing an effective Kolmogoroff constant, K_{eff}. Deacon (1988) defined K_{eff} as the value required to obtain the correct friction velocity from Eqn. (2.13). In effect, the effective Kolmogoroff value may compensate for any imbalance between production

and dissipation terms under neutral conditions. Allowing for an additional imbalance, ϕ_{Deff}, for non-neutral conditions, Eqn (2.13) can be written;

$$\phi_m - \frac{z}{L} - \phi_{Deff} = \phi_\varepsilon \propto \frac{1}{K_{eff}^{3/2}} \tag{2.38a}$$

or, equivalently;

$$\phi_m - \frac{z}{L} - \phi_{Dtrue} = \phi_\varepsilon \propto \frac{1}{K_{true}^{3/2}} \tag{2.38b}$$

Hence;

$$\phi_{Dtrue} = \left(\phi_m - \frac{z}{L}\right)\left(1 - \left(\frac{K_{eff}}{K_{true}}\right)^{3/2}\right) + \left(\frac{K_{eff}}{K_{true}}\right)^{3/2} \phi_{Deff} \tag{2.39}$$

Under neutral conditions ϕ_{Deff} is zero and $\left(\phi_m - \frac{z}{L}\right) = 1$, which implies that, for $K_{eff} > K_{true}$, the effective Kolmogoroff value compensates for an excess of dissipation over production. However, it must be noted that the true value is not well known, with suggested values ranging from 0.50 (Champagne et al., 1977) to 0.59 (Fairall et al., 1990; Dyer and Hicks, 1982). Estimates of the effective value vary from 0.50 to 0.77 (Deacon, 1988).

The assumption of local isotropy in the Kolmogoroff hypothesis leads to the one-dimensional Kolmogoroff constant assuming a different value for the transverse (v) or vertical (w) wind spectra (Busch, 1972);

$$K_v = K_w = \frac{4}{3} K_u \tag{2.40}$$

Equivalently, the spectral levels of the transverse and vertical wind spectra should be 4/3 that of the alongwind spectra. The analysis in this study was designed to reproduce that of Large and Pond (1981) since they had validated their method against the eddy correlation data of Smith (1980). Since Large and Pond obtained wind speed spectra using a propeller-vane anemometer, the total horizontal wind speed from the sonic anemometer (Section 4.3) was used instead of the longitudinal component only. If local isotropy holds over the ocean, this implies that the effective Kolmogoroff constant (if larger than the true value) could be compensating for the inclusion of the

transverse wind speed component in the wind spectra, rather than for an imbalance in the TKE budget. That the flow over the oceans is indeed isotropic is lent some support by Henjes (1996) who re-analysed 28 of the wind stress data runs used in this study. During the 12 hour period considered the wind speed and direction were stationary, and good agreement was found with Eqn. (2.40). The value of the true Kolmogoroff constant and the implied imbalance under neutral stability, is, however, still not known.

2.3 Error analysis.

There are various sources of error in the estimates of wind stress obtained via the dissipation method. These include; a) experimental uncertainties, such as instrument calibration and disturbance to the air flow by the ship, b) uncertainties in the values of the Kolmogoroff and von Kármán constants, and the forms of C_{T10N}, C_{q10N} and the dimensionless profile ϕ_m, and c) the application of the method under different atmospheric conditions. These three areas will be discussed in the remainder of this section. The validity of applying Taylor's hypothesis to our data is examined in Section 4.7.

2.3.a Experimental uncertainties.

In order to obtain estimates of the wind stress and the 10 m neutral wind speed, various parameters must be measured. These are; the relative wind speed, U_{rel}, the true wind speed (which is the measured wind speed adjusted for ship motion), U_{true}, the power spectral density (PSD) estimate in the inertial range of the of the wind spectra, the wet bulb air temperature (for the calculation of humidity), T_w, the air temperature, T, the sea surface temperature, T_s and the atmospheric pressure, P. Temperatures in this section are expressed in ºC rather than Kelvin. From here onwards, "PSD" refers to the estimate of the power spectral density in the inertial region of the wind spectrum which has been normalised by multiplying $S(f)$ by $f^{5/3}$.

To investigate the sensitivity of the calculated parameters (u_*, U_{10N} and C_{D10N}), each of the measured parameters was reduced by 5% or 0.5ºC. The heights of the instruments were also reduced; z_u, the anemometer height, was changed from 18.5 m to 17.5 m, and z_t, the height of the air temperature sensors, was altered from 17.0 to 16.0 m. The resulting change in the calculated parameters was then expressed as a percentage of the original values, for three different wind speeds. The results are summarised in Table 2.1, where the standard deviation of the mean change is also shown. It must be noted that the effect on the drag coefficient to wind speed relationship will be a combination of the changes to U_{10N} and C_{D10N}.

The calculation of u_*, U_{10N} and C_{D10N} is an iterative process involving all the measured parameters (Section 2.2.a), and the importance of a given parameter depends on the conditions of wind speed and atmospheric stability. For example, changes to the temperature measurements are much more significant at low than at high wind speeds, since at high wind speeds the mechanical production of turbulence dominates the buoyant production.

The calculated parameters appear more sensitive to changes in the sea surface temperature than to the air temperature because slightly unstable atmospheric conditions predominate over the ocean. A reduction in the sea temperature which causes a change from unstable to apparently stable conditions would imply a relatively large difference in the stability corrections (Figure 2.1). A similar reduction in the air temperature would simply make the conditions appear a little more unstable. Hence if the temperatures had been increased rather than decreased, the calculated parameters would appear more sensitive to air than sea temperature.

At low wind speeds, the effect of a systematic temperature error would have little effect on the mean C_{D10N} to U_{10N} relationship, since both these calculated parameters are affected in the same sense and to a similar degree on average. However, the effect of a temperature error on individual data can be very large if the apparent stability conditions are changed as a result. Hence small errors in the

temperature measurements would introduce a large scatter into the drag coefficient estimates obtained at low wind speeds.

Measured parameter and change.		change, at 5 m/s, to;			change, at 10 m/s, to;			change, at 20 m/s, to;		
		u_* }	U_{10N}	C_{D10N}	u_*	U_{10N}	C_{D10N}	u_*	U_{10N}	C_{D10N}
U_{rel}	-5%	+3 ±1	1	+6 ±3	+2 ±1	1	+4 ±1	+2	1	+4
U_{true}	-5%	+1 ±1	-5	+14 ±3	0	-5	+12 ±1	0	-5	+11
PSD	-5%	-4 ±1	0 ±1	-8 ±3	-3 ±1	0 ±1	-6 ±2	-2	0	-5
T_w	-0.5ºC	+1 ±3	+1 ±1	+1 ±5	0	0	0 ±1	0	0	0
T	0.5ºC	+5 ±10	+4 ±2	+2 ±16	+1 ±2	+1 ±1	+1 ±4	0	0	0
T_s	0.5ºC	-7 ±10	-6 ±3	-3 ±17	-2 ±3	-1 ±1	-2 ±5	0	0	0
P	-5%	1 ±1	1	1 ±1	0	0	0	0	0	0
z_u	-1.0 m	-2 ±1	+1	-5 ±1	-2	+1	-5	-2	+1	-5
z_t	-1.0 m	0	0	0 ±1	0	0	0	0	0	0

Table 2.1. Percentage change in calculated parameters, resulting from a decrease in the measured parameters, for 3 different wind speeds.

At moderate and high wind speeds, the measured wind parameters are the most significant sources of error. There are three main causes of error in the wind measurements; the estimate of the ship's speed, the anemometer calibration, and the airflow disturbance caused by the presence of the ship. These are discussed in turn.

To obtain the true wind speed, the measured wind speed should be corrected for ship's speed through the water, since U_{10N} is defined as the 10 meter neutral wind speed relative to the sea surface. However, except in conditions of strong tidal

currents (Geernaert et al., 1986, and Smith et al., 1992), it is usual for researchers to calculate the true wind speed with respect to the ground, hence incorporating the surface wind driven-currents into the parameterisation of the drag coefficient. Section 4.9 includes an evaluation of the likely error in the measured ship speed and the implication for the wind speed estimate.

An anemometer calibration error of -2.5% would affect the U_{rel} and U_{true} estimates directly (assuming a small ship speed), and would introduce an error of -5% in the PSD. These errors would cancel out in part, with the combined result of reducing the calculated U_{10N} by 2.5%, reducing the friction velocity by 1.7%, and increasing the calculated C_{D10N} by about 1.6%. The resulting C_{D10N} to U_{10N} relationship would, for a given wind speed, suggest an increase in the drag coefficient of about 3% to 4%.

The flow of air to the anemometer will usually have been disturbed by the presence of the ship: both a vertical displacement and an acceleration of the mean flow are possible. An acceleration of the flow would affect the estimate of U_{true} only, since U_{rel} is the actual wind speed at the anemometer, inclusive of ship speed or flow disturbance. For a reduction in U_{true} of 5%, the U_{10N} value is decreased by 5% while the C_{D10N} value is increased by 11% or more. The effect on the resulting C_{D10N} to U_{10N} relationship would be an overestimate of 16% or more in the drag coefficient for a given wind speed. Reducing z_u, the height to which the turbulence is assigned, decreases the calculated drag coefficient. Hence if the turbulence is assigned to the anemometer height, with no allowance made for a 1 m upwards displacement of the flow, the drag coefficient would be overestimated by about 5%. This assumes that the vertical displacement of the flow takes place rapidly enough for the turbulent properties of the flow to remain unchanged. This is a reasonable working assumption given that the majority of the displacement takes place within 1 second of the flow reaching the anemometer site (Section 6.4.c), and that the correlation, or "memory", time of the turbulence has been estimated to be of the order of 5 seconds or more (Henjes, 1996).

Yelland, M. J., 1997: Wind stress over the open ocean. *PhD thesis*, University of Southampton, U.K.,

A ship-mounted anemometer will move vertically, but the error caused by this motion through the vertical wind gradient is insignificant (Ramnstorf, 1988).

2.3.b Other parameters.

The sensitivity of the calculated parameters to the Kolmogoroff constant, the von Kármán constant, the bulk formulae for the heat transfer coefficients and the dimensionless profile function, ϕ_m, was also investigated in the fashion described in Section 2.3.a. The results are summarised in Table 2.2.

The Kolmogoroff value of 0.55 used in this study is generally agreed as the best effective value (Section 3.2). For the purpose of the sensitivity study, the values of u_*, U_{10N} and C_{D10N} were recalculated assuming an effective Kolmogoroff of 0.50, the lowest suggest value (Deacon, 1988). The same procedure was carried out for the von Kármán constant, again using the lowest suggested value of 0.35 (Businger et al., 1971) rather than the more usual value of 0.4. In both cases, the effect on the calculated parameters was constant at moderate or high wind speeds, with little scatter introduced. At lower wind speeds both the mean effect and the scatter were increased due to the sensitivity of the calculated parameters to the calculated atmospheric stability.

parameter	change, at 5 m/s, to;			change, at 10 m/s, to;			change, at 20 m/s, to;		
and change	u_* }	U_{10N}	C_{D10N}	u_*	U_{10N}	C_{D10N}	u_*	U_{10N}	C_{D10N}
Kolmogoroff from 0.55 to 0.50	+5 $\pm$2	0 $\pm$1	+10 $\pm$5	+3 $\pm$1	0	+7 $\pm$2	+3	0	+6
von Kármán from 0.4 to 0.35	-4 $\pm$1	-1 $\pm$1	-6 $\pm$3	-4	0	-8 $\pm$1	-4	0	-8
C_{T10N} from Smith '88 to L&P '81	+6 $\pm$6	+3 $\pm$3	+8 $\pm$8	+1 $\pm$2	0 $\pm$1	0 $\pm$3	0	0	0

C_{q10N} from Smith '88 to L&P '81	1 $\pm$1	1	1 $\pm$1	0	0	0	0	0	0
ϕ_m, $z/L < 0$ α from 20 to 30	+1 $\pm$1	+1 $\pm$1	0 $\pm$2	+1 $\pm$1	+1	+1 $\pm$1	+1	0	+1
ϕ_m, $z/L > 0$ Γ from 5 to 8	-17 $\pm$4	-9 $\pm$3	-17 $\pm$3	-5 $\pm$4	-2 $\pm$1	-7 $\pm$5	-1 $\pm$1	0	-2 $\pm$2

Table 2.2 Percentage change in calculated parameters for 3 different wind speeds.

The original heat transfer coefficients used were those of Smith (1988), Eqns. (2.27) and (2.28). However, Large and Pond (1982) used;

$$C_{q10N} = 1.15 \times 10^{-3} \qquad (2.41)$$

$$C_{T10N} = 1.13 \times 10^{-3} \qquad (z/L \le 0) \qquad (2.42a)$$

$$C_{T10N} = 0.66 \times 10^{-3} \qquad (z/L > 0) \qquad (2.42b)$$

As would be expected, the small change to the latent heat transfer coefficient, C_{q10N}, produced no significant difference in the calculated parameters. The large effects at low wind speeds due to the change in the sensible heat transfer coefficient, C_{T10N}, are attributable mainly to the cases where atmospheric conditions were stable.

Finally, the constants in the dimensionless profile function ϕ_m (Eqn. (2.15) and (2.16)) were increased to the limits of the suggested range (Fig. 2.1). Again, the effect on the calculated parameters was small for moderate and high winds, and for unstable conditions, but was much larger for low wind speeds and stable conditions.

In summary, the low wind speed (5 m/s) data are not only sensitive to the temperature measurements (Section 2.3.a), but also to the calculation of the stability parameter. The form of ϕ_m for stable conditions and low wind speeds is not well enough known. However, at moderate and high wind speeds, where unstable or near-neutral conditions predominate (Section 5.1), the calculations of u_*, U_{10N} and C_{D10N} are insensitive to either the temperature measurements, the form of the heat transfer coefficients or to the form of ϕ_m.

2.3.c Atmospheric conditions.

To estimate the wind stress, the measurement height must be within the surface layer, in which the stress is assumed to be approximately constant with height. The top of the surface layer is defined as the height at which the stress has decreased by 10% of the surface value. The height of the surface layer, H, can be approximated by (Geernaert, 1990);

$$H = A U_{10N} \tag{2.43}$$

where A is about 10 s. Hence, for a measurement height of 20 m, a wind speed of 2 m/s is the minimum at which stress estimates could be made.

It has been suggested (e.g. Donelan, 1990; Geernaert, 1990) that the friction velocity at a height z is related to that at the surface, u_{*0}, by;

$$u_{*z}^2 = u_{*0}^2 \left[1 - \frac{z f_c X}{u_{*0}} \right] \tag{2.44}$$

where f_c is the Coriolis parameter;

$$f_c = 1.454 \times 10^{-4} \sin(\text{latitude}) \tag{2.45}$$

and X is related to the height of the surface layer. However, Geernaert (1990) suggests 2.5 for the value of X, whereas Donelan (1990) suggests a value of 12. For this study, where the measurement height was about 18 m and typical latitudes were 60º, the predicted underestimate of the friction velocity for a U_{10N} of 10 m/s would therefore be either 1% or 4% depending on the value assumed for X. These underestimates would decrease with increasing wind speed. Since the size of the correction is uncertain, and is not usually applied, no height corrections will be made to the measured friction velocities in this study.

The Monin-Obukhov similarity argument (Section 2.1) breaks down under large values of $|z/L|$. The mechanical production and buoyant production of turbulent kinetic energy are of equal magnitude for (Stull, 1988);

$$|z/L| \approx 0.5 \tag{2.46}$$

As z/L becomes increasingly negative, the conditions of free convection are approached and u_* ceases to be a meaningful scaling parameter. As conditions become more stable, the height of the surface layer decreases and may become lower than the measurements height. The theory described in this Section should apply over the approximate range (Garratt, 1992);

$$-2 < \frac{z}{L} < 1 \qquad (2.50)$$

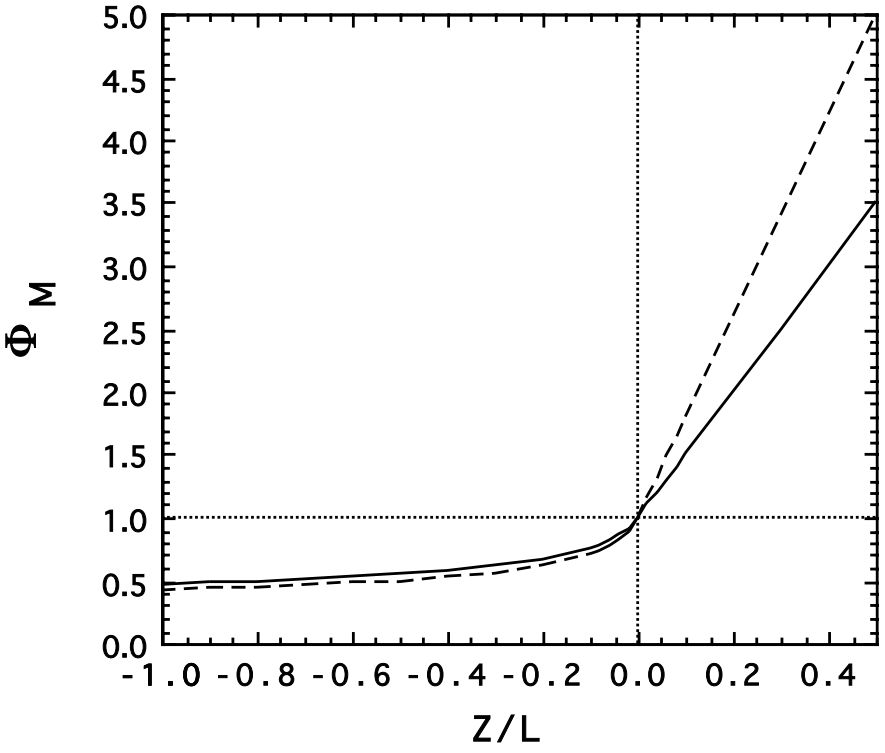

Figure 2.1. The form of the dimensionless profile function, ϕ_m. for different values of α ($z/L < 0$) and Γ ($z/L > 0$). The solid line indicates $\alpha = 20$ and $\Gamma = 5$, and the dashed line, $\alpha = 30$ and $\Gamma = 8$.

Yelland, M. J., 1997: Wind stress over the open ocean. *PhD thesis*, University of Southampton, U.K.,

3 EVALUATION OF THE INERTIAL DISSIPATION METHOD.

3.1 Introduction

There are a number of methods that have been used in the past to estimate the wind stress. Those used in early studies are reviewed by Roll (1965). More recently, the eddy correlation, the inertial dissipation and the wind profile methods have been preferred. Previous attempts to validate the dissipation method are discussed in Section 3.2, and the advantages and disadvantages of the method are discussed in Section 3.3.

3.2 Validation of the dissipation technique.

Since the inertial dissipation method was first suggested by Hicks and Dyer (1972) there have been various attempts to validate the technique, usually by comparison with the eddy correlation method (Dunckel et al., 1974; Schmitt et al., 1978; Large and Pond, 1981; Geernaert et al., 1988; Edson et al., 1991). These comparisons are discussed in turn.

Dunckel et al. (1974) obtained wind stress measurements over the tropical Atlantic for wind speeds of 4.5 to 11 m/s and near-neutral conditions ($-0.027 < z/L < -0.001$). Wave heights varied from 1 to 3 m. Data were obtained via the profile method using seven lightweight cup anemometers, arranged at heights of between 1 and 8 m, on a surface following buoy. Eddy correlation and inertial dissipation measurements were also obtained from hot-wire anemometers mounted at a height of 2.4 m on a tilt-stabilised mast on a second surface following buoy. Drifts in the hot-wire anemometers were corrected for by adjusting the horizontal wind speed to those from the cup anemometers. The mast was kept to within 1º of the vertical and accelerometers were used to obtain the buoy-motion. The eddy correlation estimates of the wind stress were increased by about 65% after corrections

for buoy motion were applied. Residual mean tilts were corrected for by rotating the axes to obtain a zero mean vertical wind speed. Twenty six estimates of the 10 m drag coefficient were obtained from the eddy-correlation method for wind speeds of between 5.5 and 8 m/s. These showed no wind-speed dependency and produced a constant value of 1.39×10^{-3}. A rather larger data set was obtained from the profile method, for wind speeds between 4.5 and 11 m/s, which also resulted in a constant drag coefficient. In this case, however, the mean value of 1.90×10^{-3} was 35 % larger than that obtained from the correlation method. The 26 estimates from the dissipation method resulted in a mean drag coefficient of 1.26×10^{-3}, about 10% less than that from the eddy correlation method. However, the results from the profile method were very sensitive to distortion of the wind profile near the water surface: when measurements from the anemometers below 2.3 m were ignored the stress estimates became much more scattered but the agreement with the eddy correlation results was much improved. Although there was reasonable agreement between the eddy correlation and dissipation methods, it was found that the spectral levels of the vertical wind speed component were, on average, equal to those of the along wind component, i.e. that the assumption of local isotropy, implicit in the dissipation method, did not hold (Section 2.2.b). However, it should be noted that of the three methods, the results from the dissipation method agreed best with the results from other (later) open-ocean studies (Figure 3.1). Dunckel et al. used a Kolmogoroff constant of 0.48 for their dissipation analysis: if this is replaced by an effective value of 0.55 (see Section 3.3) the dissipation data agree very well with later open ocean results.

Schmitt et al. (1978) performed a comparison of stress measurements obtained via the eddy correlation and the inertial dissipation methods. A sonic anemometer was mounted 8 m above sea level on a tower in 20 m of water, and levelled to within 0.1 degree. Six runs were obtained for a wind speed of around 6 m/s. Bulk formulae were used to estimate stability. The dissipation-derived drag coefficient estimate was 30% higher on average than that found by the eddy correlation method, with values

of $0.99 \pm 0.37 \times 10^{-3}$ and $0.77 \pm 0.10 \times 10^{-3}$ respectively. Again, if an effective Kolmogoroff constant of 0.55 is assumed, rather than the 0.50 used by Schmitt et al., the dissipation results would be reduced by 10%. The ratio of the vertical to the alongwind velocity spectra in the inertial region was found to be 1.06 ± 0.16 on average. A similar value was found for the crosswind to alongwind spectral ratio which suggested that the departure from isotropy was not due to buoyancy forces. Schmitt et al. reviewed other attempts to measure the ratio of the spectral levels over water, and notes that the 4/3 ratio was generally observed where the measurement height was 12 m or more. It was suggested that the degree of anisotropy increases as the ratio of the measurement height to the wave height decreases, with the effects of anisotropy becoming significant for ratios of less than 5 to 10.

Large and Pond (1981) obtained 192 estimates of the wind stress using both the eddy correlation and the dissipation methods over a wind speed range of 4 to 20 m/s. A modified Gill propeller-vane anemometer was used, mounted at a height of 12.5 m on the Bedford Institute tower (Smith, 1980). The results from the two methods agreed to within 4% except for the most stable cases. For the six estimates obtained where $z/L > 0.1$, the drag coefficient values from the dissipation method were 5 to 10 % higher than those from the eddy correlation method. On average, the results from this study agreed well with the independent eddy correlation measurements of Smith (1980), who found that the drag coefficient increased with wind speed;

$$1000\, C_{D10N} = 0.61 + 0.063\, U_{10N} \qquad 6 < U_{10N} < 22 \ \text{m/s} \qquad (3.1)$$

Both these studies are discussed in more detail in Section 7.4.

During the 3 day TOWARD experiment 2 km off the Californian coast, Geernaert et al. (1988) compared 30 minute averages of wind stress from the dissipation technique (using a hot film instrument) and the eddy correlation technique (using a sonic anemometer) for wind speeds of less than 9 m/s. Both instruments were mounted on a tower at a height of 22 m above sea level. The results of this

comparison showed that the two techniques agreed well under near neutral conditions, but for stable conditions (and especially during non-stationary conditions) the dissipation method underestimated the stress by up to 40% compared to the eddy correlation method. However, the stable data were obtained during wind speeds of less than 6 m/s. For low wind speeds and stable conditions, the anemometers may well have been above the surface layer (Section 2.3.c) and the results from either method may not be reliable.

The most recent, and most exhaustive, comparison of the dissipation and eddy correlation techniques was performed during the HEXOS experiment in the autumn of 1986. Edson et al. (1991) presented the results from the stress comparisons obtained, under near neutral or slightly unstable conditions, during the HEXOS main experiment (HEXMAX). Various anemometers were mounted on the Meetpost Noordwijk platform in the North Sea. Two sets of anemometers were deployed, each containing sonic anemometers and hot wire or film anemometers. One set was located on a boom extending out from the platform at a height of 5-8 m above sea level, and the other was on a mast above the platform, at a height of 26 m. The mast site was deliberately located in a region which suffered from distortion of the air flow in order to study the effect of such distortion on the wind stress measurements. The mean vertical and crosswind components of the wind speed were forced to zero in order to allow for instrument tilt. The results showed that the wind stress from the dissipation and eddy correlation methods agreed to within 5%. It was concluded that the dissipation method was superior to the eddy correlation method in regions where the flow distortion was severe, and also in regions of weak distortion if the effects on the eddy correlation data could not be adequately corrected. Assuming a balance between the production and dissipation of TKE, the Kolmogoroff constant was found to be 0.55±0.01, which is in agreement with that used by Large and Pond (1981).

3.3 Drawbacks and advantages of the dissipation method.

The dissipation method is often criticised since it is an indirect way of estimating the wind stress, unlike the eddy correlation method, and depends on a number of assumptions.

As described in Section 2.1, the Kolmogoroff hypothesis is fundamental to the inertial dissipation method. The hypothesis is in turn based on the assumption of local isotropy in the inertial subrange of the wind speed spectrum. The presence of local isotropy predicts a 4/3 ratio between vertical or cross-wind spectral levels and the spectral level of the alongwind component. Wucknitz (1979) and Neugum (1996) have shown that the presence of an $f^{-5/3}$ slope in the wind spectrum is not sufficient to guarantee the presence of isotropy, and that the ratio of the spectral levels of the different wind components should also be checked. Some authors (above) have shown that near to the surface, the ratio is nearer 1:1, with an "excess" of energy in the along wind spectra and an energy "deficiency" in the vertical spectra (Wucknitz). However, Wucknitz also suggests that it is possible to correct for anisotropy if the vertical wind speed spectral levels are known.

Neither Large and Pond (1981) nor Edson et al. (1991) investigated the degree of isotropy in their data. However, the review of Schmitt et al. (1978) suggested that the degree of anisotropy found over the oceans may decrease with increasing measurement height, with isotropy being present at heights of about 12 m or more. This is supported by Henjes (1996) who found a 4/3 ratio from the RRS Discovery data (obtained at a height of about 18m) used in this study. In addition, Dupuis et al. (1997) also found a 4/3 ratio of the spectral levels for a measurement height of 15 m. Dunckel et al. (1974), who report measurements from a height of 2.4 m, and Schmitt et al., using a measurement height of 8 m, both found ratios closer to 1:1. This would suggest that the HEXOS dissipation data, obtained at a height of 5 to 8 m, may have been affected by anisotropy, whereas the measurements of Large and

Pond, at a height of 12.5 m on the BIO tower, were probably unaffected by anisotropy.

This begs the question of the value found in those two studies for the effective Kolmogoroff constant. In both studies, a value of 0.55 was found to give best agreement (under near-neutral conditions) with simultaneous eddy correlation measurements. However, in the HEXOS experiment, the alongwind spectral component was used for the estimate of the dissipation rate, whereas Large and Pond (1981) measured the total horizontal wind speed spectrum. It is therefore thought that, although both experiments obtained the same value for the Kolmogoroff constant, in the HEXOS experiment this value may have compensated for an increased spectral level due to anisotropy, whereas in the study of Large and Pond, the value may have compensated for an increased spectral level due to the measurement of the total horizontal wind speed, rather than just the alongwind component.

Another criticism of the dissipation method is that of the assumptions made in using the TKE budget. This subject is dealt with in detail in Section 5, and will only be summarised here. It is sometimes assumed that the production and dissipation of TKE balance, and that the vertical divergence terms are either negligible or cancel out. It has been found, however, that this assumption does not always hold, and various empirical forms of the "imbalance" term have been proposed (Section 5.3). Many of these terms have been found by comparison of dissipation-derived wind stress data with simultaneous eddy-correlation data. Again, an effective Kolmogoroff constant is used in some studies to compensate for an imbalance of TKE observed under neutral conditions, and a stability dependent formulation of the imbalance term is found for non-neutral conditions. These studies are discussed in Section 5.3. It must be noted that the relationship between the imbalance term in the TKE budget and the effects of anisotropy is not known.

It can be seen that the major uncertainty in the use of the dissipation method lies in determining the appropriate value of the Kolmogorov constant. In this study, a value of 0.55 was used since this was the value found by Large and Pond (1981), who obtained good agreement between their open ocean dissipation and eddy correlation wind stress estimates. The experimental conditions of their study were similar in many crucial respects to those of this study, i.e. the measurement heights were above the region where the effects of anisotropy may be significant, and both studies use the total horizontal wind speed spectrum to determine the dissipation rate. For these reasons it is thought that the Kolmogoroff value used in this study is appropriate. However, even if the appropriate value were really 0.50 (rather lower than found by most researchers (Section 5.3)), this would imply an increase of the mean drag coefficient of about 7% for a wind speed of 10 m/s (Section 2.3.b). Although a significant effect, this is small in comparison to the biases introduced by the effects of flow distortion. For example, in Section 2.3.a it was shown that a fairly small error of 5% in the estimate of the true wind speed introduces a 17 % bias of the drag coefficient for a wind speed of 10 m/s. Hence the uncertainties inherent in the use of the dissipation method are much less critical than the correct determination of the mean wind speed. The effects of flow distortion on the results of this study are determined, and corrected for, in Section 6.

Most open ocean wind stress data has been obtained using the dissipation method (Section 7.4) since it is the most practical method for use on moving platforms such as ships. The eddy correlation method depends on accurate measurements of the vertical as well as the horizontal fluctuations of wind speed, integrated over all length scales, and is therefore much more sensitive to the effects of flow distortion on the turbulent structure of the flow than is the dissipation method. The ship motion is large compared to the fluctuations of the vertical wind speed which means that very sophisticated motion packages are required for the eddy correlation method to be employed successfully. In addition, the distortion of the flow of air around a ship has a much greater impact on either the eddy correlation or

the wind profile method than on the dissipation technique (Edson et al., 1991). Small errors in the vertical alignment of the anemometer can have a large effect on the eddy-correlation derived wind stress. For example, Oost et al. (1994) describes the 50% average disagreement in the concurrent wind stress estimates from 3 sonic anemometers which was ascribed to misalignments of 1º (Kaimal and Haugen, 1969). Even when these misalignments are corrected for, the effects of flow distortion are still significant. Oost et al. developed a method to correct for the effects of flow distortion around the anemometer support structures (booms etc.) used during the HEXOS experiment. In addition to the mean tilt correction, an average correction of 11% was required to correct the wind stress results for an anemometer misaligned with the flow by less than 2.5º. The errors described above were all found from instruments deployed on stable platforms. On a moving platform, the degree of instrument misalignment and the effects of flow distortion will vary rapidly in time: correcting for these effects presents a severe experimental challenge if the eddy correlation is to be used successfully.

All methods of determining the wind stress require stationary conditions. However, whereas the eddy correlation method requires sampling times typically of the order of 30 minutes or more, the dissipation method only requires sampling periods long enough to determine the spectral level at frequencies of a few Hertz. Typical sample periods used are of the order of 10 or 20 minutes, and Marsden et al. (1993) successfully used the dissipation method with a sampling period of about 1 minute.

3.4 Discussion

For open ocean studies, where instruments are usually mounted on a moving platform, the inertial dissipation method is the most practical. The wind stress results from this method have been shown to agree to within a few percent with measurements made using the more direct eddy correlation method. The dissipation method is much less sensitive to low frequency platform motions than the eddy

correlation method, and is also much less sensitive to distortions of the air flow since it uses only the high frequency part of the spectrum. The insensitivity of the dissipation method to flow distortion suggests that, for eddy sizes within the inertial sub-range (order 1m or less), the spectral level is not significantly affected.

The major uncertainty in the use of the dissipation method is the choice of the effective Kolmogoroff constant. However, a 10% error in the value of the constant has a relatively small effect on the drag coefficient to wind speed relationship. It is suggested that, whichever method is employed to estimate the wind stress, the effects of flow distortion and the accurate determination of the true wind speed are the largest sources of error. This subject is investigated in detail in Section 6.

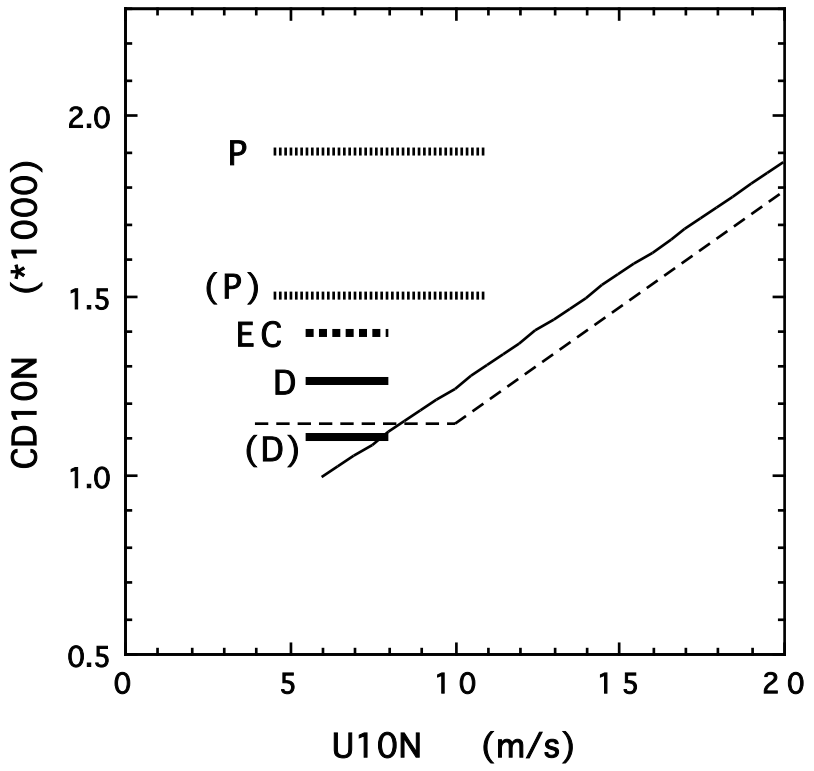

Figure 3.1. Open ocean drag coefficient data from the profile method (heavy dotted lines, marked P), the eddy correlation method (heavy dashed line, EC) and the dissipation method (thick solid lines, D) from the intercomparison of Dunckel et al. (1974). The line marked (P) represents data from the profile method using anemometers above 2.3 m only. The line marked (D) represents the dissipation results with an assumed Kolmogoroff constant of 0.55. The thin lines show the open ocean relationships suggested by Large and Pond (1981) (dashed) and Smith (1980) (solid).

4 INSTRUMENTATION AND DATA PROCESSING

This Section describes the instrumentation, logging systems and initial data processing employed during the R.R.S. Discovery Southern Oceans cruises D199, 200 and 201 and the R.R.S Charles Darwin cruise 43. The Darwin cruise took place in the Faeroes region of the North Atlantic (Figure 4.1) during the Autumn of 1989. The later cruises on the Discovery took place in the Southern Oceans (Figure 4.2) from the end of December 1992 to the start of May 1993. The system used on the Discovery will be described in greater detail, since the majority of the data used in the later sections were obtained during this cruise. The Darwin system differed only in the addition of extra fast sampling anemometers, and in the degree of automation of the initial data processing.

All manipulation and analysis of data was carried out on a Sun UNIX workstation or an Apple Macintosh machine networked to the UNIX system. Most of the analysis was performed using "PEXEC", a suite of in-house FORTRAN programs.

4.1 Instrumentation on the Discovery Southern Ocean cruises.

A Solent Sonic Research Anemometer (manufactured by Gill Instruments Ltd.) was mounted on the foremast of the RRS Discovery, 18.5 m above sea level, as shown in Figure 4.3. The asymmetric head version of the anemometer was used with the 240° open sector facing the bow of the ship (Figure 4.4). The anemometer had a sampling rate of 168 Hz, and output digital 3-component wind estimates at 21 Hz. These data were logged to a NEC APC IV portable microcomputer for periods of 12 minutes, each beginning on the quarter-hour.

In addition to the Solent sonic anemometer, an R.M. Young propeller anemometer was also mounted on the foremast platform. Two Vector Instrument aspirated psychrometers were mounted near the sonic anemometer at a height of 17 m

above the water line. An aneroid barometer was located in the main laboratory of the ship and a hull-mounted platinum resistance thermometer was used to obtain the sea surface temperature. The ship's GPS system and the hull-mounted two-component electromagnetic log (em log) system produced values for the speed of the ship over the ground and through the water respectively. All these instruments were sampled by the RVS "metlogger" system at 1 Hz, and 1 minute average values were recorded.

The temperature sensors were accurate to a few tenths of a degree or better, and the air pressure sensor has a specified accuracy of 0.3 mb. These are sufficient for the calculation of the atmospheric stability corrections, as discussed in Section 2.3. The accuracy of the em log varies, depending on how recently and well the calibration was performed, but should be better then 0.5 m/s, whereas the GPS ship speed is accurate to 0.1 m/s (Kent et al., 1992). Ship speed data are discussed further in Section 4.8. The Solent sonic anemometer has a specified accuracy of 1.5 % over a 10 second sample for wind speeds between 0 and 30 m/s. However, the calibration certificates for this instrument suggest that, for the 20 m/s wind speed used during the calibration, the errors do not exceed 0.5%.

Apart from the Solent sonic and mean meteorological systems, the Discovery was also equipped with a Ship Borne Wave Recorder (SBWR). The SBWR had a sampling period of 10 minutes and produced 102 spectral estimates ($E(f)$) between 0 and 1 Hz. These data were logged to an NEC PC.

4.2 The Charles Darwin cruise 43.

The Charles Darwin was equipped with similar mean meteorological instruments as the Discovery. The psychrometers, R.M. Young propeller anemometer, sea temperature and air pressure sensors were sampled at 1 Hz using the MultiMet data logger (Birch and Pascal, 1987) and one minute means were produced. One minute means of the speed of the ship over the ground and through the water were recorded from the ship's GPS and em log systems respectively. A

SBWR was also installed on the Darwin, and was operated as described in Section 4.1.

The Solent sonic installed on the foremast platform of the Darwin was a prototype model that differed slightly from the production model used on the Discovery cruises. The 21 Hz output from the prototype was based on a 42 Hz sampling rate (rather than 168 Hz), and the internal calibration was a generic one based on tests carried out in a 2' by 3' wind tunnel, whereas the production models were individually calibrated in a 7' by 5' wind tunnel. Additionally, the three support struts around the sensor volume of the prototype were arranged symmetrically (Figure 4.5). A full evaluation of the prototype Solent sonic is given by Yelland et al. (1991), who demonstrated that uncontaminated spectra could not be obtained within 20∞ of a support strut. This result led to the development of the asymmetric version of the anemometer, used later on the Discovery. However, the prototype instrument was mounted on the Darwin with the "North" strut facing aft, and collection of wind spectra was restricted to periods when the wind was blowing within 30∞ of the ship's bow, i.e. was more than 30∞ from a support strut. The three component wind speed data from the Solent sonic were logged over 20 minute periods.

In addition to the Solent sonic anemometer, there were four other fast response anemometers mounted on the foremast platform (Figure 4.6). The Solent sonic was mounted 15.1 m above the waterline. The R.M. Young propeller vane anemometer was mounted on the port side of the foremast platform at a height of 15.6 m. The Kaijo-Denki sonic and the R.M. Young Bivane anemometers were mounted on the starboard side of the platform at heights of 14.35 and 15.7 m respectively. The R.M Young tri-axis anemometer did not function successfully and produced no useful data. The latter three instruments, all mounted on the starboard side of the platform, were operated by researchers from the University of Manchester Institute of Science and Technology, who kindly provided the wind speed spectra and mean relative wind speed data from the Kaijo-Denki and Bivane anemometers.

4.3 Processing of the wind spectra during the Discovery cruises.

For the Discovery cruises, the logging program for the Solent sonic anemometer performed some initial processing of the data which is described fully in Clayson (1994), and is summarised here. The three components of wind speed were transformed into North, East and Vertical speeds, where North corresponded to a wind blowing over the bows of the ship. To obtain the wind speed spectra from a 12 minute sample, the North and East components were used to calculate the instantaneous horizontal speeds which were then treated in 28 sections of 512 values. For each section, the mean was subtracted, a partial cosine window was applied and the power spectral densities calculated using a Fast Fourier Transform. The spectra were corrected for windowing loss and normalised by multiplying by $f^{5/3}$. The 28 spectra were then averaged together. The mean value of the normalised power spectral density (PSD) was calculated by averaging the 49 spectral estimates between 2 and 4 Hz: a linear fit was also calculated over the same frequency range. The lower frequency limit was chosen to be above that of the ship motion. The upper limit was selected to be well below half the Nyquist frequency (10.5 Hz).

For each 12 minute run, the mean PSD, the slope and intercept of the fit, the mean horizontal wind speed and the vector averages of the North, East and Vertical components of the wind speed were recorded in summary files. The averaged spectra were recorded separately.

4.4 Processing of the wind spectra during Darwin cruise 43.

For the Darwin cruise, the data from the Solent sonic anemometer were manually processed in a similar fashion as described in Section 4.3. At low wind speeds (less than about 5 m/s), the spectral levels increased above the $f^{-5/3}$ relationship. This may have been due to aliasing of high frequency noise, since the production models of the anemometer, which used a higher sampling rate, did not produce spectra with this increased spectral level at the higher frequencies. As

discussed in Yelland et al. (1994) the choice of a 2 to 4 Hz range for estimating the PSD seemed effective, since the values from the Solent sonic agreed well with those from the other anemometers used during the cruise.

For the Propeller and Bivane anemometers, PSD values were calculated across a fixed frequency range of 1.6 to 2.2 Hz, whereas the Kaijo-Denki PSD values were obtained from a fixed wavenumber range from 1 to 3 (equivalent to a frequency range of 0.8 to 2.4 Hz at a relative wind speed of 5 m/s, and 2.4 to 7.2 Hz at 15 m/s). Data from the two propeller-vane anemometers and the Kaijo-Denki sonic anemometer were recorded for periods of 5 minutes, rather than the 20 minute period used for Solent sonic anemometer on this cruise.

Both the Bivane and the Propeller-vane anemometers used lightweight polystyrene propellers. In order to be able to directly compare the results from these two instruments, their spectra were processed in the same way. The spectral values from the Propeller-vane were corrected for the time response of the propeller using the formula of Brook (1977);

$$H(f) = 1 / (1 + (2 \pi f L U_{rel}^{-1})2) \qquad (4.2)$$

where H(f) is the transfer function for frequency, f, and U_{rel} the mean apparent wind as measured at the anemometer. The value for the response length, L , was determined as 1 m by the manufacturers using wind tunnel measurements. However, a separate estimate of the response length was obtained from the cruise data by determining the correction needed to give an $f^{-5/3}$ slope in the dissipation region of the spectrum. This apparent response length increased from near zero at low wind speeds to asymptotically approach a value of one for wind speeds greater than 8 m/s (Figure 4.7). If these values represent the correct response length for the propeller (rather than the effect of high frequency noise in the spectra) then the use of a constant value for L of 1m at all wind speeds will have overcorrected the data, particularly at wind speeds below 8 m/s where the estimates of spectral level will be of doubtful accuracy.

4.5 Processing of the mean meteorological data.

One minute averaged values of air pressure, wet and dry bulb air temperatures, sea surface temperature, wind speed and direction (from the Propeller-vane anemometer), em log data, GPS and compass data were averaged a second time to obtain 12 minute values which corresponded to the sampling periods used by the Solent sonic anemometer. In addition to the mean 12 minute values, the standard deviations were also calculated. The mean and standard deviations of all the variables were merged on to the summary data files obtained from the Solent sonic anemometer (Section 4.2).

For the Darwin cruise, averages of the mean meteorological and navigation data were formed to correspond to the Solent sonic 20 minute sampling period. The other anemometers used during this cruise sampled for periods of 5 minutes and these data were also averaged.

4.6 Processing of the SBWR data.

Data from the SBWR were used to estimate the significant wave height, H_s, from the zeroth moment of the spectra (Pitt, 1981);

$$H_s = 4\left[\int E(f)\,df\right]^{1/2} \qquad (4.1a)$$

$$H_s = 4\left[\sum_{0.04}^{0.4} E(f)\Delta f\right]^{1/2} \qquad (4.1b)$$

where $\Delta f = 5/512$ Hz is the width of the frequency bins. The frequency response of thie SBWR is rather poor, with no useful spectral information above about 0.4 Hz (10 m wavelength). In addition, no directional information is available from the data. It is therefore not possible to differentiate wind waves and swell waves using this data.

4.7 Quality control

Quality control criteria were applied to the data and a run was rejected if; the wind was not blowing within 30∞ of the bows; the standard deviation of the relative wind direction or of the ship's head was greater than 20∞; or if the standard deviation in the ships speed was greater than 0.5 m/s. The latter criteria were designed to reject runs during periods when the ship was manoeuvring. For the ship-borne wave recorder, data were rejected if the ship speed through the water was greater than 1 m/s.

Data were also rejected if the intercept of the fit to the wind speed spectrum was not within 30 % of the mean PSD value, i.e. the normalised wind spectrum was not flat. Figure 4.8 shows five accepted spectra from the Discovery cruise, obtained at various wind speeds. The motion of the ship is visible at about 0.1 Hz, well below the frequency range of interest. As described above (Section 4.3), spectra from 28 sections of data were averaged for each run, hence the standard deviation of the spectral estimates is 19% (Pitt, 1981). The standard deviation of the mean PSD is around 3%, since there were 49 spectral estimates in the 2 to 4 Hz frequency range used.

The calculation of the PSD (Section 2.1) requires the assumption that Taylor's hypothesis is valid, i.e. that the turbulence is "frozen". Willis and Deardorff (1976) suggest that the hypothesis is valid when $\sigma_u < 0.5\ U_{rel}$, where σ_u is the standard deviation of the relative wind speed, U_{rel}. This test was met by all the Discovery data which passed the other quality control criteria: for all data, with the exception of one very low wind speed run, the standard deviation of the relative wind speed was less than 10 % of the mean value.

4.8 Estimating the true wind speed.

The true wind speed should be calculated with respect to the water surface rather than over the ground (Section 2.2). This implies that the em log data of ship

speed through the water should be used, rather than that from the GPS. However, the em log needs careful calibration to provide accurate data, and can also be affected by use of the ship's bow thruster. The bow thruster is used to position the ship when "on station", and works by emitting a strong jet of water from beneath the hull. In the case of the Darwin, this jet can be emitted in any direction, and could pass close to the em log sensors under the hull, causing the instrument to record erroneous ship velocities. Figure 4.9 shows the mean em log ship speed against that from the GPS for the Discovery data, after the quality-control criteria have been applied. Since the data were selected for winds blowing over the bow, it would be expected that the wind drift current would generally act so that the ship's speed through the water from the em log would be larger than the ship's speed over the ground. However, it can be seen that at low ship speeds, the em log under-estimates by about 0.1 m/s. As the GPS ship speed is the derivative of the ship's position, no systematic error can be attributed to the ship speed over the ground, and it is therefore concluded that the em log had a poor calibration during the Discovery Southern Ocean cruises.

For both the Darwin and the Discovery cruises, the true wind speed was calculated by vector addition of the GPS ship speed with the relative wind speed from the Solent sonic anemometer. Hence the true wind speed may be overestimated due to the neglect of any wind drift currents. These are estimated to be of the order of $0.5\ u_*$ (Wu, 1975), i.e. about 2% of the wind speed, which is not insignificant. However, calculation of the true wind speed with respect to the ground is common practice (Section 2.3.a), and effectively incorporates the surface wind driven-currents into the parameterisation of the drag coefficient. Since a) we have no measurement of the drift currents, and b) in order to compare our results with those of other researchers, no corrections will be made to the estimates of the true wind speed.

4.9 Description of the data.

After selection according to the criteria in Section 4.6, the three Discovery Southern Ocean cruises resulted in 2633 wind stress estimates. These data covered a wide range of meteorological conditions; wind speeds ranged from near calm to 26 m/s (with a mean of 11 m/s), and the air-sea temperature difference varied from -8 to +4∞C. 1570 of these data had concurrent SBWR data during which the ship was moving at less than 1 m/s. The mean significant wave height was a little less than 4 m, with a maximum of 14 m.

Charles Darwin cruise 43 produced 146 data cycles with concurrent PSD values from three of the fast sampling anemometers: 99 values were obtained from the Bivane. These were 20 minute averages, rather than the 12 minute averages produced from the Discovery cruises. The air-sea temperature difference ranged from -6 to +0.5∞C, and winds speeds varied from 6 to 18 m/s, with a mean of 12 m/s. Only 64 concurrent SBWR spectra were available, with Hs values between 2 and 8 m.

Figure 4.1 The ship track for R.R.S. Charles Darwin cruise 43.

m/s. The mean significant wave height was a little less than 4 m, with a maximum of 14 m.

Charles Darwin cruise 43 produced 146 data cycles with concurrent PSD values from three of the fast sampling anemometers: 99 values were obtained from the Bivane. These were 20 minute averages, rather than the 12 minute averages produced from the Discovery cruises. The air-sea temperature difference ranged from -6 to +0.5°C, and winds speeds varied from 6 to 18 m/s, with a mean of 12 m/s. Only 64 concurrent SBWR spectra were available, with Hs values between 2 and 8 m.

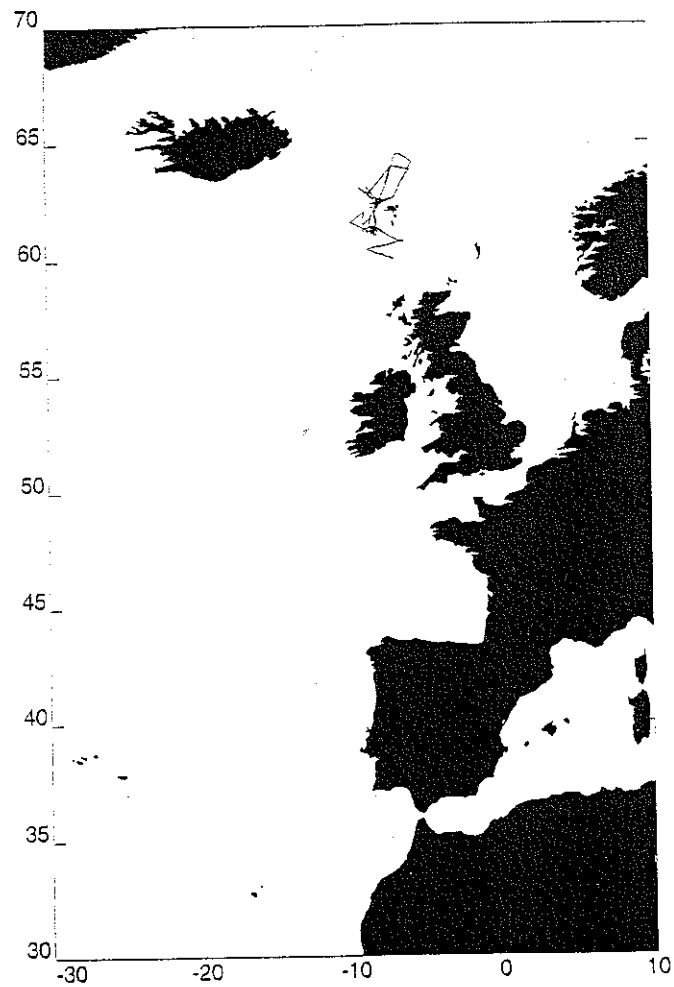

Figure 4.1 The ship track for R.R.S. Charles Darwin cruise 43.

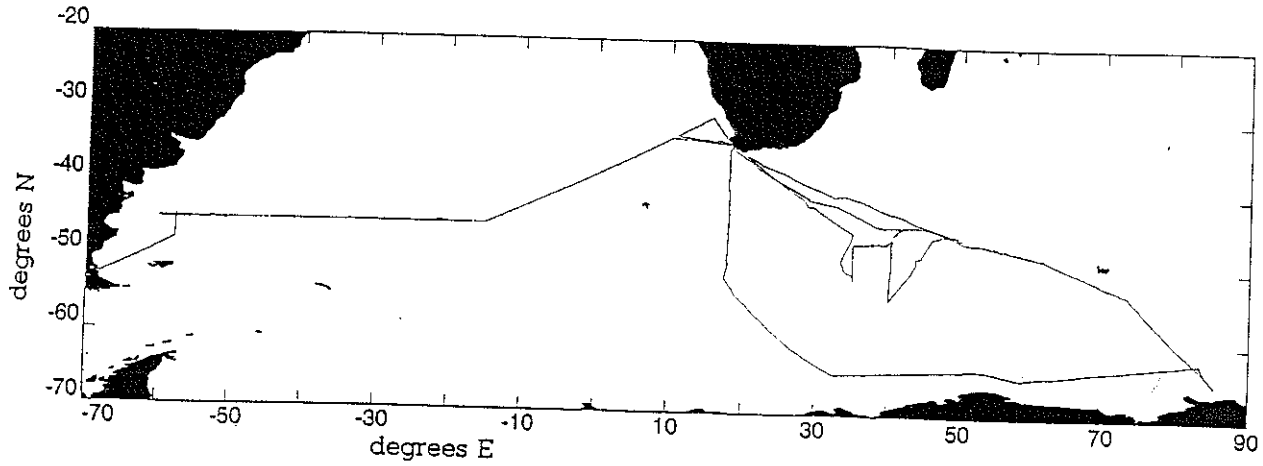

Figure 4.2 The ship track for R.R.S. Discovery cruises 199, 200 and 201.

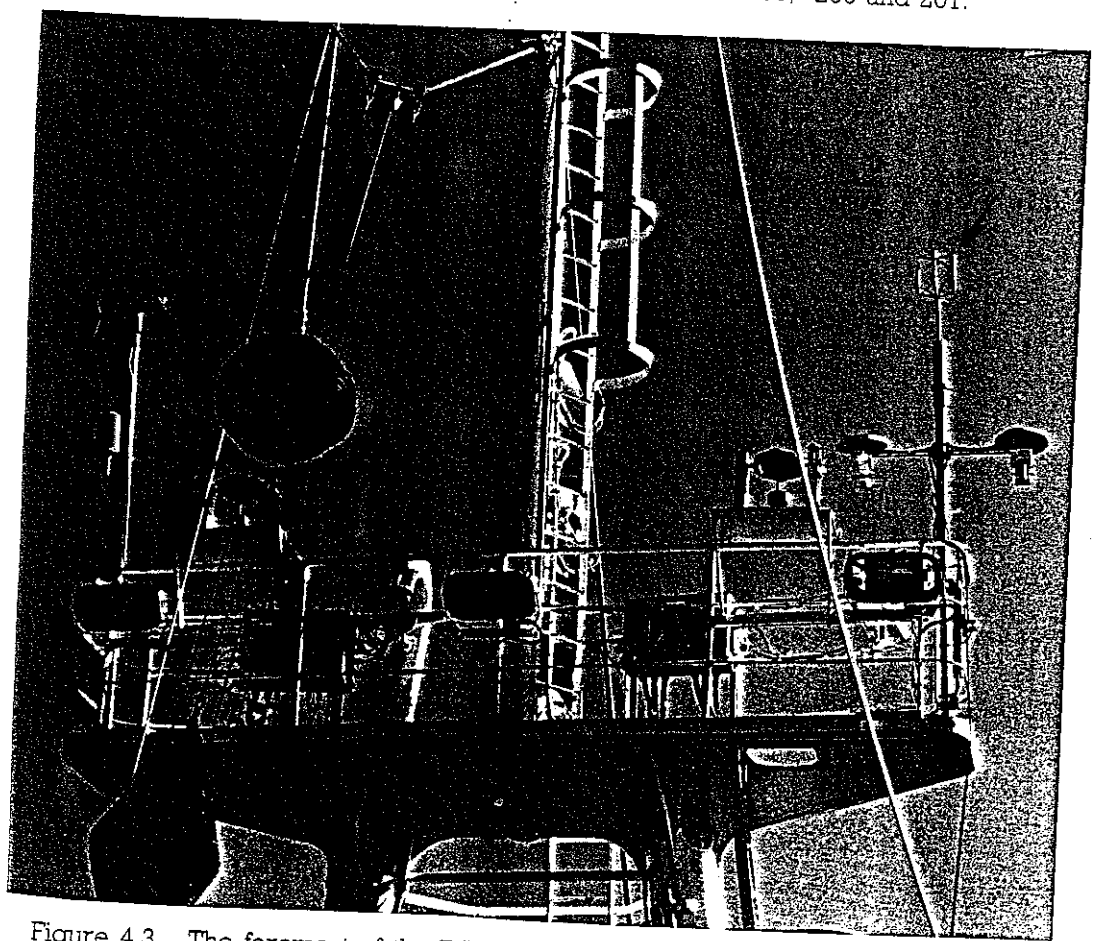

Figure 4.3 The foremast of the R.R.S. Discovery, showing the Solent sonic anemometer (indicated by the arrow) on the starboard side of the platform.

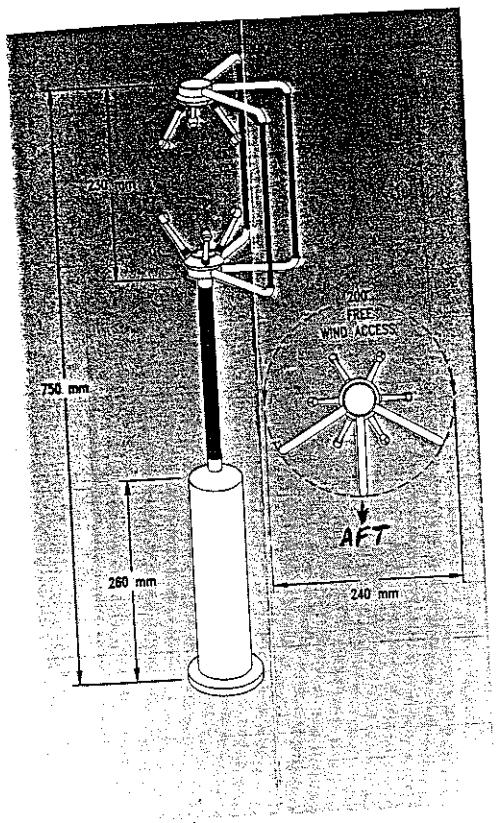

Figure 4.4 The asymmetric version of the Solent sonic anemometer.

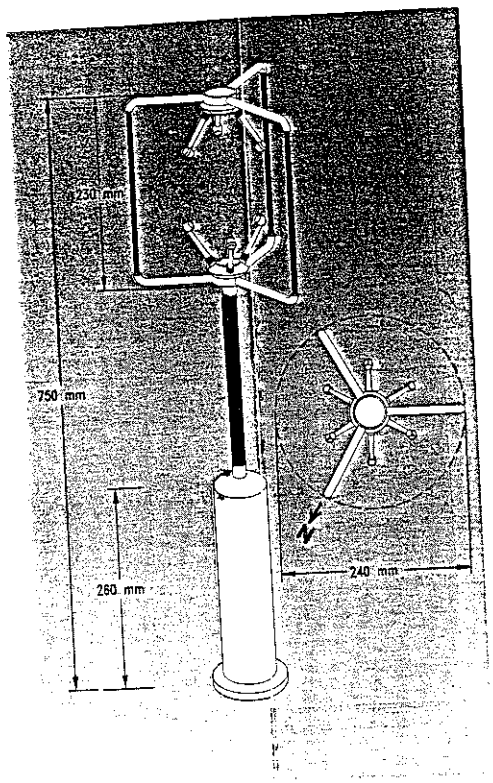

Figure 4.5 The symmetrical version of the Solent sonic anemometer.

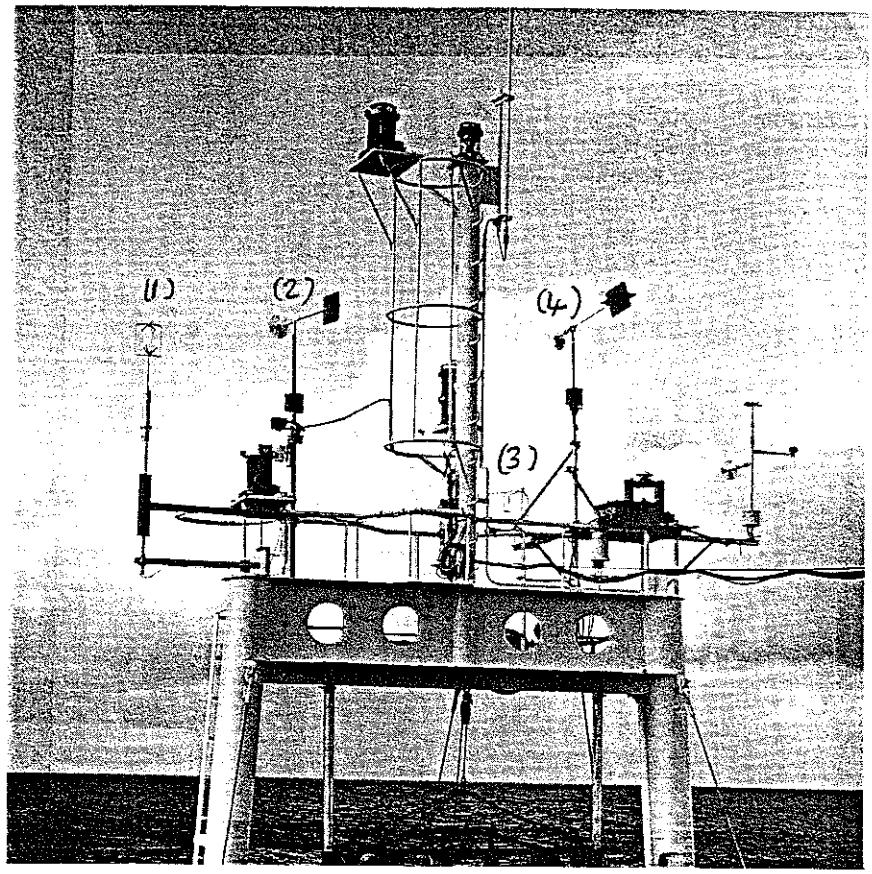

Figure 4.6 The foremast of the R.R.S. Charles Darwin, looking forward from the bridge. The fast sampling anemometers are indicated by the numbers; (1) Solent sonic, (2) Young propeller-vane, (3) Kaijo-Denki sonic, and (4) Young Bivane.

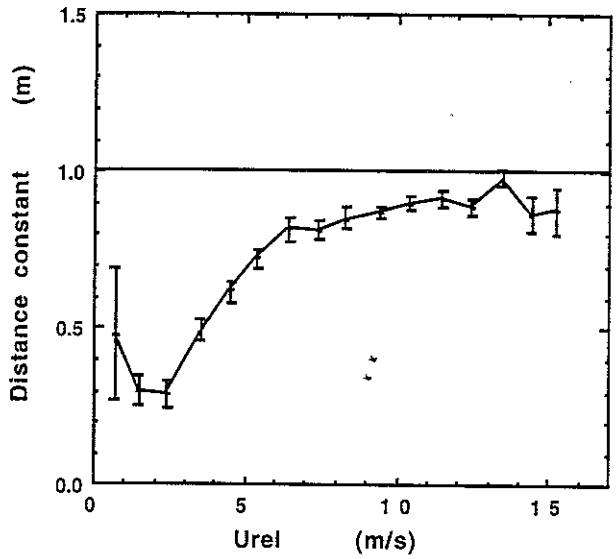

Figure 4.7 The estimated distance constant, L, against relative wind speed for the Young propeller anemometer. Error bars indicate the standard deviation of the mean.

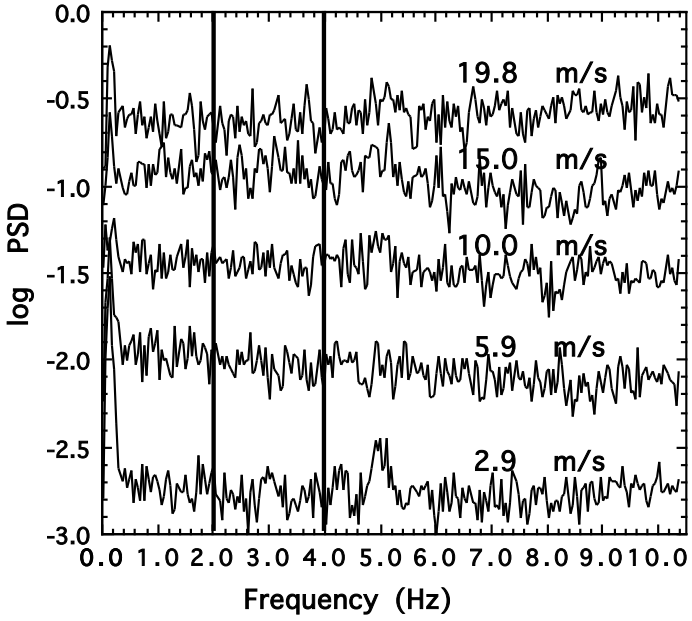

Figure 4.8 Wind speed spectra from the Solent sonic anemometer used during the Discovery Southern Ocean cruises. The average wind speed is indicated for each. The vertical lines indicate the frequency range across which the PSD is estimated.

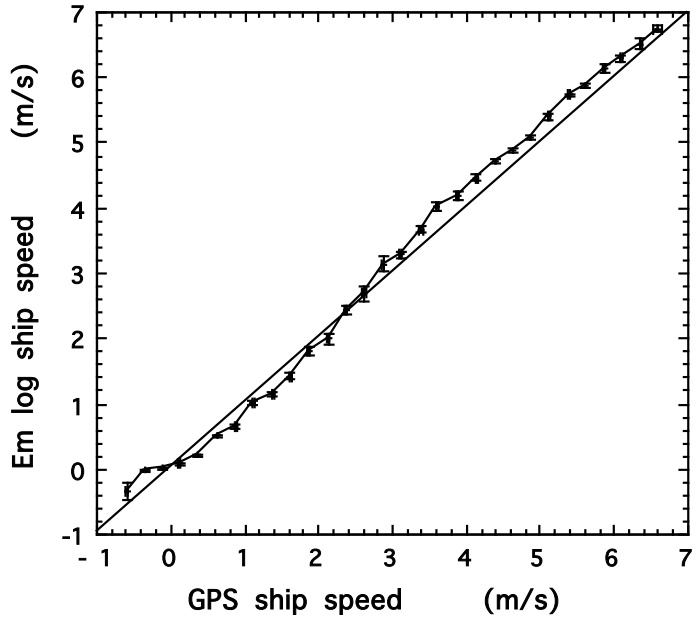

Figure 4.9 Em log against GPS ship speeds for the Discovery cruises. Error bars indicate the standard deviation of the mean.

NOTE: this chapter is superceded by Taylor, P.K. and Yelland, M.J. 2000: On the apparent 'imbalance' term in the turbulent kinetic energy budget, *J. of Atm. and Ocean. Tech.*, 17(1), 82-89

5 THE WIND STRESS CALCULATION: QUANTIFYING THE IMBALANCE TERM IN THE TKE BUDGET.

This Section describes the analysis of the data obtained from the Discovery cruises (Section 5.1) and investigates the assumption of a balance between the production and dissipation terms in the TKE budget. An empirical relationship between the imbalance term, stability and wind speed is determined in Section 5.2. The resulting form of the imbalance term is compared to the findings of previous studies in Section 5.3, and its effect on the drag coefficient are investigated in Section 5.4.

5.1 The friction velocity with the assumption of zero imbalance.

The theory behind the calculation of the wind stress was given in Section 2. Initially, the assumption was made that the terms for the vertical divergence of the turbulent transport and of the pressure transport in the TKE budget cancelled out, implying a balance between the production terms and the dissipation (Eqn. (2.18a)). This assumption is commonly made (for example, Large and Pond, 1981 and 1982, and Anderson, 1993).

The data obtained from the Discovery Southern Ocean cruises were analysed as described in Section 2.2.a, using the FORTRAN program “bfdissY.F”. Out of the 2633 data cycles which passed the quality control criteria (Section 4.6), 182 failed to converge during the iterative calculation of the stress (Section 2.2.a). These were all obtained during wind speeds of less than 10 m/s, and represent 16% of the data obtained below that speed. Data obtained at wind speeds greater than 10 m/s all converged. Figure 5.1 shows the air-sea temperature differences and true wind speeds for all the data. It can be seen that, apart from a few data where conditions were very stable, the data which failed to converge occurred during unstable conditions.

NOTE: this chapter is superceded by Taylor, P.K. and Yelland, M.J. 2000: On the apparent 'imbalance' term in the turbulent kinetic energy budget, *J. of Atm. and Ocean. Tech.*, 17(1), 82-89

Figure 5.2 shows the variation of z/L with U_{10N}. The U_{10N} values range from almost calm to 26 m/s, and the stability parameter z/L varies from -2 to +4. To examine the effectiveness of the stability functions, the data were separated according to ranges of z/L and averaged into U_{10N} bins of 1 m/s width. The results are shown separately for the stable and unstable conditions in Figure 5.3. The stable data above about 6 m/s are in good agreement with the very near-neutral ($|z/L| < 0.01$) data, except for 10 points between 15 and 20 m/s. At low wind speeds, data where $z/L > 0.1$ have smaller friction velocity values than the corresponding very near-neutral data. For unstable data and winds above 6 m/s, it can be seen that, compared to the very near-neutral data, the friction velocity is increasingly underestimated with increasingly unstable conditions. Below 6 m/s the pattern is less clear.

5.2 Estimation of the imbalance between production and dissipation.

5.2.a Analysis method and results from Yelland and Taylor (1996).

The dependence of the non-neutral friction velocity values on both the stability and wind speed conditions was investigated, by comparison with the neutral data, by Yelland and Taylor (1996) (YT96). The method and results are summarised here. The neutral ($|z/L| < 0.01$) friction velocity data were fit by a third order polynomial which was then used as a bulk formula to calculate u_{*BULK} values as a function of the measured U_{10N} for the entire data set. Figure 5.4 compares the calculated parameters obtained using the bulk relationship with those from the original dissipation calculation. It can be seen that, compared to the large amount of scatter in the friction velocity and stability parameter estimates, the calculation of U_{10N} is virtually unchanged, except for a few values below 5 m/s during which conditions were very stable. The differences between the “bulk” friction velocity values, u_{*BULK}, and those from the original dissipation method calculation, u_{*DISS}, were ascribed to an imbalance term, Φ_D, since the effect of the acceptable variation in Φ_M

NOTE: this chapter is superceded by Taylor, P.K. and Yelland, M.J. 2000: On the apparent 'imbalance' term in the turbulent kinetic energy budget, *J. of Atm. and Ocean. Tech.*, 17(1), 82-89

for unstable conditions is very limited (Section 2.3.b). The bulk method assumed zero imbalance;

$$\Phi_{\varepsilon BULK} = \Phi_{MBULK} - z/L_{BULK} \qquad (5.1a)$$

If the possible effects of sea state and sources of error or noise in the data are ignored, then an imbalance term should make u_{*DISS} equal to u_{*BULK};

$$\frac{k_v z\varepsilon}{u_{*DISS}^3} = \frac{k_v z\varepsilon}{u_{*BULK}^3} = \Phi_M - z/L - \Phi_D \qquad (5.1b)$$

Since many of the data failed to converge using the original dissipation calculation, the imbalance term was estimated using z/L from the bulk calculation as a first approximation;

$$\Phi_D = \Phi_{MBULK} - z/L_{BULK} - \frac{k_v z\varepsilon}{u_{*BULK}^3} \qquad (5.1c)$$

YT96 found Φ_D to be a function of wind speed as well as z/L. An imbalance term of the form;

$$\phi_D = \frac{z}{L}\left(2 - \frac{U_{10N}}{3}\right) \qquad z/L \le 0 \qquad (5.2a)$$

$$\phi_D = \frac{z}{L}\left(\frac{(U_{10N} - 12)^2}{15}\right) \qquad z/L > 0 \qquad (5.2b)$$

was found to remove the systematic differences between the non-neutral and neutral data. A slightly better convergence rate was also achieved, with 169 low wind speed cases failing to converge.

5.2.b Re-analysis of the imbalance term.

Subsequent analysis suggested that at least part of the discrepancy between the neutral and non-neutral data may have been due to the effects of air-flow disturbance caused by the presence of the ship, rather than wholly to the imbalance in the TKE budget. This problem, examined in Section 6, is illustrated in Figure 5.5.a, where the original friction velocity and U_{10N} values are shown after separation into three relative wind direction classes: "port" and "starboard" for relative wind directions of more than 10 (and less than 30) degrees to port or starboard of the bow,

and "bow" for relative wind directions within 10 degrees of the bow. Figure 5.5.b shows the equivalent drag coefficient to wind speed data. For a given U_{10N}, it can be seen that over most of the wind speed range the drag coefficients obtained with the wind on the starboard bow are slightly overestimated compared to the bow-on values, and those from the port bow are significantly underestimated. The mean relative wind direction is shown for each 1 m/s U_{10N} interval in Figure 5.6.a, and for each $0.1z/L$ interval in Figure 5.6.b. It can be seen that for data obtained during both the higher wind speeds and the more unstable conditions, the relative wind direction tended to be to port of the bow.

In order to remove possible spurious correlations of the imbalance term with either U_{10N} or z/L, the 1074 data obtained with the wind within 10º of the bow were selected for re-analysis. In this range, the mean relative wind directions values show little or no trend with wind speed or stability (Figure 5.6 a and b).

Figure 5.7 shows the u_* to U_{10N} relationships, calculated with the assumption of zero imbalance, for these "bow" data after separating according to stability. The friction velocities are increasingly underestimated with increasingly unstable conditions, as in Figure 5.3 for the entire data set, but the stable data show no deviation from the neutral relationship except at the lowest wind speeds where the anemometer may well have been above the surface layer (Section 2.3.c). As before, a "bulk" u_* to U_{10N} relationship was found, for the "bow" data only, by fitting a third order polynomial to data where $|z/L| < 0.03$. The bulk relationship was then used to obtain U_{10N}, u_{*BULK} and z/L values for all the "bow" data, and the imbalance term, Φ_D, was recalculated using Eqn. (5.1.c) as described above.

5.2.c A simple form of the imbalance term.

Figure 5.8 shows the Φ_D estimates averaged against z/L, after separating into different wind speed ranges. For unstable conditions it appears that, for a given z/L value, Φ_D may increase with wind speed. There is no such wind speed dependence

NOTE: this chapter is superceded by Taylor, P.K. and Yelland, M.J. 2000: On the apparent 'imbalance' term in the turbulent kinetic energy budget, *J. of Atm. and Ocean. Tech.*, 17(1), 82-89

apparent in the stable data: low wind speed data is suspect under these conditions and the data range 0 to 7 m/s should be ignored. As a first approximation, the Φ_D estimates for all data obtained at wind speeds above 7 m/s were fit by a linear regression on z/L which gave;

$$\phi_D = -0.5\frac{z}{L} \qquad z/L \le 0 \qquad (5.3a)$$

$$\phi_D = -1.6\frac{z}{L} \qquad z/L > 0 \qquad (5.3b)$$

This form of the imbalance term was then used in the re-calculation of the u_{*DISS}, U_{10N} and Obukhov length values. The averaged u_{*DISS} to U_{10N} relationships are shown after separation by z/L in Figure 5.9. The stable data at moderate and high wind speeds show no significant dependence on z/L. The discrepancies between the neutral and unstable u_{*DISS} to U_{10N} relationships have been slightly reduced (c.f. Figure 5.7), but are still significant. It was therefore thought that the simple imbalance term of Eqn. (5.3.a) was not adequate, and that a wind speed dependent term should be investigated.

5.2.d A wind speed dependent imbalance term.

It was assumed that the imbalance term could be expressed simply by;

$$\Phi_D = \frac{z}{L} f\{U_{10N}\} \qquad z/L < 0 \qquad (5.4)$$

The form of the U_{10N} function was found by dividing the Φ_D estimates by the corresponding z/L values and averaging the results against U_{10N}. This is shown in Figure 5.10 for all data where $z/L < -0.03$, and again in Figure 5.11 where the data are first separated according to stability. Figure 5.11 shows that the wind speed dependence observed in Figure 5.10 is not due to an unaccounted stability dependence of Φ_D, since all the stability classes, although noisy, show similar behaviour. The dependence of Φ_D on U_{10N} could be described by the linear relationship;

$$\Phi_D = \frac{z}{L}\left(0.8 - \frac{U_{10N}}{6.5}\right) \qquad z/L < 0 \qquad (5.5)$$

NOTE: this chapter is superceded by Taylor, P.K. and Yelland, M.J. 2000: On the apparent 'imbalance' term in the turbulent kinetic energy budget, *J. of Atm. and Ocean. Tech.*, 17(1), 82-89

Figure 5.12 shows the mean relative wind direction for each of the wind speed averages used in Figure 5.10. The very slight trend towards the starboard side of the bow with increasing wind speed would be unlikely to cause a significant change in the magnitude of the airflow disturbance, and would act, if at all, to offset rather than increase the imbalance term.

Figure 5.13 shows the friction velocity to U_{10N} values obtained using the imbalance term of Eqn (5.5). For wind speeds above 10 m/s, the agreement between the neutral and unstable data is now good. However, there is still a significant discrepancy at the lower wind speeds.

The residual imbalance, $\Delta\Phi_D$, was found from;

$$\Delta\Phi_D = \frac{k_V z\varepsilon}{u_{*DISS}^3} - \frac{k_V z\varepsilon}{u_{*BULK}^3} \qquad (5.6)$$

These estimates of $\Delta\Phi_D$, obtained from the data which converged successfully, were divided by their corresponding z/L values and averaged against U_{10N} in Figure 5.14. It can be seen that for all except the strongest winds above 5 m/s, the introduction of the imbalance term of Eqn (5.5) has removed the wind speed dependence. However, at the lower wind speeds the residual imbalance term, $\Delta\Phi_D$, has increased in magnitude compared to the original Φ_D (c.f. Figure 5.10). This is due to the non-convergence of 55 data which required a positive rather than a negative imbalance term for these wind speeds. The individual $\frac{\Phi_D}{z/L}$ estimates from the bulk formula calculation for these cases are also shown on Figure 5.14. Since data above about 9 m/s also suggest an additional positive imbalance term of the order of $-0.3z/L$, the dissipation calculation was repeated using an adjusted imbalance term of the form;

$$\Phi_D = \frac{z}{L}\left(0.5 - \frac{U_{10N}}{6.5}\right) \qquad z/L < 0 \qquad (5.7)$$

which is also a reasonable fit to the imbalance estimates shown in Figure 5.10.

With the inclusion of this form of the imbalance term all except 22 data converged, and the resulting u_* to U_{10N} relationships for the different stability classes are all now in agreement with that for the neutral case (Figure 5.15).

NOTE: this chapter is superceded by Taylor, P.K. and Yelland, M.J. 2000: On the apparent 'imbalance' term in the turbulent kinetic energy budget, *J. of Atm. and Ocean. Tech.*, 17(1), 82-89

In summary, the imbalance term for stable conditions (Eqn 5.3b) was a function of stability only, and would be zero if the constant in the dimensionless profile function Φ_M, originally 5, was replaced by a value of 6.6. For unstable conditions, the wind speed dependent imbalance term given in Eqn (5.7) removes the discrepancy observed between data obtained during non-neutral and neutral conditions, and also greatly reduces the number of data which fail to converge.

5.3 Comparison of imbalance terms.

5.3.a Estimates of the imbalance under neutral conditions.

There have been various estimates of the imbalance term in the TKE budget, the most well known being that of Wyngaard and Cote (1971) who made land based measurements of all the terms in the TKE budget except for the pressure transport term. These authors grouped the pressure transport term and the possible effects of inhomogeneity and non-stationarity (both judged to be small in comparison with the transport term) together as an "imbalance" term, I. The sum of I and the measured turbulent transport gave an imbalance term, Φ_D, of about -0.3 for unstable conditions, i.e. dissipation exceeded production by about 30%. A similar imbalance was found for stable conditions. Lenschow et al. (1980) made aircraft measurements over the ocean and also found dissipation exceeding production by up to 40% at the surface: however, this estimate is an extrapolation of data obtained between 100 and 1000 m.

More recently, the work of Wyngaard and Coté has been re-interpreted by many others using a von Kármán constant of 0.40 rather than the original value of 0.35. Edson et al. (1991) suggested that reinterpretation of the Wyngaard and Coté results was consistent with their HEXMAX result of an excess of dissipation over production of about 12%. On the other hand, Fairall and Edson (1994) analysed the HEXMAX data along with data from RV FLIP and RV Iselin and found that local dissipation was less than production by about 10%. Frenzen and Vogel (1992) used a von Kármán constant of 0.387, and found that their land-based dissipation

measurements suggested that production exceeded dissipation, by about 20%. They too reinterpreted the data of Wyngaard and Coté and found that dissipation was about 16% less than production.

The determination of the imbalance is further complicated by the choice of Kolmogoroff constant. As discussed in Section 2.2.b, the true value of this constant is not well known, and an "effective" value (Deacon, 1988) is sometimes found by comparison of eddy correlation and dissipation data (e.g., Edson et al., 1991). It is thought that the use of this effective value compensates for any imbalance under neutral conditions, but since there is much debate as to both the true and effective values, the implied magnitude and even sign of the imbalance is still not known. For example, a balance between dissipation and production was found, or assumed, by Large (1979), Large and Pond (1981 and 1982) and Anderson (1993) who all used K=0.55 and k_v=0.4. Edson et al (1991) also found a balance using K_{eff}=0.55 and k_v=0.4, although their K_{true} of 0.51 led to the result of an excess of dissipation by 12% mentioned above. A balance was also found by Schacher et al. (1981) using K=.52 and k_v=.35, and Khalsa and Businger (1977) using K=0.50 and k_v=0.4

5.3.b Estimates of the imbalance under non-neutral conditions.

Table 5.1 summarises the imbalance terms found by various researchers from recent experiments over the ocean: only terms obtained under unstable conditions are presented, since these conditions predominate over the ocean and few estimates of the term have been made for stable conditions. It can be seen that the range of wind speed and stability conditions of each study vary widely.

These results are illustrated in Figure 5.16. Where an original Kolmogoroff value of other than 0.55 has been used in obtaining the imbalance, the results have been adjusted using Eqn (2.39) so that a direct comparison can be made.

NOTE: this chapter is superceded by Taylor, P.K. and Yelland, M.J. 2000: On the apparent 'imbalance' term in the turbulent kinetic energy budget, *J. of Atm. and Ocean. Tech.*, 17(1), 82-89

Study (no. of data)	Imbalance term	z/L range	U_{10N} range	value of constants
this study (716 x 10 min.)	$\Phi_D = \frac{z}{L}\left(0.5 - \frac{U_{10N}}{6.5}\right)$	-2 to 0	0 to 26	K = 0.55 k_V=0.40
Yelland and Taylor, 1996 (1660 x 10 min.)	$\phi_D = \frac{z}{L}\left(2 - \frac{U_{10N}}{3}\right)$	-2 to 0	0 to 26	K = 0.55 k_V=0.40
Dupuis et al, 1996 (950 x 13 min.)	$\Phi_D = -0.65\frac{z}{L}$	-8 to 0	3 to 12	K=0.55 k_V=0.40
Edson et al., 1991 (HEXMAX 328 x 50 min.)	$\Phi_D = 0$ (K_{tru}=0.51, $\Phi_D = -0.12$)	-0.3 to 0	< 20	K_{eff}=0.55 k_V=0.40
Fairall and Edson, 1994 (HEXMAX, FLIP + Iselin)	$\phi_D = 0.1\frac{z}{L} + \frac{1}{7 - z/L}$	-10 to 0	not known	K=0.52 k_V=0.40

Table 5.1 Imbalance terms found from various studies over the oceans.

It can be seen that the imbalance term given by Eqn. (5.7) shows a reduced wind speed dependence in comparison with that from the analysis of Yelland and Taylor (1996). As described in Section 5.2.b, the larger wind speed dependence found by YT96 is likely to have been caused by the varying effects of air flow disturbance with relative wind direction. The re-analysis resulted in an imbalance term which is positive, i.e. production exceeds dissipation, for all wind speeds above 3.25 m/s: estimates of the wind stress are not thought reliable for wind speeds much below this (Section 2.2.c).

The results from this study are in agreement with those of Dupuis et al. (1996) for their typical wind speed of around 7 m/s. Although the result of Dupuis et al. confirms that from this study, it should perhaps be viewed with caution. The data used by Dupuis et al. was obtained from two separate cruises of the research

NOTE: this chapter is superceded by Taylor, P.K. and Yelland, M.J. 2000: On the apparent 'imbalance' term in the turbulent kinetic energy budget, *J. of Atm. and Ocean. Tech.*, 17(1), 82-89

ship "Le Suroit": the two cruises produced systematically different wind stress to wind speed relationships (their Figure 9). Friction velocity estimates from the SOFIA cruise were about 5% lower, for a given wind speed, than those from the SEMAPHORE experiment. The two cruise data were treated as one data set for estimating the imbalance term, with no explanation of, or correction for, the disparity between the two. It is possible that the resulting imbalance term was, in part at least, a correction for this disparity rather than an estimate of the imbalance between production and dissipation of TKE.

The imbalance terms from this study, YT96 and Dupuis et al. all resulted from a comparison of non-neutral to (near) neutral data, obtained using the inertial dissipation technique, with an assumed balance between production and dissipation under neutral conditions. In all cases, an effective Kolmogoroff constant of 0.55 was used since this had been found by Large (1979) and Edson et al. (1991) to compensate for any imbalance under neutral conditions.

In contrast, the results from Edson et al. (1991) and Fairall and Edson (1994) were arrived at by comparing data obtained from the inertial dissipation method to eddy-correlation derived data. Despite the fact that both used data from the same experiment, HEXMAX, the results from these two studies differ substantially. However, the latter authors combine this coastal data, obtained from the MPN platform in the southern North Sea, with data obtained from the ships R/V Iselin in the Atlantic and R/V FLIP (effectively a large spar buoy) off the West coast of California. The difference between the imbalance terms from the two studies could either be real, caused by different wind speed or sea state conditions prevailing in the different regions, or spurious, due to the various platforms causing different patterns of air-flow disturbance at the measurement sites, a problem to which the eddy correlation method is particularly sensitive.

The wide range of published estimates of the imbalance term may be partially explained if it does indeed depend on wind speed (or some other wind speed

NOTE: this chapter is superceded by Taylor, P.K. and Yelland, M.J. 2000: On the apparent 'imbalance' term in the turbulent kinetic energy budget, *J. of Atm. and Ocean. Tech.*, 17(1), 82-89

dependent factor, see Section 5.5) as shown in this study, but the published results do not contain enough information to test this. On the other hand, the lack of consensus between different studies may simply be an illustration of the difficulty of making such estimates. A comprehensive study of the TKE budget over the ocean, similar to that of the land-based study of Frenzen and Vogel (1992), would be needed to ascertain the absolute magnitude and form of the imbalance term. Such a study would be extremely difficult to perform since data covering a large range of stabilities and wind speeds would have to be obtained from a platform where flow disturbance was minimised, i.e. preferably from a mast-like spar buoy. Similar conditions would have to be met even for the less direct method of comparing eddy correlation and dissipation data to estimate the imbalance.

5.4 Effect of the imbalance term on the Drag Coefficient data from the Darwin and the Discovery.

Figure 5.17a shows the mean C_{D10N} to U_{10N} relationships obtained from the Discovery data after analysis both with and without the imbalance term of Eqn. (5.7). The results from the Solent sonic anemometer used on Charles Darwin cruise 43 are shown likewise in Figure 5.17b. In both cases, only data obtained with the wind within 10º of the bow was used in the analysis. The relationships suggested by Smith (1980) and YT96 are also shown for comparison.

It can be seen that the application of the imbalance term increased the mean drag coefficient for a given wind speed by about 5 % for the Discovery data. With zero imbalance, the mean relationship was similar to that of Smith (1980), but with a slightly greater wind speed dependence. Application of the imbalance term resulted in a mean relationship which gave drag coefficients which were similar to those of Smith (1980) at moderate wind speeds, but were closer to those of YT96 for wind speeds above 15 m/s. The original drag coefficients from the Darwin were increased by up to 30 % after the imbalance term was included in the re-analysis, since the low wind speed data were all obtained under very unstable conditions. Use of the

NOTE: this chapter is superceded by Taylor, P.K. and Yelland, M.J. 2000: On the apparent 'imbalance' term in the turbulent kinetic energy budget, *J. of Atm. and Ocean. Tech.*, 17(1), 82-89

imbalance term lessens the agreement between the original Discovery results and those of Smith (1980).

The values of the imbalance term for the unstable Discovery data are shown against U_{10N} in Figure 5.18. For all except the lowest wind speeds, the term is positive, implying an excess of production over dissipation. For wind speeds above 12 m/s, production exceeds dissipation by between 5 and 10 % on average, with individual values up to 20%. Between 4 and 12 m/s, there is a wide range of values observed for the imbalance, from zero to 85%. Use of the imbalance term reduced the scatter in the Discovery friction velocity estimates by about 10 % on average. For wind speeds of around 10 m/s, where the range of the imbalance term was largest, the scatter was reduced by 50%.

5.5 Summary

This section described a re-analysis of the Discovery Southern Ocean data used by Yelland and Taylor (1996) in order to estimate the imbalance between local production and dissipation in the turbulent kinetic energy budget, with the assumption of a balance under neutral conditions. A subset of the original data was used in order to minimise the effects of airflow distortion, which vary with relative wind direction (Section 6). Since both wind speed and stability also showed a weak correlation with wind direction it was thought that the stronger wind speed dependence of the imbalance term found by YT96 may have been due in part to the varying effects of the airflow disturbance.

The re-analysis showed no evidence for any wind speed dependence of the dimensionless profiles for stable data, unlike the results of YT96. For slightly stable data, use of a dimensionless profile function of the form;

$$\Phi_M = 1 + 6.6\frac{z}{L} \qquad 0 < z/L < 0.2$$

resulted in a balance between production and dissipation.

For unstable conditions, an imbalance term of the form (Eqn. 5.7);

NOTE: this chapter is superceded by Taylor, P.K. and Yelland, M.J. 2000: On the apparent 'imbalance' term in the turbulent kinetic energy budget, *J. of Atm. and Ocean. Tech.*, 17(1), 82-89

$$\Phi_D = \frac{z}{L}\left(0.5 - \frac{U_{10N}}{6.5}\right) \qquad z/L < 0$$

removed the discrepancy observed between data obtained during non-neutral and neutral conditions, and greatly improved the proportion of low wind speed data which converged successfully. If a balance between production and dissipation is assumed under neutral conditions, then, for unstable conditions, production was found to exceed dissipation by about 10 % on average.

A less empirical formulation of the imbalance term may be obtained if, as described in Section 5.3.b, a more comprehensive study of the TKE budget over the ocean is carried out in the future. At this point, there is no consensus on either the sign or the magnitude of the imbalance between production and dissipation in the TKE budget over the oceans. However, the results from this study are the first to show that the imbalance term may be related to a wind-speed dependent factor. The form of the imbalance term for unstable conditions is not dimensionally correct: it is likely that the imbalance should be expressed as a function of some other non-dimensional wind speed dependent term. Edson (pers. comm. 1997) has recently reported initial results from a experiment on the RV FLIP which seem to show that the imbalance term is a function of sea-state, which is also wind-speed dependent. It was not possible to test this hypothesis due to the very limited wave data available from this study.

NOTE: this chapter is superceded by Taylor, P.K. and Yelland, M.J. 2000: On the apparent 'imbalance' term in the turbulent kinetic energy budget, *J. of Atm. and Ocean. Tech.*, 17(1), 82-89

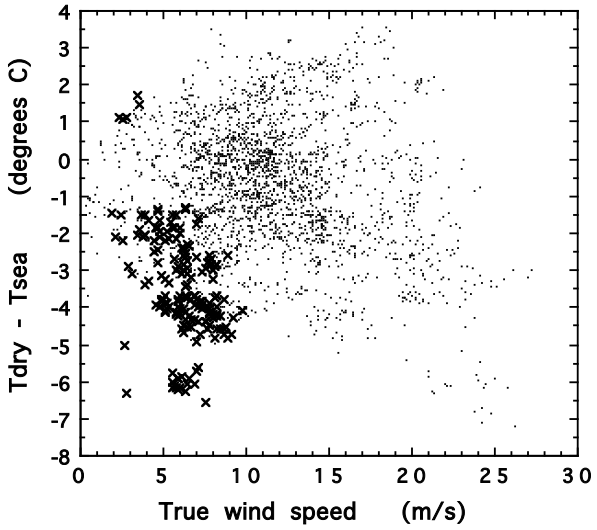

Figure 5.1 The air-sea temperature differences for the Discovery Southern Ocean data. Data which failed to converge during the iterative calculation of the wind stress are indicated by the crosses.

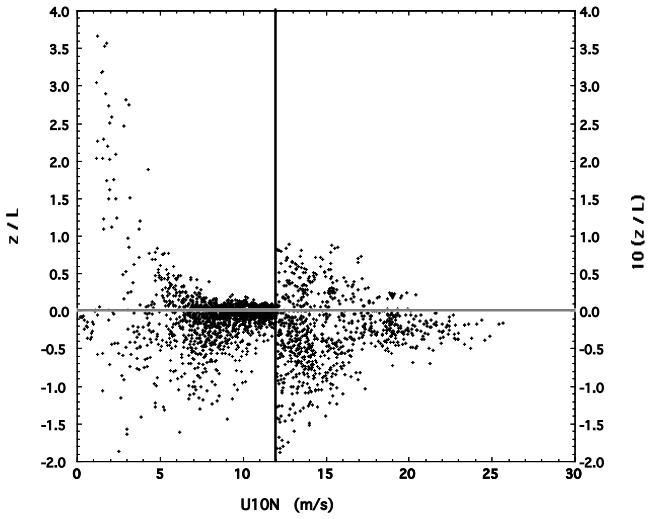

Figure 5.2 The z/L values against U_{10N} obtained with the assumption of a zero imbalance. Note change of the vertical axis scale at 12 m/s.

NOTE: this chapter is superceded by Taylor, P.K. and Yelland, M.J. 2000: On the apparent 'imbalance' term in the turbulent kinetic energy budget, *J. of Atm. and Ocean. Tech.*, 17(1), 82-89

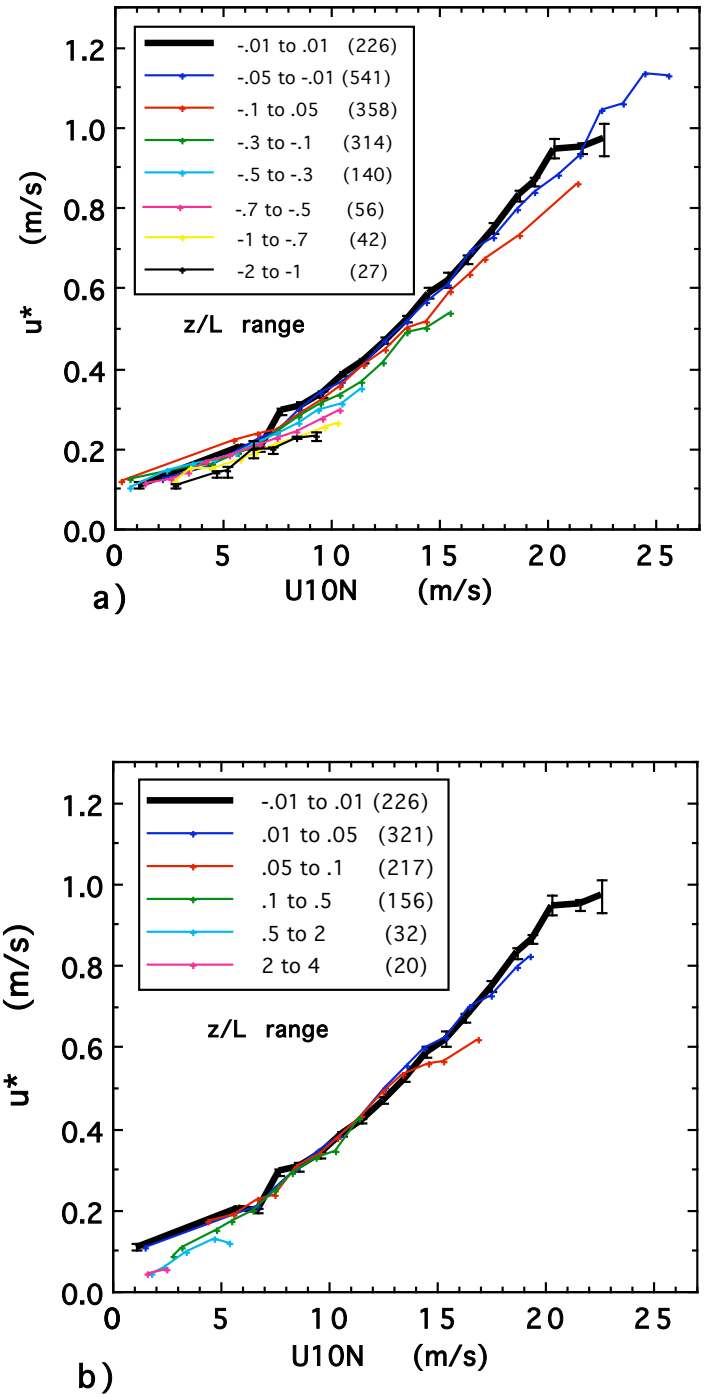

Figure 5.3 Friction velocity estimates, obtained with the assumption of a zero imbalance, averaged on U_{10N} and separated into the stability ranges shown, for a) unstable conditions, and b) stable conditions. The numbers in the brackets give the amount of data in each stability class.

NOTE: this chapter is superceded by Taylor, P.K. and Yelland, M.J. 2000: On the apparent 'imbalance' term in the turbulent kinetic energy budget, *J. of Atm. and Ocean. Tech.*, 17(1), 82-89

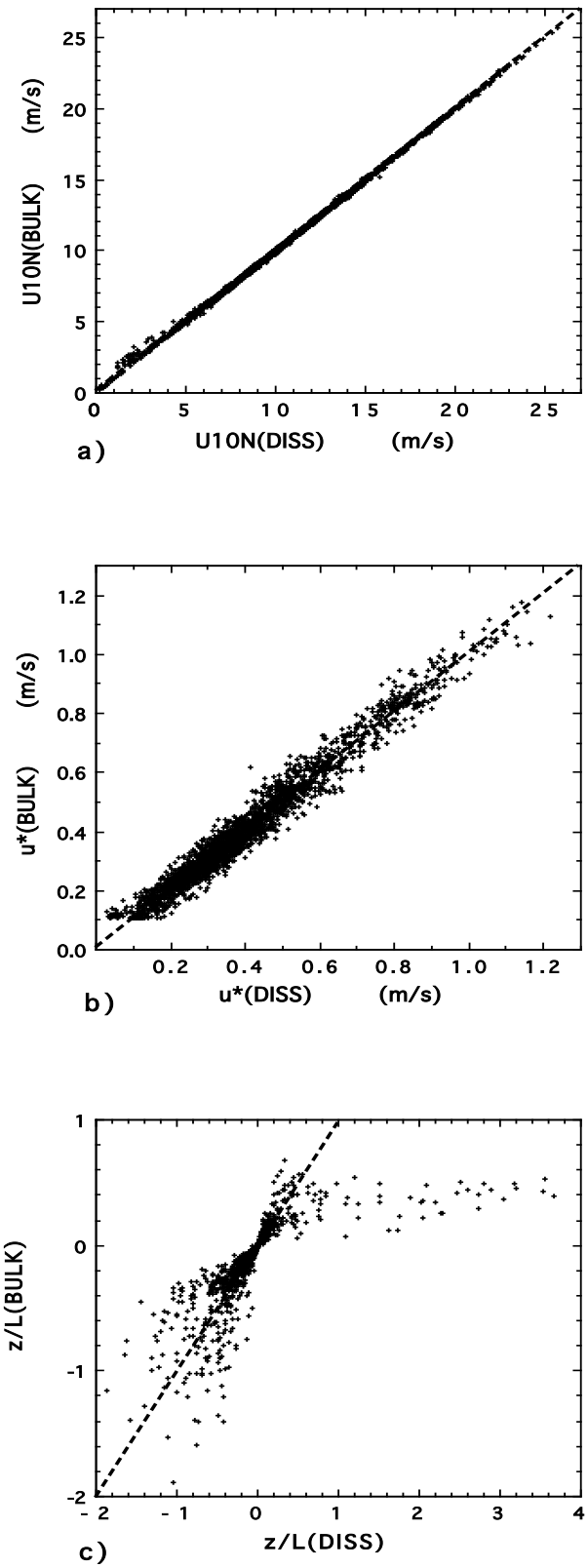

Figure 5.4 Comparison of a) U_{10N}, b) friction velocity, and c) stability estimates obtained using the dissipation (DISS) and bulk (BULK) methods. The dashed lines indicate a 1:1 agreement.

NOTE: this chapter is superceded by Taylor, P.K. and Yelland, M.J. 2000: On the apparent 'imbalance' term in the turbulent kinetic energy budget, *J. of Atm. and Ocean. Tech.*, 17(1), 82-89

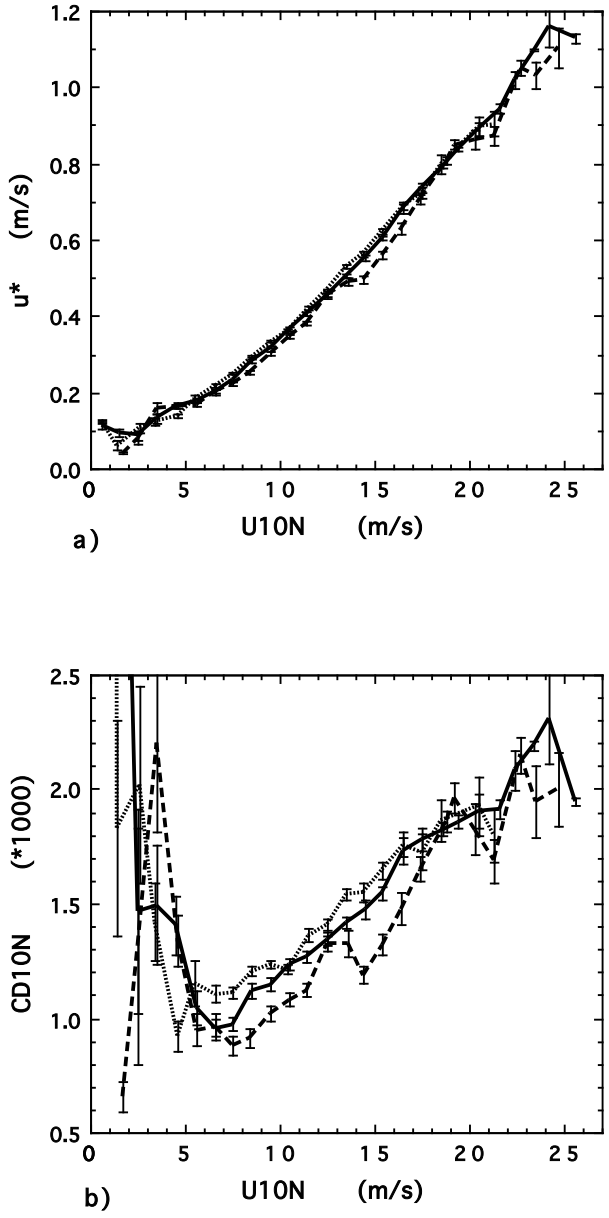

Figure 5.5 a) Friction velocity and b) drag coefficient data, calculated with the assumption of zero imbalance, separated into relative wind direction classes. Data obtained for wind directions between 10° and 30° to port of the bow are shown by the dashed line, the solid line indicates wind directions within 10° of the bow and the dotted line indicates data obtained with the wind 10° to 30° on the starboard bow.

NOTE: this chapter is superceded by Taylor, P.K. and Yelland, M.J. 2000: On the apparent 'imbalance' term in the turbulent kinetic energy budget, *J. of Atm. and Ocean. Tech.*, 17(1), 82-89

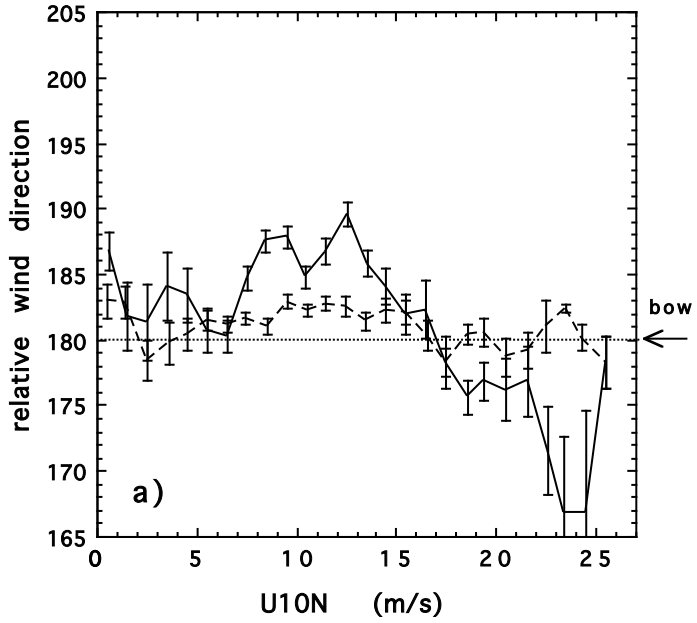

Figure 5.6a Relative wind direction (180° represents wind blowing directly over the bow) against wind speed for all data within 30° of the bow (solid line), and for data within 10° of the bow (dashed).

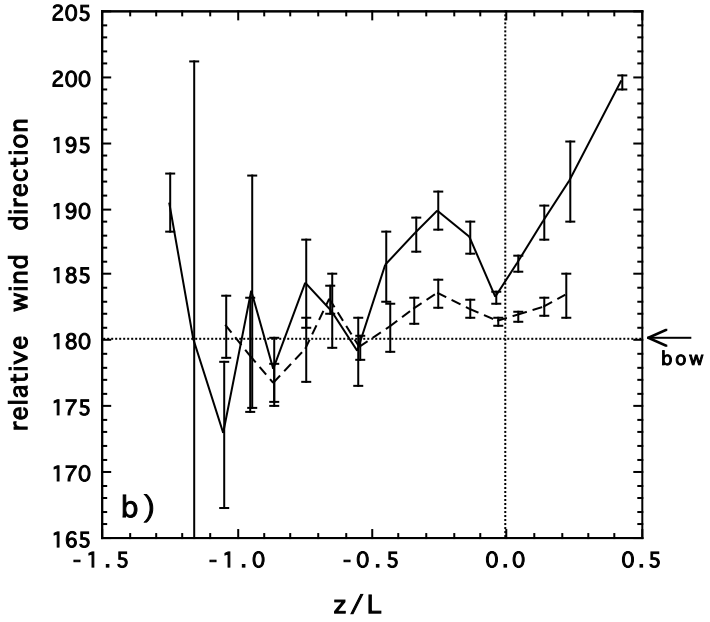

Figure 5.6b Relative wind direction against stability for all data within 30° of the bow (solid line), and for data within 10° of the bow (dashed).

NOTE: this chapter is superceded by Taylor, P.K. and Yelland, M.J. 2000: On the apparent 'imbalance' term in the turbulent kinetic energy budget, *J. of Atm. and Ocean. Tech.*, 17(1), 82-89

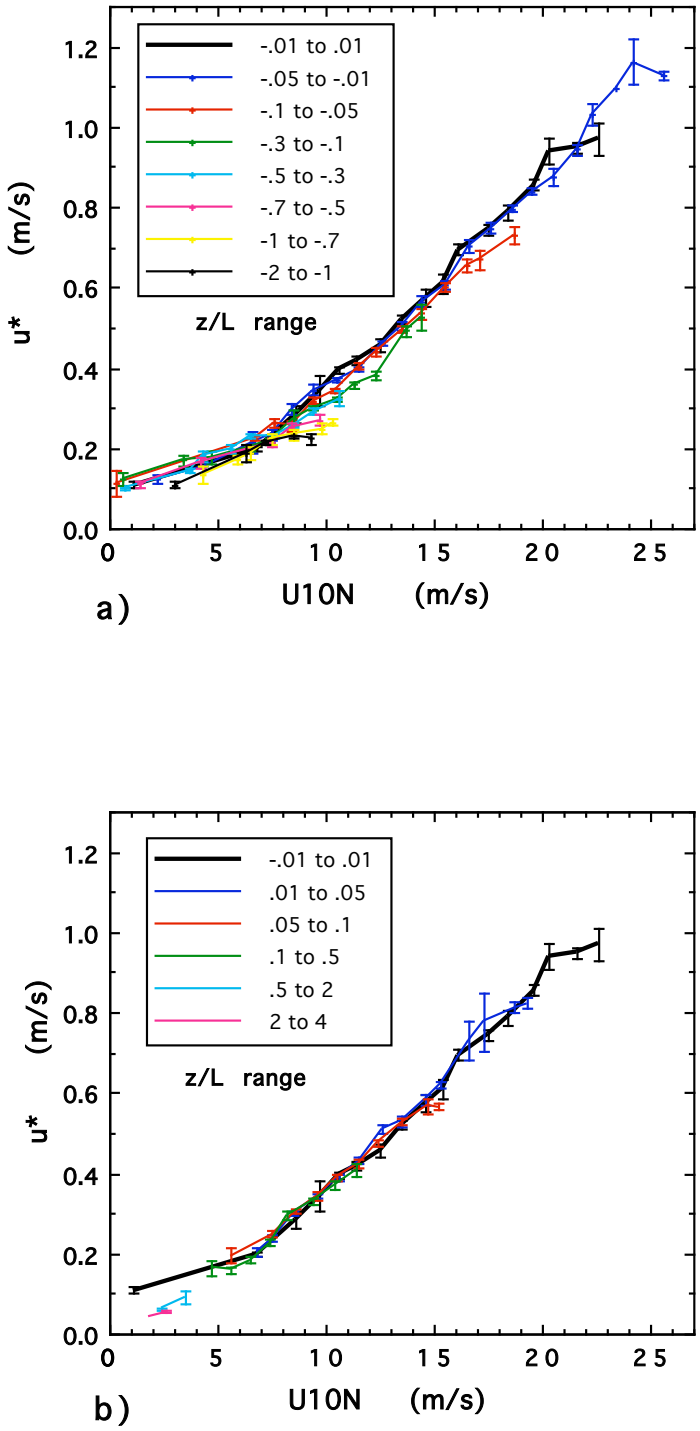

Figure 5.7 As Figure 5.3 but for relative wind directions within 10° of the bow only.

NOTE: this chapter is superceded by Taylor, P.K. and Yelland, M.J. 2000: On the apparent 'imbalance' term in the turbulent kinetic energy budget, *J. of Atm. and Ocean. Tech.*, 17(1), 82-89

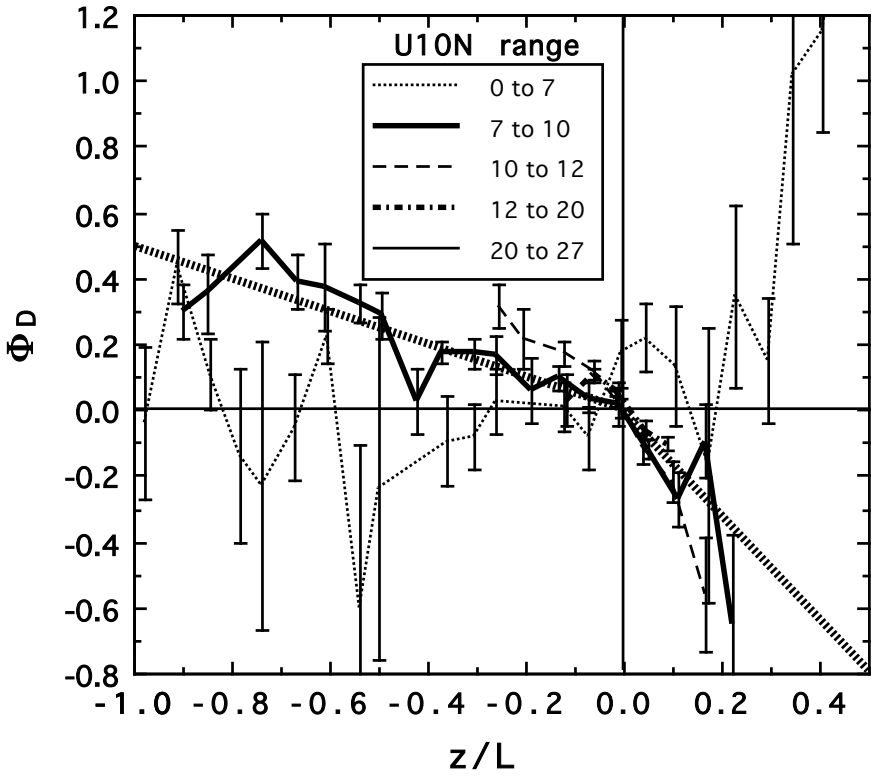

Figure 5.8 Estimates of the imbalance term, Φ_D, against stability for different wind speed classes. The heavy dotted line indicates the fit to all data obtained for wind speeds over 7 m/s.

NOTE: this chapter is superceded by Taylor, P.K. and Yelland, M.J. 2000: On the apparent 'imbalance' term in the turbulent kinetic energy budget, *J. of Atm. and Ocean. Tech.*, 17(1), 82-89

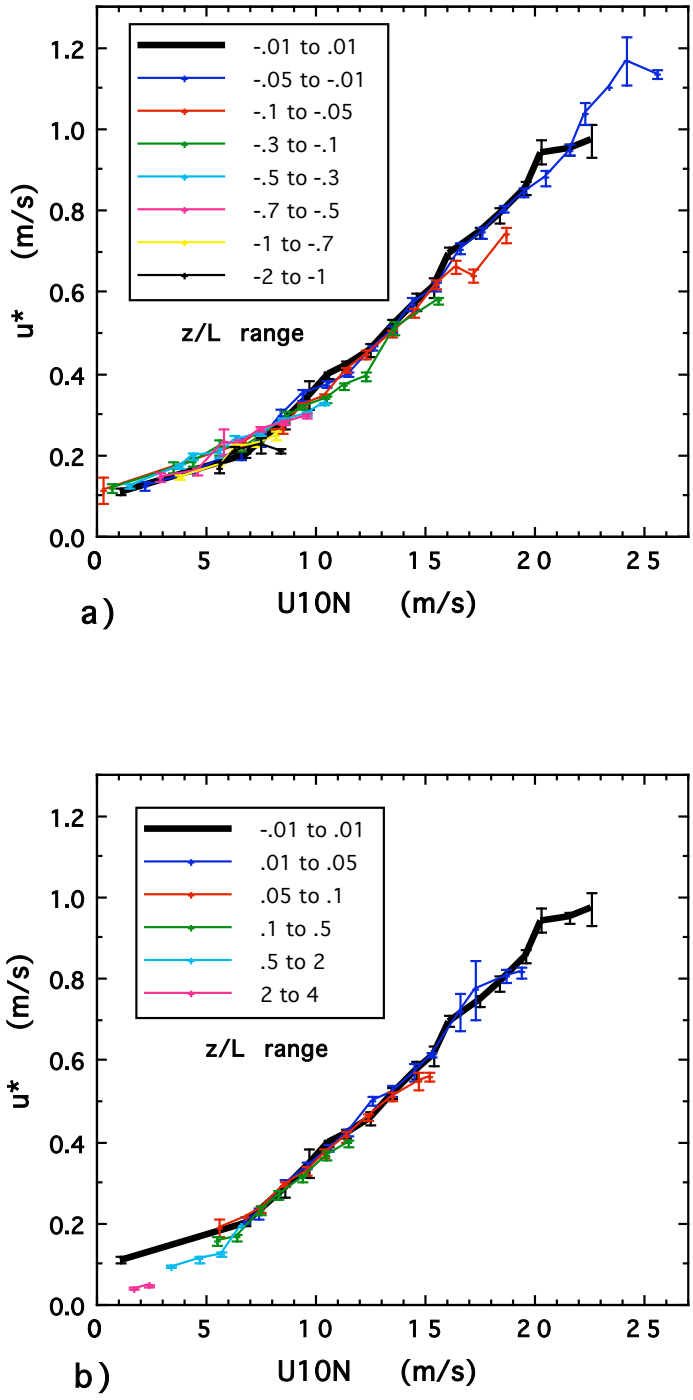

Figure 5.9 Averaged u_{*DISS} to U_{10N} relationships for a) unstable, and b) stable data, after application of the imbalance terms given in Eqn 5.3

NOTE: this chapter is superceded by Taylor, P.K. and Yelland, M.J. 2000: On the apparent 'imbalance' term in the turbulent kinetic energy budget, *J. of Atm. and Ocean. Tech.*, 17(1), 82-89

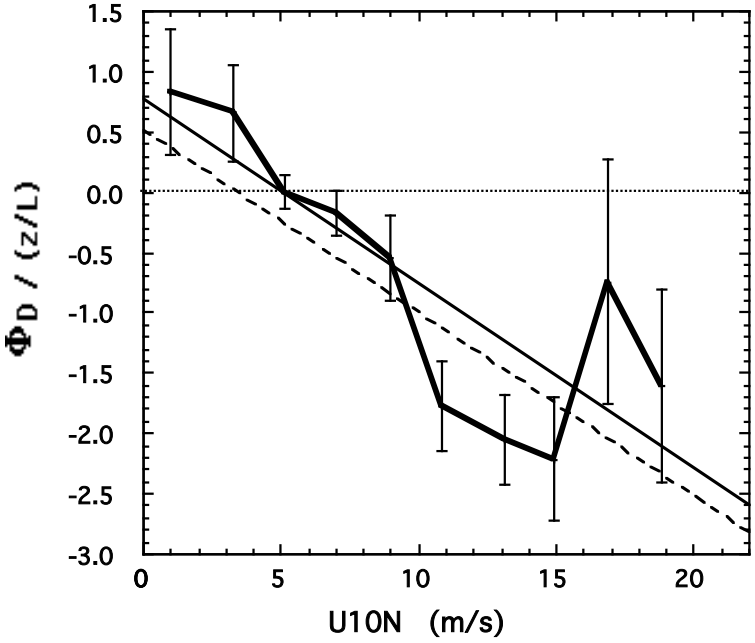

Figure 5.10 $\Phi_D/(z/L)$ against U_{10N} for all data where $z/L < -0.03$. The fit to the averaged data is shown (solid), as is the relationship of Eqn. (5.7) (dashed)

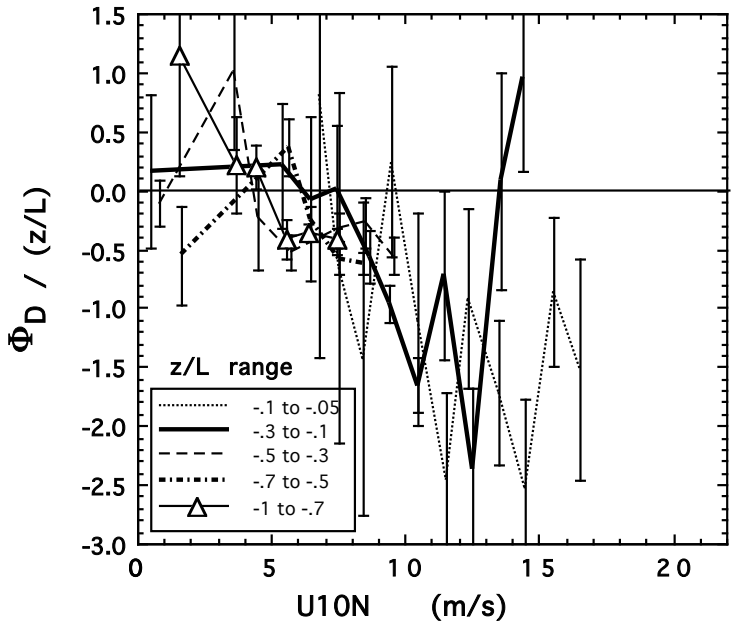

Figure 5.11 As Figure 5.10 but after separation of data into the stability classes shown.

NOTE: this chapter is superceded by Taylor, P.K. and Yelland, M.J. 2000: On the apparent 'imbalance' term in the turbulent kinetic energy budget, *J. of Atm. and Ocean. Tech.*, 17(1), 82-89

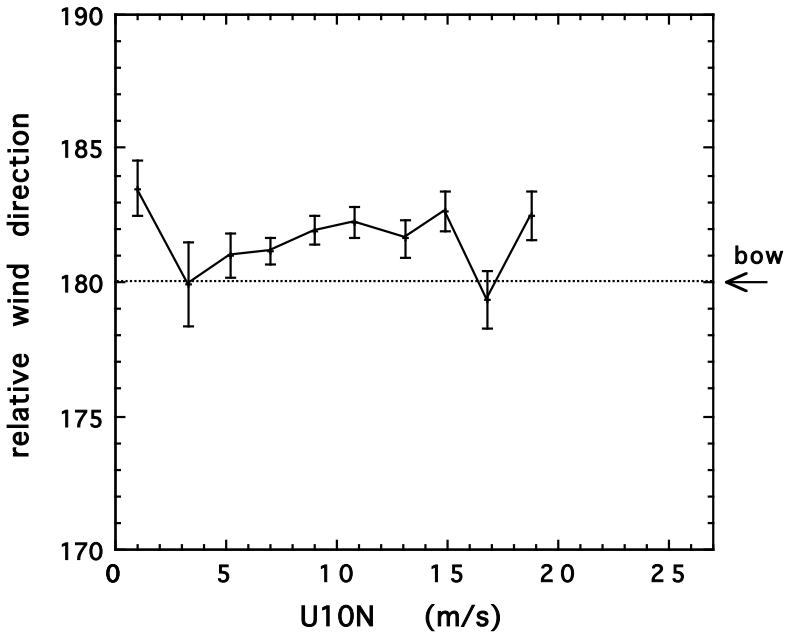

Figure 5.12 The mean relative wind direction for each of the wind speed averages used in Figure 5.10.

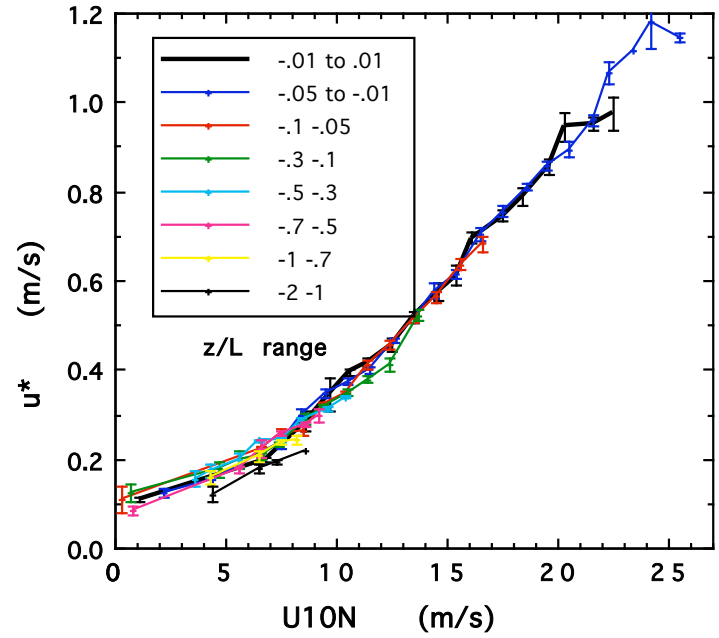

Figure 5.13 The u_* to U_{10N} values obtained using the imbalance term of Eqn (5.5).

NOTE: this chapter is superceded by Taylor, P.K. and Yelland, M.J. 2000: On the apparent 'imbalance' term in the turbulent kinetic energy budget, *J. of Atm. and Ocean. Tech.*, 17(1), 82-89

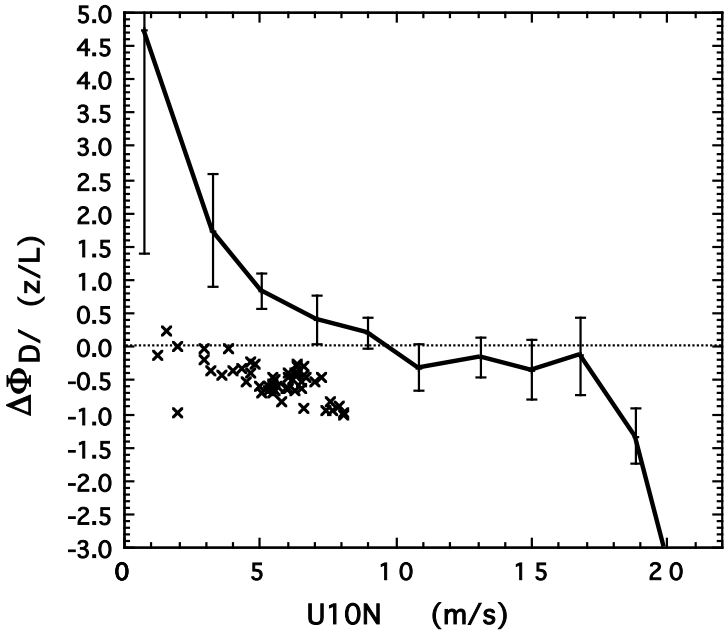

Figure 5.14 Values of $\Delta\Phi_D / (z/L)$ averaged against U_{10N}. For data which failed to converge, the individual bulk estimates of $\frac{\Phi_D}{z/L}$ are shown as crosses.

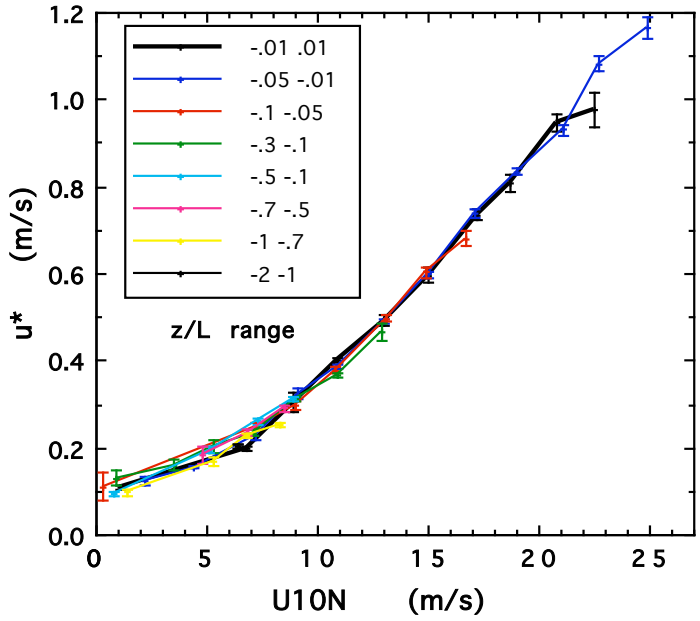

Figure 5.15 Friction velocity to U_{10N} relationships after analysis of the data using the imbalance term of Eqn 5.7.

NOTE: this chapter is superceded by Taylor, P.K. and Yelland, M.J. 2000: On the apparent 'imbalance' term in the turbulent kinetic energy budget, *J. of Atm. and Ocean. Tech.*, 17(1), 82-89

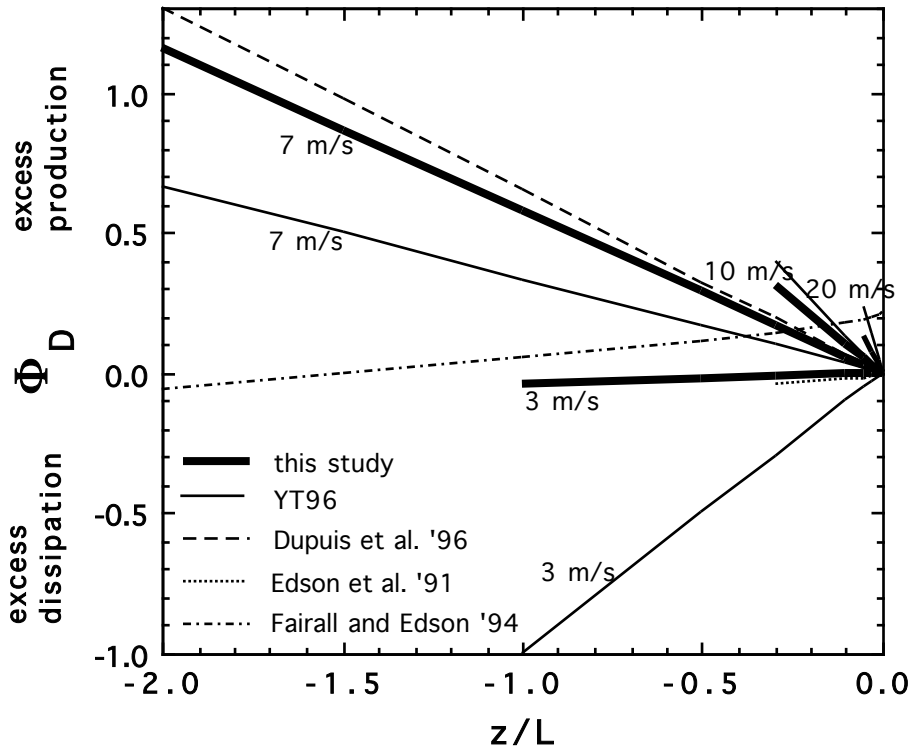

Figure 5.16 Estimated imbalance terms from; this study (thick solid lines), YT96 (thin solid), Dupuis et al. 1996 (dashed), Edson et al. 1991 (dotted) and Fairall and Edson 1994 (chain). The terms from this study and YT96 are shown for four different wind speeds, as indicated on the figure. The Edson et al. and Fairall and Edson terms have been adjusted to a Kolmogoroff value of 0.55.

NOTE: this chapter is superceded by Taylor, P.K. and Yelland, M.J. 2000: On the apparent 'imbalance' term in the turbulent kinetic energy budget, *J. of Atm. and Ocean. Tech.*, 17(1), 82-89

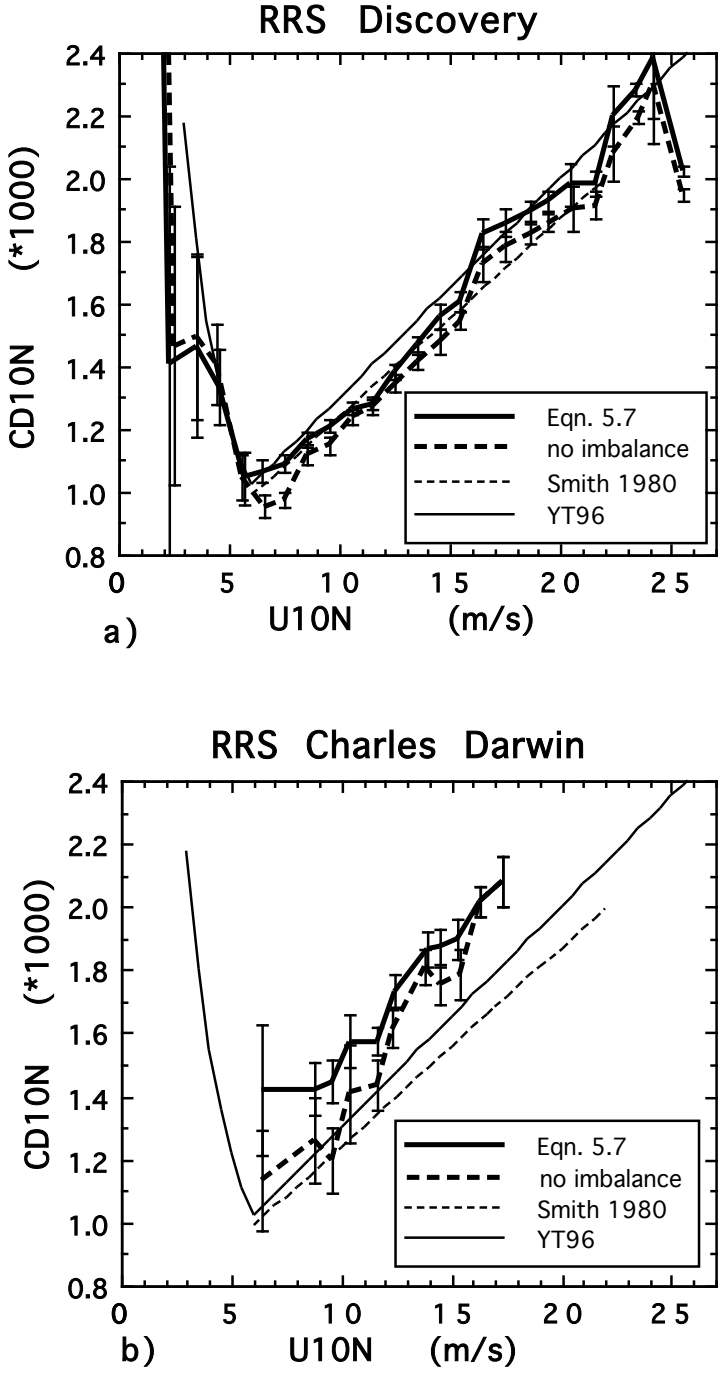

Figure 5.17 Effect of the imbalance term on the mean drag to wind speed relationship for a) the Discovery data, and b) the data from the Solent sonic anemometer on the Darwin. Results obtained with the assumption of a zero imbalance are shown by the thick dashed line, and those obtained using the imbalance term of Eqn. (5.7) are shown by the thick solid line. For comparison, the relationships suggested by Smith (1980) and YT96 are indicated by the thin dashed and thin solid lines respectively.

NOTE: this chapter is superceded by Taylor, P.K. and Yelland, M.J. 2000: On the apparent 'imbalance' term in the turbulent kinetic energy budget, *J. of Atm. and Ocean. Tech.*, 17(1), 82-89

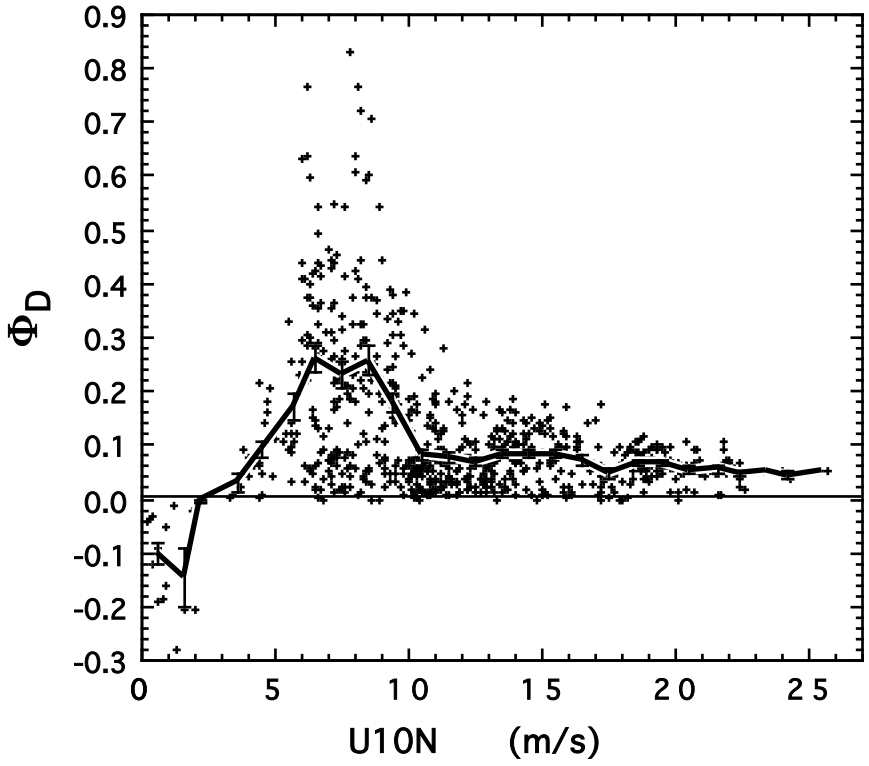

Figure 5.18 Magnitude of the imbalance term for the unstable Discovery data.

6 THE EFFECTS OF AIR FLOW DISTURBANCE ON THE MEASUREMENT OF THE DRAG COEFFICIENT.

6.1 Introduction

Section 5 described the empirical determination of the imbalance between production and dissipation of turbulent kinetic energy. The imbalance term was used in the derivation of drag coefficient estimates from data obtained from the Solent sonic anemometers used during cruises of the Discovery and the Charles Darwin. These results were shown in Figure 5.17: it can be seen that the results from the two ships are significantly different. It was thought that the effects of airflow distortion could be a cause of this difference. This Section investigates the flow distortion around the two ships.

The flow of air to the anemometer can be distorted by a) the sensor itself, b) the local supporting structure such as the mast that the anemometer is mounted on, and c) the larger scale obstruction caused, in this case, by the presence of the ship. In this study, the first of these is corrected for by the instrument calibration which results from wind tunnel tests of the instrument (Section 4.2). This Section discusses the effect of the other causes of flow distortion.

Two possible sources of error in the determination of the drag coefficient lie in the measurement of the true wind speed, U_{true}, and in the estimation of the measurement height, z (Section 2.3.a). Both these sources of error can be caused by the ship's hull, superstructure and foremast presenting an obstruction to the air flow. The flow of air at the anemometer site can have been displaced and/or accelerated (decelerated) compared to its free stream values. As shown in Section 2.3.a, a vertical displacement of the flow affects the calculation of the friction velocity, whereas an error in the U_{true} estimate will mainly affect the calculated U_{10N}. Relatively modest errors in U_{true} or z can have a significant affect on the calculated

C_{D10N}: a 5% underestimate of U_{true} would result in a 12% overestimate of C_{D10N}, and a 5% overestimate of z would cause the calculated C_{D10N} to also be overestimated by 5% (Table 2.1). The two sources of error are unlikely to occur in isolation, and the effects of the two on C_{D10N} can either tend to cancel, or can act in the same sense.

In the past (Section 6.2), there have been few attempts to quantify the acceleration of the flow over ships, and almost no estimates of the vertical displacement. Section 6.3 describes the Computational Fluid Dynamics (CFD) package used in this study to model the flow around ships in three dimensions and hence quantify both errors. Validation of the package is described in Section 6.4, and the results from the modelling of air flow over the RRS Discovery are discussed in Section 6.5.

6.2 Previous estimates of the flow distortion around ships.

6.2.a Estimates of the vertical displacement of the flow.

Tillman et al (1994) used wind tunnel studies and potential flow theory to estimate the vertical displacement of the flow at an anemometer located on a Martian Lander, and used the estimates to correct the friction velocities obtained from wind speed spectra. Large and Pond (1982) speculated on the problem of vertical displacement of the flow over the ships they used, but concluded that the streamlines were displaced horizontally rather than vertically when the flow was over the bows of the ship. It is believed that, to date, there have been no quantitative estimates of the vertical displacement of the air flow reaching the measurement site in any previous study of wind stress over the oceans.

6.2.b Estimates of the acceleration of the flow.

There have been various attempts to estimate the acceleration of the airflow over ships. These have been summarised by Dobson (1981) and Taylor et. al (1995), with particular emphasis on the likely errors implied for wind speed measurements

made from Voluntary Observing Ships (VOS). Dobson described "our abysmal lack of understanding" of the problem, and cited the work of Augstein et. al. (1974) and Kidwell and Seguin (1978). These studies showed that flow distortion effects could cause errors in the wind speed estimate of up to 20% in data obtained from meteorological research vessels; ships which could be supposed to have relatively reliable and well sited instrumentation.

There have, in the past, been three methods used to estimate the error in the wind speed measurement caused by flow distortion: in situ comparisons between data from ships and buoys, or between anemometers located at different sites on the same ship; wind tunnel studies of air flow around model ships; simple potential flow theory or 2-dimensional numerical models of the flow. These will be discussed in turn.

6.2.c In situ comparisons.

In situ comparisons, whether between ships and buoys or between anemometers located at different sites on the same ship, rely on the assumption of a reliable datum. Various researchers have compared data from an anemometer located on the ship's main mast to that from an instrument boomed out from the ship's bow (Ching, 1976; Kidwell and Seguin, 1978; Large and Pond, 1982). However, even when the ship is head to wind the data from the bow boom site are unlikely to be free from the effects of flow distortion, since these can still be significant upstream of the ship and will also vary with relative wind direction (Sections 6.2.d and 6.4.b). Data from buoy mounted anemometers should be less affected by flow distortion, but obtaining reliable wind speeds from buoys has proved difficult. For example; during the GATE experiment (Godshall et al., 1976), the results varied from one intercomparison of ship and buoy data to another; Weller et al. (1990) examined wind speed data from an array of meteorological buoys and concluded that it was less reliable than that from the research ship Meteor; and Queffeulou (1991) suggested

that wind speed data from ship mounted instruments was needed to calibrate wind speed data from an array of buoys.

Although in situ comparisons can provide useful information about the relative wind speed errors at different anemometer sites, no estimate can be made of the absolute magnitude of the wind speed errors, nor of the vertical displacement of the flow.

6.2.d Wind tunnel studies.

Wind tunnel studies of the air flow around ships have been described by, for example, Romanov et al. (1983), Blanc (1986, 1987), Surrey et al. (1989) and Thiebaux (1990). The latter two were studies of two Canadian research ships, and will be used below as part of the evaluation of the CFD software used in this study. Romanov et al. also studied a research ship, and found, for wind over the bows of the ship, wind speed errors of +1% at a mainmast site, -3% at the foremast and -5% at the anemometer location at the end of a boom in the ship's bows. For wind on the beam of the ship, the errors were +5%, +10% and +2% respectively. Blanc studied the flow around two warships: in both cases, the wind speed was overestimated by about 10% at a main mast site for flow over the bows. No estimate of the vertical displacement of the flow was made in these studies.

Wind tunnel studies rely on the assumption that self-similarity holds at large Reynolds numbers, i.e. that the ratio of the velocities at two points, the anemometer site and some free stream site say, will be the same for the ship as for the ship model. Romanov et al. suggest the critical Reynolds number, R_e, for ships should be in the region of 5×10^5, where;

$$R_e = \frac{UL}{\upsilon} \qquad (6.1)$$

L represents the model or ship length, U is the wind speed and υ is the kinematic viscosity of air. Self-similarity may not hold for the smaller-scale features of a model, such as the ship's masts (Thiebaux, 1990), since there are practical limits to the

maximum wind speed that can be obtained in a wind tunnel, or withstood by a model. The results from wind tunnel studies can also be affected by the ship blocking the flow through the tunnel, causing the flow in the vicinity of the ship to be accelerated, and by other experimental errors such as anemometer inaccuracies.

Although such wind tunnel studies can give estimates of the wind speed error for many different relative wind directions, the tests are very time consuming and can be prohibitively expensive. Access to a suitably large wind tunnel, capable of simulating a surface layer flow, is also not always easily available. Because of these difficulties, very few research ships have been studied in wind tunnels.

6.2.e Numerical Modelling

The flow around ships has been examined by, for example, Kahma and Lepparanta (1981) who used potential flow models, and by Dupuis, 1994) who used a CFD model. Both studies were of research ships: the former found an overestimate of the wind speed of 15% for a main mast site, and the latter 20%. Very simple 2-dimensional models were used in both cases, and only flow directly over the bows of the ship was studied. A 2-dimensional model effectively simulates flow over an infinitely wide ship, hence the effects of flow distortion may have been overestimated due to the displacement of the streamlines being constrained solely to the vertical.

Potential flow models, which assume the fluid to be inviscid and irrotational, have been used in the past to estimate the flow distortion around simple shapes such as a cylindrical mast (Wucknitz, 1980). The results of such studies have often been applied to land based wind stress measurements where the instruments are supported on a structure which can be represented by such an idealised shape (e.g. Wieringa, 1980). More sophisticated models have been used by Wyngaard (1981) and Oost (1991) in order to estimate the distortion around more complex geometries. However, Oost et al (1994) concludes that none of the potential flow methods he examined (including that of Wyngaard (1981)) was suitable for simulating the distortion caused by large objects such as ships which are of a comparable scale to the measurement

height, i.e. where the scale of the turbulence is not large compared to the scale of the object.

CFD models should produce a more realistic simulation of fluid flow compared to potential flow theory, since turbulence is included by parameterisation and the flow is allowed to be both viscous and compressible. However, the use of CFD models has been limited in the past because they are computationally very expensive compared to simpler numerical methods.

6.3 The CFD software "VECTIS".

A CFD software package, "VECTIS", was used in this study to model the distortion of the air flow over research ships. It is believed to be the first such use of a fully 3-dimensional modelling package. VECTIS is a commercially available finite volume model, produced by Ricardo Consulting Engineers Ltd. (Shoreham-by-Sea, U.K.), and was designed to model flow inside automobile engines. Following our suggestions, Ricardo adapted the software to improve the simulation of surface layer flows. These changes allowed the user to specify 1) the roughness length of a surface and 2) the shape of the vertical wind profile at the inlet.

The behaviour of the fluid flow is calculated in VECTIS by solving the Navier-Stokes equations for the fluid motion and the equations for the conservation of mass and energy. Turbulence closure is obtained by a standard two-equation k-ε model (see Garratt, 1992 and Stull,1988). In this, covariance terms are represented by eddy diffusivities, which are themselves parameterised in terms of the TKE (k). Two separate transport equations are solved for the TKE and for the dissipation rate (ε). These equations involve the use of five empirically determined "constants": the values used in the VECTIS software are those recommended by Launder and Spalding (1974). Some of the constants have been determined by measurement, but others are not know and are sometimes selected by comparing model results with laboratory data (Detering and Etling, 1985). The accuracy of the CFD results will be affected, to

some degree, by the validity of the parameterisations used. However, the largest source of error is likely to be in the complexity of the ship geometry. In this study, validation of the software was performed by comparison with results from a wind tunnel study and results from in situ data.

The use of the software is described by Moat et al. (1996), and is summarised here. A finite element surface geometry of the ship was created from digitised 1:100 scale general arrangement ship plans using the finite element pre-processor "FEMGEN" (produced by Femsys, Leicester, U.K.). This geometry was enclosed in the centre of a "wind tunnel" 600 m long, 300 m wide and 150 m high (compared to maximum ship dimensions of 100 m length, 15 m breadth and 20 m height), and imported into the VECTIS CFD software. The models discussed below all simulate an air flow directly over the bows of the ships.

The software allows a variable density of cells within the computational volume. The density of cells in each region of the wind tunnel is specified by the user, and the mesh is then generated automatically. This allowed regions of interest to be well resolved without creating an unfeasibly large number of computational cells. A typical model in this study would contain in the region of 2×10^5 cells, the smallest of which were located in the region of the foremast platform and were about 20 cm on a side. In comparison, the largest were a few metres long and were located well aft of the ship.

The type of each surface was also specified. The walls and ceiling of the wind tunnel were "zero gradient" boundaries (i.e. symmetry planes), and the floor of the tunnel was a "wall boundary" with a roughness length of 10^{-4} m. The speed of the air flow at all heights at the inlet of the tunnel was specified: a logarithmic surface profile of the sort given by Eqn. 2.22 was generally used.

Preparation of the models took upwards of two weeks. The computational phase took two to three weeks to run on a dedicated Silicon Graphics Indigo^2 R8000 machine with 288 Mb of memory before converging on a steady solution. During the

computational period, data were extracted from about eight locations in the tunnel: near the inlet and outlet and at different points around the ship structure. When velocity data from all of these monitoring points had become constant to within 0.05 m/s for a few tens of iterations, the model was halted and the last iteration was used to extract the results. After each model run, the flow at the edges of the tunnel was examined to ensure that free stream conditions existed, i.e. that the tunnel was large enough for the ship not to cause a significant blockage to the flow.

The vertical displacement of the flow, Δz, from its free stream height, z_f, was found by tracing the streamline which intersected the anemometer site back to the tunnel inlet. The percentage wind speed error at the anemometer site was obtained from;

$$\Delta U = \left(\frac{U_z}{U_f} - 1\right) 100 \qquad (6.2)$$

where U_z is the wind speed at the anemometer site and U_f is the free stream wind speed at height z_f. Since the shape of the vertical wind profile changed slightly along the length of the tunnel for some of the model runs (causing a difference between the 10 m wind speed at the inlet and at the outlet of less than 1%), the free stream wind speed was always obtained using data from the edge of the tunnel, directly abeam of the anemometer site.

In the calculation of the friction velocity from the cruise data, z_f was substituted for the measurement height, z (Eqn. 2.13). To obtain the true wind speed (Eqn. 2.21), U_{true}, the wind speed measured by the anemometer, U_{rel}, was corrected for the wind speed error before allowing for the speed of the ship.

6.4 Validation of the CFD software.

6.4.a Comparison with wind tunnel studies.

VECTIS was initially evaluated by modelling the flow over two Canadian research ships, the CSS Hudson and the CSS Dawson, and comparing the results to

those from wind tunnel studies of the same ships carried out by Surrey et al. (1989) and described by Thiebaux (1990). The wind tunnel study did not include any estimates of the vertical displacement of the flow, hence only the wind speed errors could be directly compared.

Both ships were modelled using the CFD software for a bow-on flow (Hutchings et al, 1995). The model wind velocity at a height of 10 m was 13 m/s, compared to the wind tunnel scale velocity equivalent to a U_{10N} of 27.2 m/s for the Hudson and 15.7 m/s for the Dawson. For both ships, Surrey et al. measured the wind speed error at the main mast anemometer site and at a site in the ship's bows for all relative wind directions at intervals of 10 degrees. These results, reproduced from the tables given in Thiebaux, are shown in Figure 6.1 along with the CFD results: a negative wind speed error implies that the flow has been decelerated compared to the free stream value. The agreement between the wind tunnel and CFD errors is excellent for the main mast Hudson site and for the Dawson bow site. For the Dawson main mast site, the wind tunnel study suggest that the flow has been accelerated by 7% whereas the CFD results suggest an acceleration of 5.5%. Given estimated errors in the wind tunnel results of 1% due to tunnel blockage and a possible 1.5% anemometer inaccuracy, the discrepancy between the wind tunnel and CFD results is not significant. The difference between wind tunnel and CFD results is rather larger for the Hudson bow anemometer site; the two methods give wind speed errors of -1% and -3.3% respectively. However, it seems that in this case the wind tunnel result may be suspect since there is no obvious cause for the relatively large change in wind speed error with relative wind direction (up to 3% for a 10º change). If this is so, then the wind tunnel results from both ships imply that one bow-on wind speed correction could be used for winds blowing within about 20 degrees of the bow. For other wind directions, significantly different and more rapidly varying correction factors would be needed.

As mentioned above, the wind tunnel studies gave no estimate of the vertical displacement of the flow. However, the estimates of the displacement obtained from

the CFD modelling are partially supported by wind stress data obtained from the two ships. Compared to the Dawson, the superstructure of the Hudson is situated much closer to the bows of the ship and presents a more abrupt blockage to the flow of air (Figure 6.2). This causes a larger vertical displacement of the flow at the bow anemometer site: for the Dawson, the flow is displaced by 0.4 m, whereas the flow over the Hudson has been displaced by 1.1 m. Dobson et al. (1994; 1995) presented drag coefficient results from the Hudson which were about 10 to 30% greater than those obtained on the Dawson by Anderson (1993): both data were obtained using the bow anemometer sites. The difference in wind speed errors for the two ships would suggest that the Hudson drag coefficients should be 5 to 15% larger than those from the Dawson, but the 0.7 m difference in the vertical displacements (nearly 5% of the measurement height) would explain an additional 5% of the observed difference. An exact analysis can not be made using the observational results since they were obtained over a large range of relative wind directions: Dobson et al. accepted data within 60º degrees of the bow and Anderson accepted data within 45º.

This initial evaluation of the CFD software was encouraging. Further confirmation of the software was provided by modelling the airflow over the RRS Charles Darwin.

6.4.b The drag coefficient estimates from RRS Charles Darwin cruise 43.

The measurement program and data processing for Darwin cruise 43 have been described in Sections 4. Wind stress estimates were obtained from each of four fast-response anemometers, all located on the foremast platform. Yelland et al. (1994) described in detail the intercomparison of the data from these instruments. However, their analysis assumed a balance between dissipation and production of turbulent kinetic energy. In this study, the data have been reprocessed using the empirical imbalance term determined in Section 5 (Eqn. 5.7), with a resulting increase of the calculated drag coefficients of around 10% on average. Yelland et al. (1994) accepted data where the wind was blowing within 30 degrees of the bows, whereas the wind

tunnel studies of the Hudson and Dawson discussed above suggest that a limit of 20º or less would be more suitable. This is confirmed by the Discovery results discussed in Section 5.2.b, where significantly different mean C_{D10N} to U_{10N} relationships are found for relative wind directions 10º to 30º to port of the bow, ±10º of the bow and 10º to 30º to starboard of the bow. In this analysis, a limit of ±10º has been chosen since the orientation of the anemometers along the centre line of the ship can not be performed to better than about 5º. This criteria reduced the number of concurrent 20 minute stress estimates to 73 from each anemometer.

Figure 6.3 shows the mean drag coefficient to U_{10N} relationships for each of the anemometers after the data were re-processed. It can be seen that, at the lowest wind speeds (about 6 m/s), the drag coefficients from the two sonic anemometers (Solent and Kaijo-Denki) differ by about 5%. This differences increases to 30% at high wind speeds. There is a similar pattern to the comparison of the propeller anemometers (the Bivane and the Young propeller-vane): at low wind speeds the two give similar C_{D10n} values which are both about 20% greater than those from the sonic anemometers. Except for the lower wind speeds, the Young propeller-vane measurements produced C_{D10N} values about 15% larger for a given wind speed than those from the Bivane anemometer. As a reference level, the relationship suggested by the open ocean data of Smith (1980) is also shown: in comparison, the drag coefficients from the Darwin anemometers are between 15% and 60% high.

The differences between the friction velocity data from the four Darwin anemometers is shown in Figure 6.4.a, expressed as a percentage difference from the values from the Solent sonic anemometer. It can be seen that the data from the Kaijo-Denki results in u_* values which are 5% larger than those from the Solent over most of the wind speed range. In contrast, the values from the two propeller anemometers agree reasonably well with those from the Solent for the higher wind speeds. At lower wind speeds, the propeller anemometer results are also greater than those from the Solent sonic. However, Yelland et al. (1994) indicated that the elevated friction velocities from the two propeller instruments at low wind speeds was probably due

to an over-correction of the propeller response (Section 4.4). If this is so, then the friction velocity estimates from the Kaijo-Denki would seem to be anomalous.

The difference in U_{10N} estimates from the four anemometers was rather more marked than the differences in friction velocities (Figure 6.4.b). Compared to those from the Solent sonic, the results from the Young were between 5 and 10 % low, those from the Bivane were in agreement to within 3% , and those of the Kaijo-Denki sonic were low by about 3% at low winds and up to 7% at the higher wind speeds. Since the Bivane and the Solent sonic were the two best exposed instruments, being situated furthest away from the foremast extension (Section 4, Figure 4.6), Yelland et al. (1994) concluded that the data from these two anemometers were the more reliable and that the other instruments were more affected by air flow distortion.

It is likely that the difference in the results from the four instruments is due, in the main, to the effects of flow distortion, since anemometer calibration errors would affect the u_* and U_{10N} estimates in the same sense. For example, if the U_{10N} estimates from the Kaijo-Denki were low by around 5% on average because of a large calibration error, then the friction velocity should also be low, by around 3.5%, whereas the comparison in Figure 6.4.a shows the u_* values from the Kaijo-Denki to be high by around 5%. In addition, such a calibration error would result in an overestimate of C_{D10N}, from the C_{D10N} to U_{10N} relationship, of between 6 to 7% rather than the 5 to 30% over-estimate observed in Figure 6.3. A similar argument can be used for the Young propeller-vane results. The disparities in the data from the four instruments allow a test of the ability of the CFD software to provide corrections for the effects of airflow distortion.

6.4.c Modelling the airflow distortion over the RRS Charles Darwin.

A model of the Charles Darwin was created as described above (Section 6.3), and the CFD software was used to simulate a flow of air directly over the bows of the ship, with a wind speed of 13.7 m/s at a height of 10 m. A full description of the model run is given in Moat and Yelland (1996a). The flow at the edge of the tunnel

abeam of the centre of the ship had been accelerated by less than 0.2% at a height of 15 m: abeam of the foremast platform, the acceleration was about 0.05% at the same height. These results confirmed that the presence of the ship in the wind tunnel caused insignificant blockage to the flow of air at the edges of the tunnel, i.e. that free stream conditions existed abeam of the ship.

Figure 6.5 shows model data on a vertical plane which intersects the site of the Solent sonic anemometer. The length and shading of the arrows represent the ratio between the wind speed at that point and the free stream value, i.e. the wind speed at that point undistorted by the presence of the ship. The direction of the arrow indicates the direction of the flow over the ship. Ratios greater than one represent an acceleration of the flow. The values from each computational cell are represented by a separate arrow: the greater mesh density around the foremast is clearly visible.

The superstructure of the ship forms an abrupt blockage relatively close to the foremast. The region of severely decelerated air in front of the superstructure extends forwards to the foremast platform and causes large wind speed errors at the anemometer sites. Also visible is a region of decelerated flow in front of and above the bows of the ship, caused by both the ship's hull and by the extended area of blocked flow in front of the superstructure. This region would encompass an anemometer mounted on a boom extending forwards from the bows.

To estimate the vertical displacement of the flow reaching the anemometers, streamlines were traced from the inlet of the tunnel to the anemometer sites. The flow was displaced from its free stream height of 14.0 m by almost 1.2 m by the time it had reached the site of the Solent sonic. The displacement began 40 m (or 2.9 seconds) upstream of the site, but half of the displacement took place within 8 m (0.6 seconds) of the anemometer (Section 2.3.a). Similar streamlines were obtained for the other anemometer sites: for the two propeller anemometers the displacement was also found to be about 1.2 m, and at the lower Kaijo-Denki site the flow had been displaced by about 1.0 m.

Anemometer	Height (m)	ΔU (%)	Δz (m)	γ (°)
Solent sonic	15.1	-3.5 $\pm$ 1	1.2	6
Propeller-vane	15.6	-8 $\pm$ 5	1.2	9
Bivane	15.7	-6 $\pm$ 1.5	1.2	8
Kaijo-Denki	14.3	-12 $\pm$ 3	1.0	7

Table 6.1. CFD model results for the Charles Darwin. Wind speed errors, ΔU, vertical displacement of air flow, Δz, and the angle of the flow to the horizontal, γ, at the anemometer sites on cruise 43.

The acceleration of the flow at all four sites was found as described in Section 6.3. The angle of the flow to the horizontal at each anemometer site was also calculated. The results are summarised in Table 6.1. The accuracy of the wind speed error was determined by assuming a positional error of 0.5 m. Although the anemometer sites are known to within about 10 or 20 cm, the 0.5 m estimate was used to allow for additional errors due, for example, to possible inaccuracies in the modelling of the foremast platform. The Young propeller vane and the Kaijo-Denki sonic anemometers were both sited in regions where the wind speed errors were relatively large and varied quite rapidly with position. The gradient of the error at the Kaijo-Denki anemometer site was greatest in the vertical direction, whereas at the site of the Young anemometer the gradient was largest in the horizontal. As expected, the errors at the Solent sonic and Bivane sites were smaller and had smaller gradients. The vertical displacement can generally be obtained to within less than 5 cm and is relatively insensitive to errors in the anemometer position, as illustrated by the similarity in the displacements found at the four anemometer sites.

6.4.d The Charles Darwin drag coefficients, corrected for flow distortion effects.

The results from the CFD modelling were applied to the Darwin data selected for relative wind directions within 10 degrees of the bow. The precise vertical

alignment of the anemometers is difficult to determine but the wind speed components obtained from the Solent sonic suggested a tilt to the vertical of 7 degrees, which is in good agreement with the 6 degree angle obtained from the model. Although the Kaijo-Denki sonic also measured all three components of wind speed, these were not available and no comparison of the tilt estimates could be made. The Bivane anemometer oriented itself into the mean wind and would be unaffected by a non-zero vertical component of the mean wind, but the propeller vane instrument only measured the horizontal component. A cosine response was assumed for this latter anemometer and the data were corrected by an additional 1% to allow for the possible 9 degree angle of the mean flow with the vertical.

The data from the four anemometers were corrected for flow distortion using the information in Table 6.1, and new u_*, U_{10N} and C_{D10N} estimates were obtained. Figures 6.6.a and b illustrate the direct comparison of the estimates of the friction velocity and U_{10N} between the four Darwin anemometers (c.f. Figure 6.4). As expected, the ratios of the friction velocity estimates are virtually unchanged since the vertical displacements were similar at all four anemometer sites. The friction velocity values from each instrument were reduced by about 2%.

The U_{10N} comparisons show that the large discrepancy in wind speeds between the Young and the Solent sonic anemometers has been removed by the application of the flow distortion corrections. The corrected U_{10N} data from the Bivane is now a few percent high in comparison to the Solent sonic, and that from the Kaijo-Denki is now also high, by around 5%. At first sight, the corrections to the Bivane data appear to have slightly worsened the agreement with the data from the Solent, and the Kaijo-Denki wind speed data appear to have been vastly over-corrected. However, the results are now compatible with possible differences in anemometer calibration. When the ratios of corrected U_{10N} values are compared to the u_* ratios, it can be seen that the differences between the results from each anemometer could now be caused by errors in instrument calibration, i.e. both the u_* and U_{10N} values from the Bivane are high by a few percent, and both the u_* and U_{10N}

estimates from the Kaijo-Denki are high by about 5%. Given that the anemometers specifications claim an accuracy of 2% or better, this could account for most of the differences in wind speed estimates. However, as shown in Section 2.3.a, a calibration error should affect the U_{10N} estimate slightly more than the u_* estimate: for example, a calibration offset of -2.5% should results in a U_{10N} error of -2.5%, but would cause a friction velocity error of around -1.7%. Hence either the friction velocity estimates from the Bivane and Kaijo-Denki have been slightly over-corrected for flow distortion in comparison with those from the Young and the Solent, or the wind speeds have been slightly under-corrected. Since the vertical displacement of the flow was very similar for all four instruments, and was relatively insensitive to the exact position of the instruments, it seems probable that the estimate of the wind speed errors is at fault. An additional deceleration of the flow of 3% (see Table 6.1) at the Kaijo-Denki site would make the results from that instrument consistent with those from the other anemometers.

The differences in the u_* and U_{10N} estimates from the Kaijo-Denki and those from the other anemometers could, for the sake of argument, be ascribed solely to errors in the results from the CFD modelling, with the assumption that none of the instruments had any calibration error. This would imply that the wind speed error due to flow distortion at the Kaijo-Denki site should have been 6% rather than 12 % and that the vertical displacement of the flow at the site should have been about 2 m rather than 1 m. Given that the model and the wind tunnel results agreed to within 2 % or better, this size of inaccuracy in the model results seems unlikely. However, since the Kaijo-Denki was sited in a region of relatively severe flow distortion, the discrepancy between the results from that anemometer and the others could well be due to a mixture of model inaccuracy and instrument calibration error as described above.

The mean C_{D10N} to U_{10N} relationships for each of the four anemometers are shown, after correction for flow distortion, in Figure 6.7 (c.f. Figure 6.3). For a given wind speed, the C_{D10N} values were reduced by a maximum of 40 % of their

original value for the Kaijo-Denki data, 30% for the Propeller vane, 20 % for the Bivane and 15 % for the Solent sonic. The two sonic anemometers are now in close agreement as are the two propeller anemometers. As before, the C_{D10N} estimates from propeller anemometers are relatively high at lower wind speeds, probably due to the over-correction of the propeller response, but they are now in fair agreement with the data from the sonic anemometers for the higher wind speeds. In addition to the vastly improved agreement between all four instruments, the lower C_{D10N} to U_{10N} relationships are now very similar to that expected for open ocean conditions.

In conclusion, although validation of the CFD software is not yet complete (Section 9), the results to date are very encouraging. The model-derived wind speed errors are in good agreement with those found from wind tunnel studies, and the estimates of vertical displacement account qualitatively for the difference in the drag coefficients results obtained from the CSS Hudson and CSS Dawson. Most importantly, the results from the CFD software reconcile the very disparate drag coefficient relationships from the four anemometers on the RRS Charles Darwin foremast. The results also support the suggestion (Yelland et al., 1994) that the measurement of wind stress is much less affected by distortion of the airflow than is the measurement of the true wind speed.

6.5 Airflow over the RRS Discovery.

Following initial validation of the software, the air flow around the R.R.S. Discovery was simulated. As for the Darwin and the Canadian ships, the Discovery ship model was enclosed in the centre of a wind tunnel as described in Section 6.3, and a logarithmic profile with a 10 metre wind speed of 13.7 m/s was used (Moat et al., 1996). The flow at the edge of the tunnel abeam of the centre of the ship had been accelerated by less than 0.3%: abeam of the foremast platform, the acceleration was less than 0.1%. This confirmed that the presence of the ship in the wind tunnel caused insignificant blockage to the flow of air at the edges of the tunnel, i.e. that free stream conditions existed abeam of the ship.

Since the data from the Discovery covered a much larger range of wind speeds than that obtained on the Darwin, the CFD software was used to model flow over the Discovery for two other speeds (Moat and Yelland, 1996b). The model was run with a 10 m wind speed of 20.5 m/s, above which the number of drag coefficient data obtained during the cruises decreases sharply, and again for a wind speed of 6 m/s. This lower wind speed was chosen since it represents the point at which the observed C_{D10N} to U_{10N} relationship is at a minimum. In addition, it is likely that at some wind speed less than 6 m/s the pattern of flow around the ship may change, as described in Kidwell and Seguin (1978). The presence of the ship did not cause a significant blockage to the flow at the edge of the tunnel in any of the three model runs.

Figure 6.8 shows model data, for the 13.7 m/s run, on a vertical plane through the port side end of the foremast platform. Although the Solent sonic was situated on the starboard edge, the flow in the region of the platform was symmetrical about the centre line of the ship. This Section is shown for direct comparison with the equivalent Darwin simulation (Figure 6.5). It can be seen that superstructure on the Discovery is rather more streamlined than that of the Darwin, and presents less of a blockage to the airflow. This results in significantly smaller errors in the wind speed estimates made from the Solent sonic anemometer site on the foremast.

The results from all three Discovery simulations are summarised in Table 6.2. The wind speed errors at the Solent sonic anemometer site are less than 1%, and the vertical displacement of the flow is of the order of 1m, for all three runs. The foremast site is much less affected by flow distortion than the equivalent sites on the Darwin and this is reflected both by the smaller wind speed errors and the smaller gradients associated with them. The vertical displacement of the flow, caused largely by the presence of the ship's bows, is similar for both ships.

model U_{10} (ms^{-1})	ΔU (%)	Δz (m)	γ (°)
6	-0.3 ± 0.3	1.2	2
13.7	-0.5 ± 0.2	1.0	2
20.5	-0.8 ± 0.2	0.7	2

Table 6.2. Wind speed errors, ΔU, vertical displacement of air flow, Δz, and the angle of the flow to the horizontal, γ, at the site of the Solent Sonic anemometer (height 18.5m) on RRS Discovery for three CFD model runs with different values of the 10m wind speed.

The results from the three different Discovery simulations were each applied to all data for wind speeds over 6 m/s obtained for relative wind directions within 10 degrees of the bow. The three resulting mean C_{D10N} to U_{10N} relationships are shown together in Figure 6.9. The corrections from the 6 m/s run result in fractionally lower drag coefficients than those from the 13.7 m/s run over the entire range of wind speed. The results from the 20 m/s run result in C_{D10N} values which are insignificantly different except at the higher wind speeds where they are less than 1.5% greater than those from the 13.7 m/s run. Since these differences between the results from the different model runs have little significant effect on the mean C_{D10N} to U_{10N} relationship, and because only 15% of the data considered were obtained when U_{10N} was greater than 17 m/s, the results from the 13.7 m/s model run will be used to correct all data where the wind speeds exceeded 6 m/s.

Figure 6.10 shows the mean C_{D10N} to U_{10N} relationship for the data from the Discovery, both before and after the corrections for airflow disturbance are applied. For a given wind speed, the drag coefficient value has been reduced by between 5 and 6% by the application of the corrections. Also shown are the equivalent relationships from the two sonic anemometers on the Charles Darwin. The corrected Darwin C_{D10N} estimates are in closer agreement with the uncorrected Discovery data,

and are therefore also about 5 or 6% greater than the corrected Discovery data. It is assumed that this discrepancy between the corrected data from the two ships is caused by inadequacies in the airflow modelling and the resultant flow distortion corrections, i.e. is not due to a real difference in the wind stress relationship over the open ocean in the North Atlantic compared to the South Atlantic and Southern Oceans. If this is so, then an additional wind speed error of 1.5% or an additional displacement of about 1 m, applied to one of the two ships only, would account for the discrepancy. The wind speed errors for the Darwin anemometers are the most likely cause, since an additional error of 1.5% is both small compared to the estimated errors for that ship and is also within the expected accuracy of those estimates (Table 6.1). It is unlikely that the estimate of vertical displacement is the cause: the displacement is similar for both ships and any error in the estimate of the displacement would therefore be expected to apply in a similar fashion to both.

It must be noted that this residual difference in the corrected C_{D10N} relationships from the two ships is small compared to the original differences of between 15 and 20% in the case of the Solent sonic, and between 40 to 50% in the case of the Kaijo-Denki anemometer.

6.6 Summary.

This Section has described the use of a fully 3-dimensional CFD model to simulate the flow distortion around research ships. For anemometers sited in the bows of these ships, the flow of air was raised by about 1m from its free stream height. The effect on the speed of the flow varied more widely between the ships, and depended largely on the shape of the ship's superstructure and its proximity to the mast on which the instruments were located. Comparisons of the model results with wind tunnel studies of the same ships showed agreement to within 2% or better for the wind speed error. The model-derived estimate of the vertical displacement of the flow could not be validated directly. However, the results from the simulation of the flow over the RRS Charles Darwin successfully reconciled the drag coefficient data

from four anemometers. For example, the C_{D10N} to U_{10N} relationships from the two sonic anemometers, which originally differed by up to 30%, became indistinguishable. Validation of the CFD software is continuing: future work in this area is discussed in Section 9.

Although the instruments on the Charles Darwin were thought to be well sited at the time of the cruise, the effects of the airflow distortion caused the original drag coefficient results to be overestimated by up to 60% when the wind was directly over the bows of the ship. This demonstrates that the effects of airflow distortion can not be ignored when making wind stress measurements from ships or other large platforms (Section 7). In addition, the wind tunnel results for the Canadian ships (Thiebaux, 1990) show that these effects are also likely to vary rapidly with relative wind direction: this has usually been ignored in previous studies on the effects of wave age on the wind stress (Section 8).

The site of the Solent sonic anemometer on the foremast platform of the RRS Discovery was affected relatively little by flow distortion in comparison to the anemometer sites on the RRS Charles Darwin. The wind speed error at the anemometer site on the Discovery was very small (0.5% compared to between 3.5% and 12% for the Darwin anemometers), as was the gradient of the error (0.2% compared to between 1% and 5%). However, the 1m vertical displacement of the flow had a significant effect on the C_{D10N} estimates. Correcting the Discovery data for flow distortion effects resulted in a C_{D10N} to U_{10N} relationship which would suggest a reduction in the mean C_{D10N} estimates of around 5% compared to their original values. The mean drag coefficient to wind speed relationship obtained from the corrected Discovery data is discussed in Section 7.

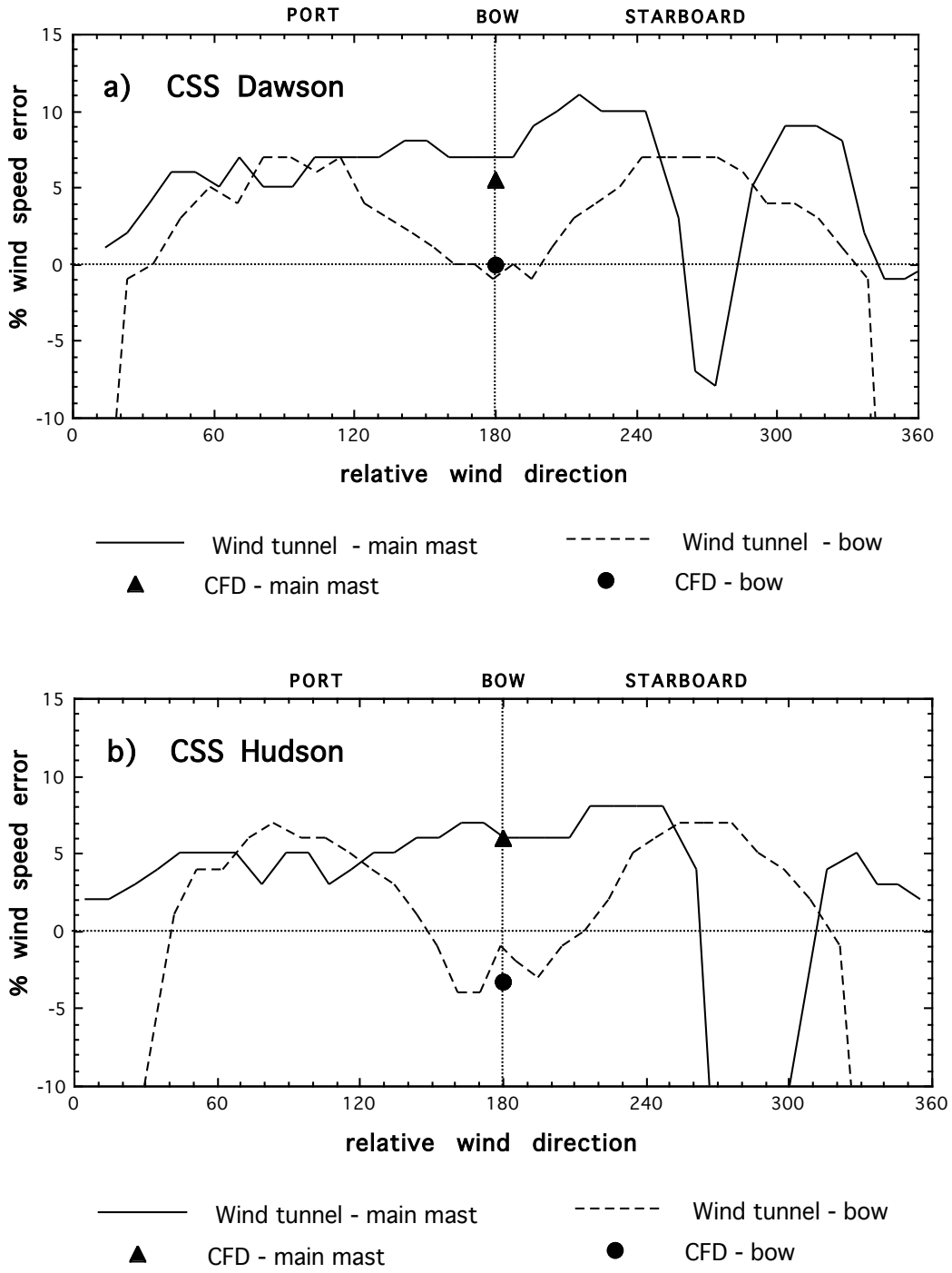

Figure 6.1 The variation of wind speed errors with relative wind direction from wind tunnel studies of a) the CSS Dawson and b) the CSS Hudson. A relative wind direction of 180º represents a flow directly over the bows of the ship. Both ships had anemometer sites on the main mast (solid line) and in the bows (dashed line). The equivalent results from the CFD modelling of the two ships are also shown.

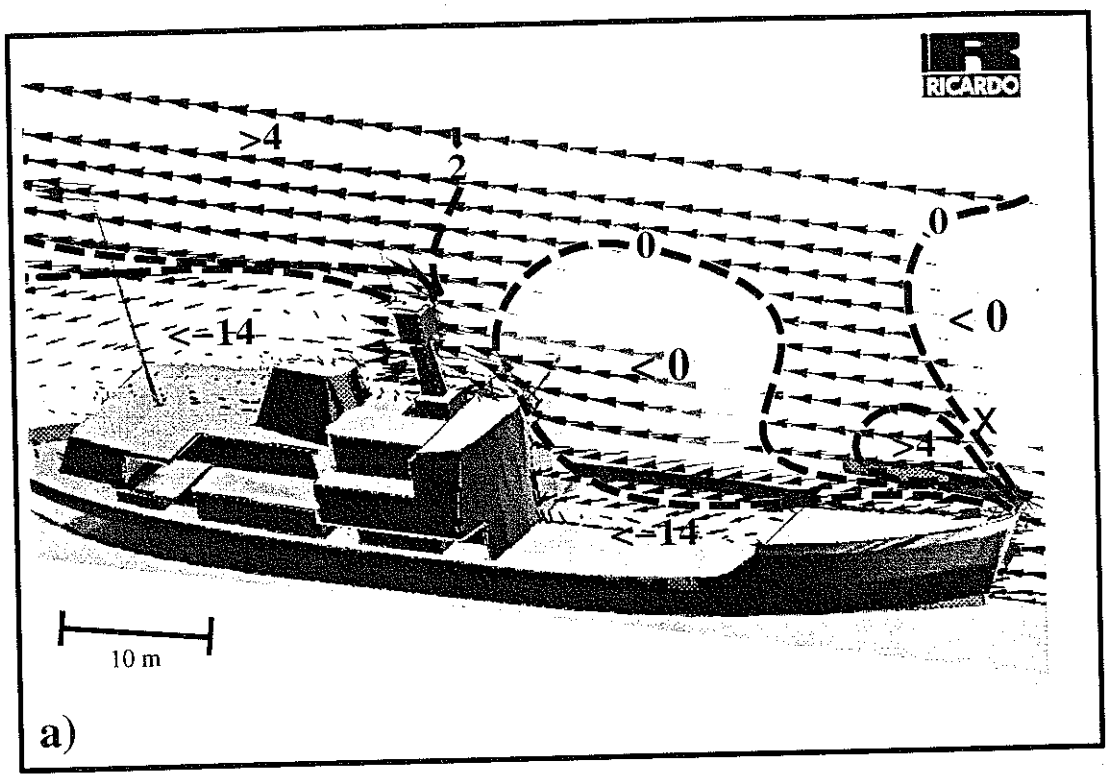

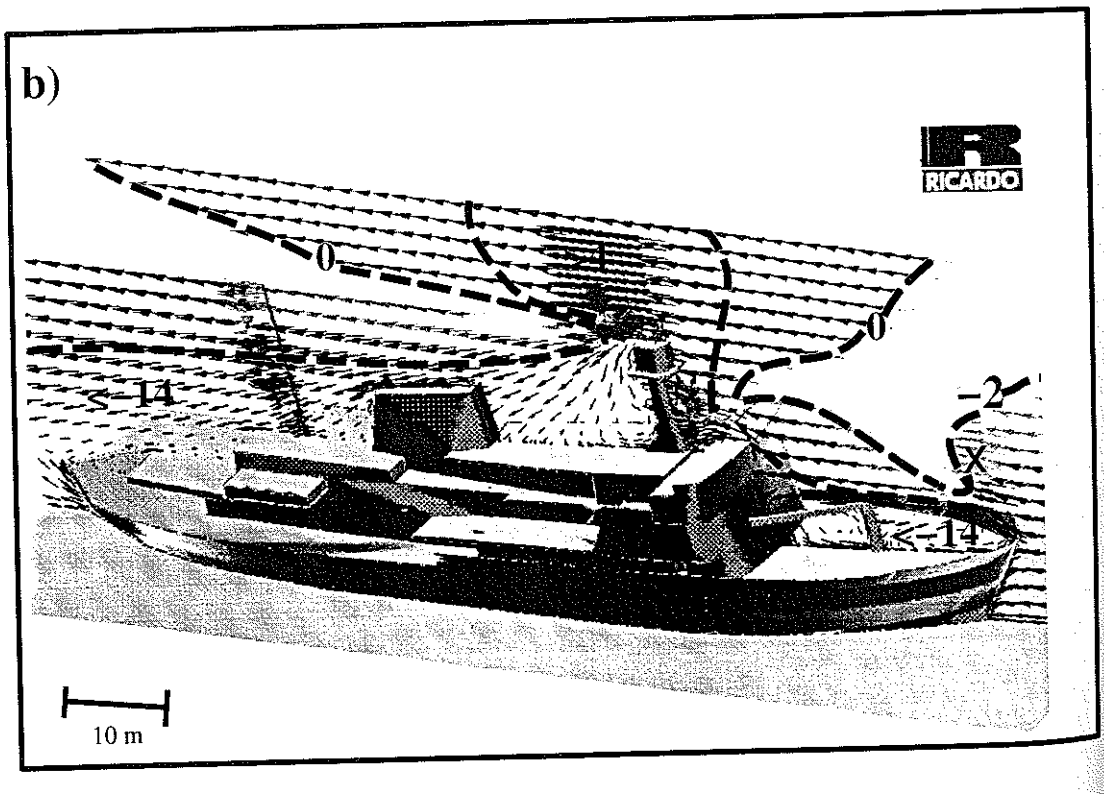

Figure 6.2 CFD model data on a vertical plane through the centre line of a) the C.S.S. Dawson, and b) the C.S.S. Hudson. The position of the bow anemometer is indicated by a cross. The arrows indicate wind velocity, and the dashed lines show the contours for percentage wind speed error, with a region of deceleration shown by a negative percentage error.

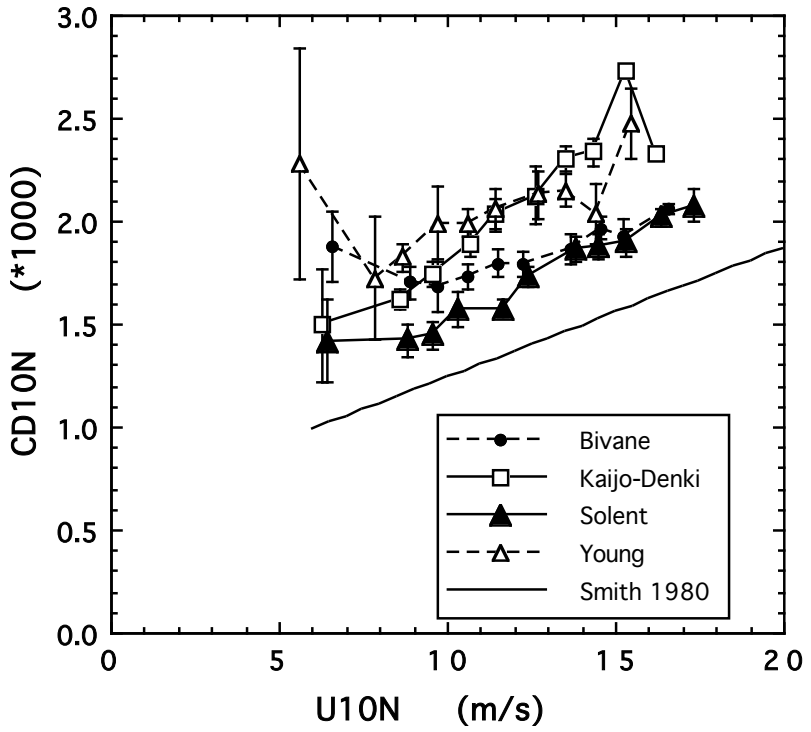

Figure 6.3 The mean drag coefficient to U_{10N} relationships for each of the four anemometers on the foremast platform of the Darwin. The data were selected for relative wind directions within 10º of the bow, and were processed using the imbalance term given in Eqn. 5.7. The relationship suggested by Smith 1980 is also shown.

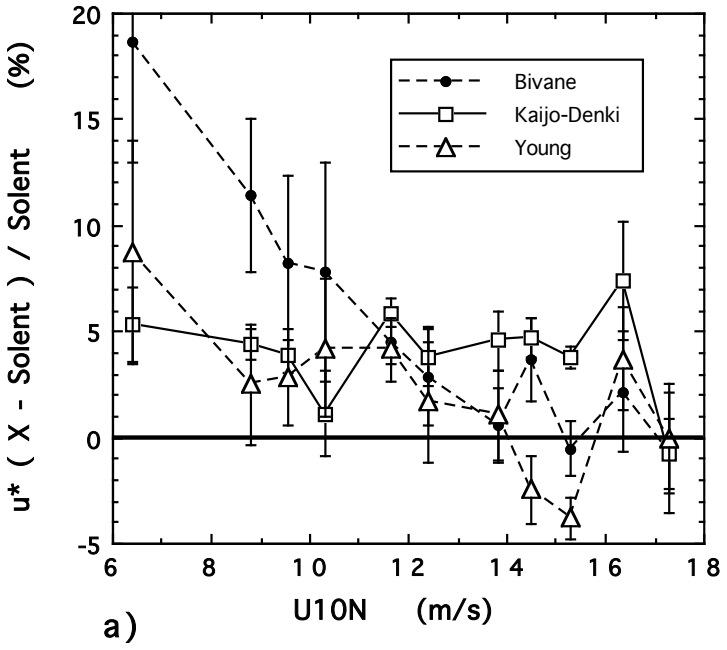

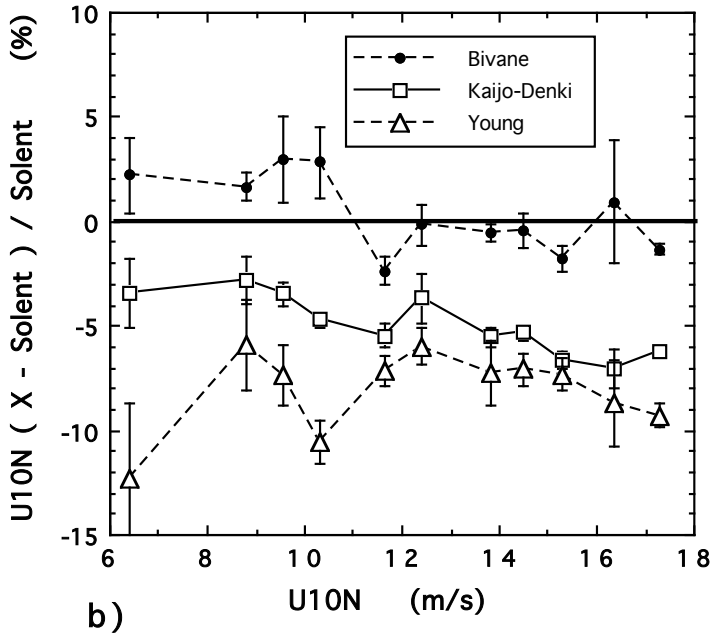

Figure 6.4 a) The differences between the friction velocity data from the Bivane, Kaijo-Denki and Young anemometers expressed as a percentage difference from the values from the Solent sonic anemometer. b) The percentage difference in U_{10N} estimates between the anemometers.

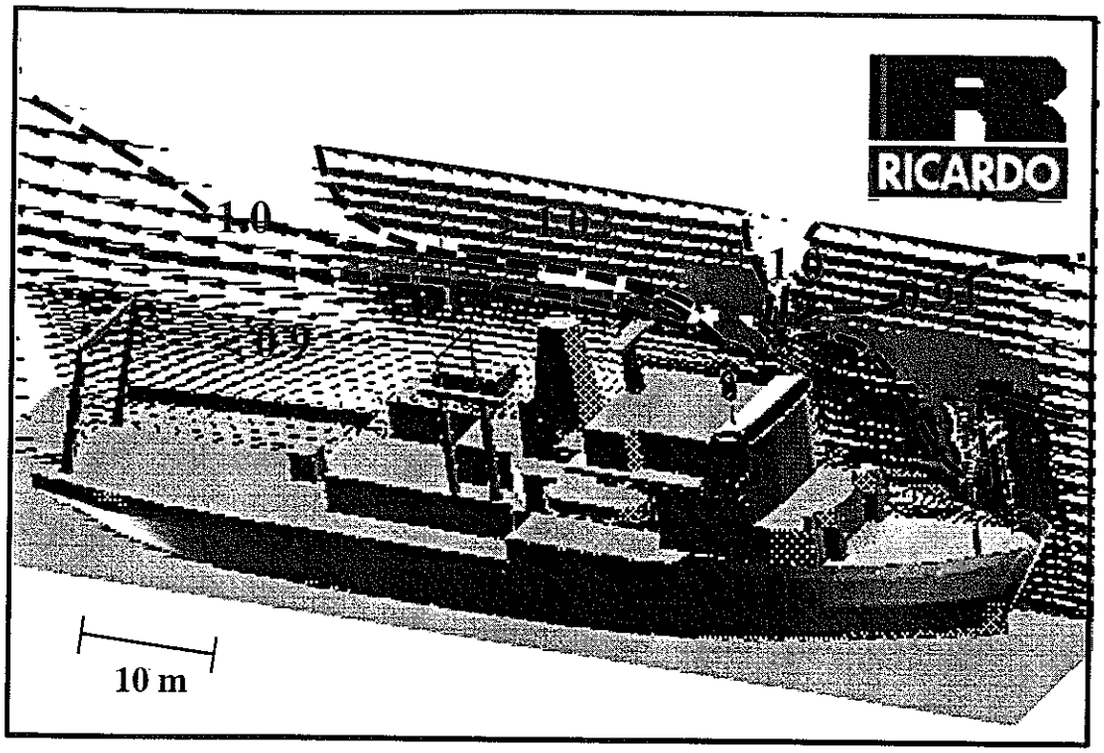

Figure 6.5 CFD model results for flow over the RRS Charles Darwin. Only data on a vertical plane intersecting the Solent sonic anemometer site are shown. The results are expressed as the ratio between the actual wind speed at a point and the free stream wind speed (i.e. the wind speed at that point undistorted by the presence of the ship). This ratio governs the length and shading of the arrows, the direction of which indicates the direction of flow around the ship. Each arrow is associated with a single computational cell.

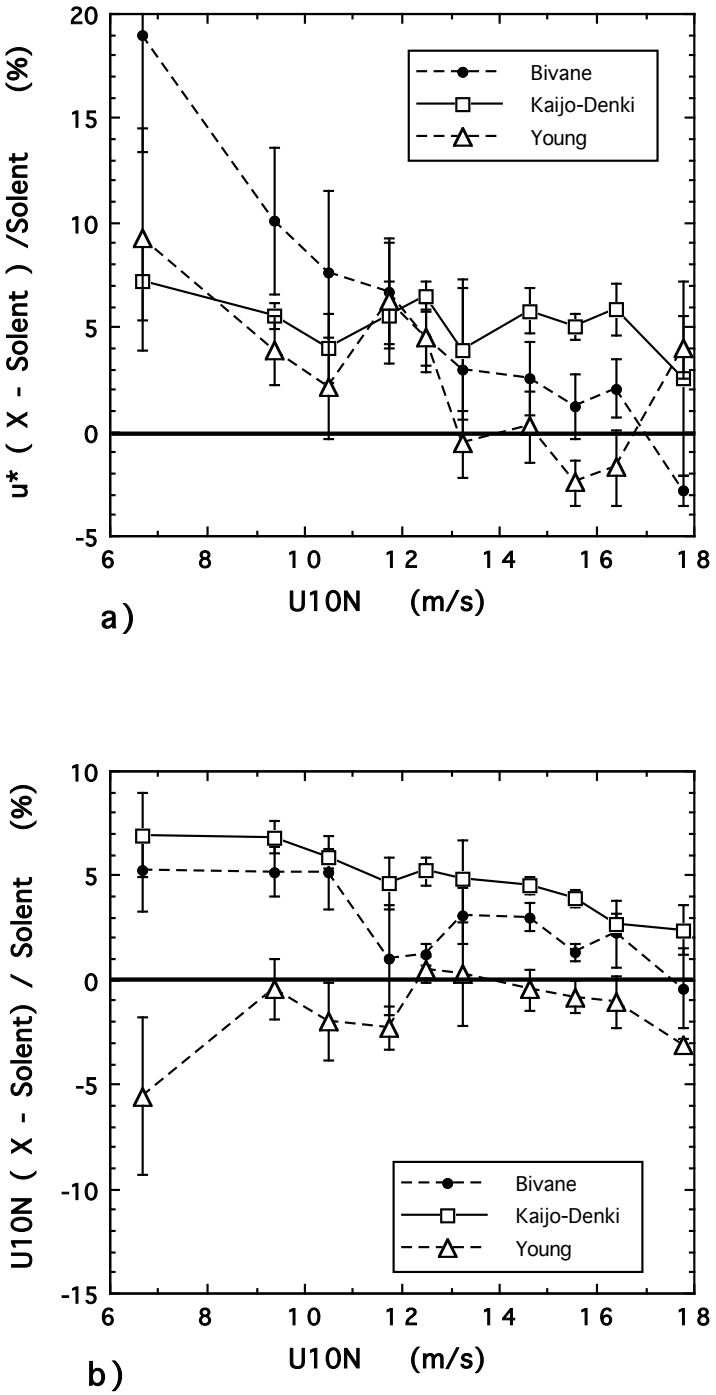

Figure 6.6 Percentages differences between a) the friction velocity estimates and b) the U_{10N} estimates from the four Darwin anemometers, after the data are corrected for airflow distortion effects. See Figure 6.4 for the equivalent data prior to the application of the corrections.

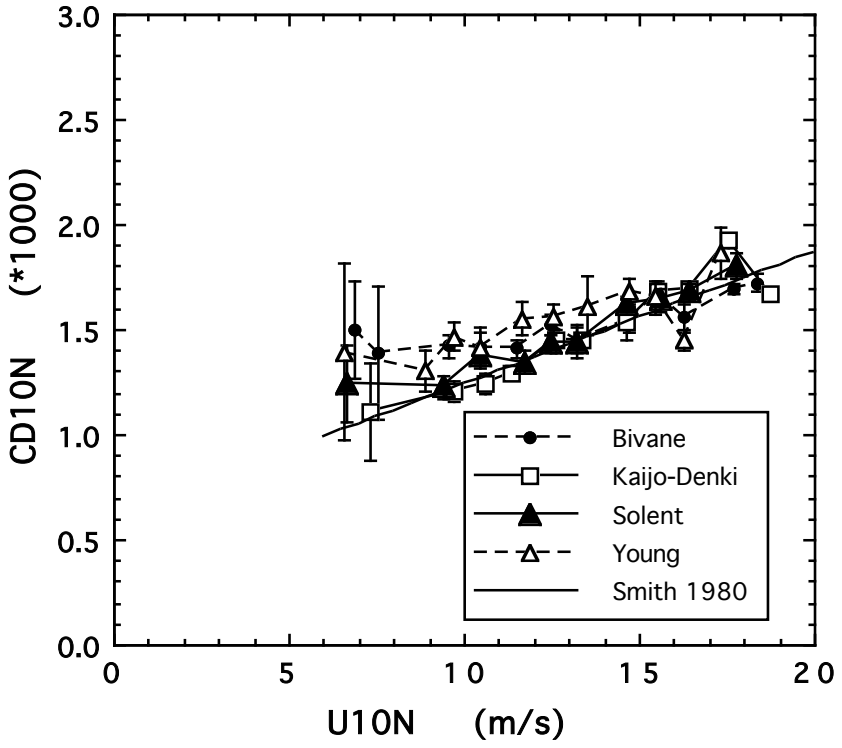

Figure 6.7 The mean C_{D10N} to U_{10N} relationships for each of the four anemometers on the foremast of the Darwin, after the data are corrected for the effects of airflow distortion (c.f. Figure 6.3). The relationship suggested by Smith 1980 is also shown as a reference.

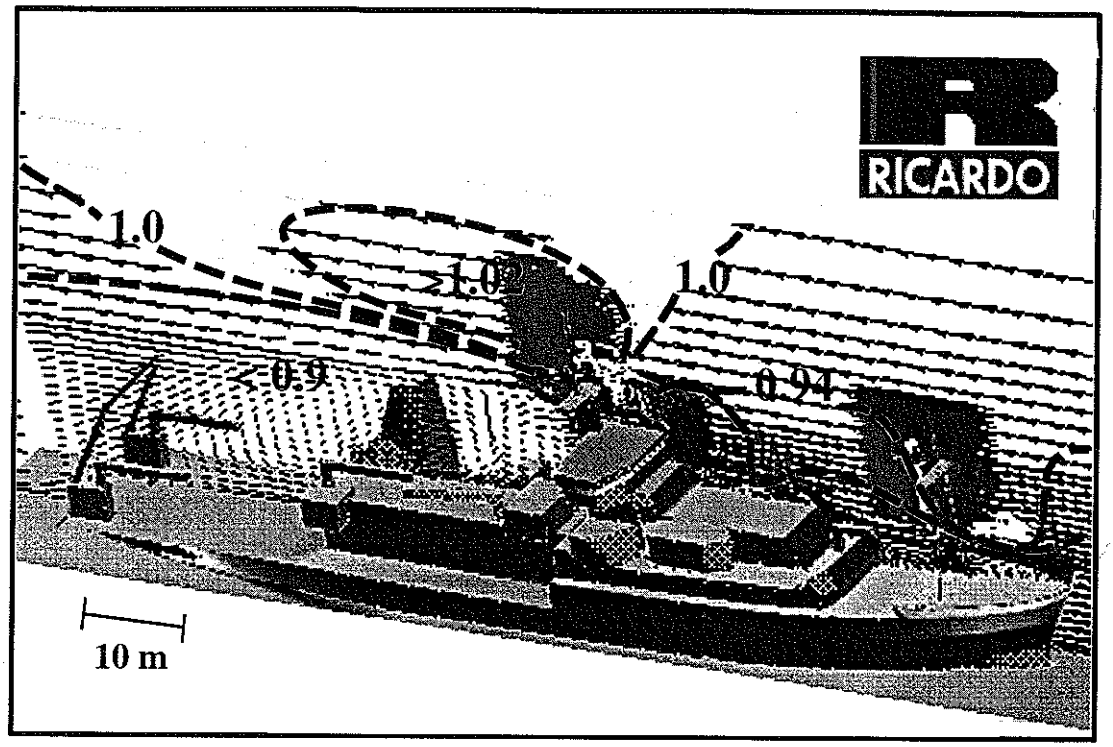

Figure 6.8 CFD modelresults for flow over the RRS Discovery (cf. Figure 6.5 for the RRS Charles Darwin model). The length and shading of the arrows indicate the ratio between the distorted and undistorted wind speeds, and the direction of the arrows is that of the distorted flow.

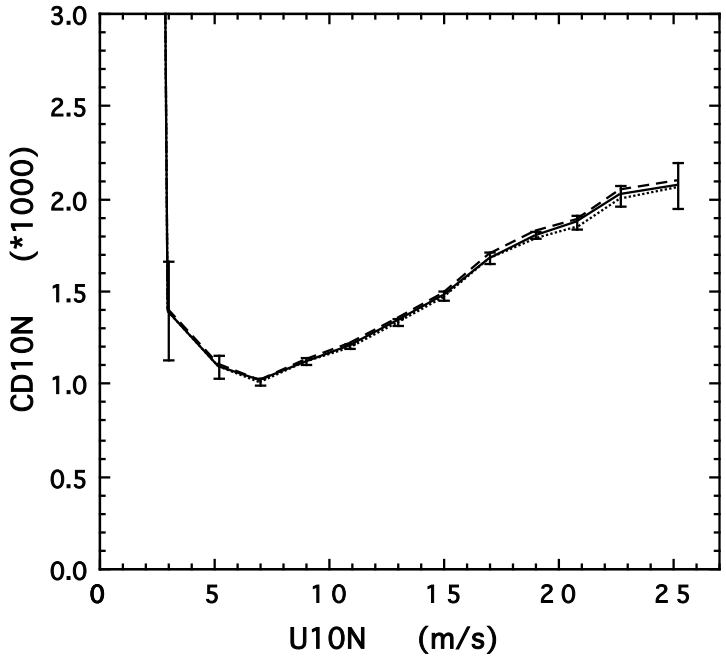

Figure 6.9 Mean C_{D10N} to U_{10N} relationships from the Discovery data after application of three different sets of airflow distortion corrections, obtained from simluations of the flow at 6.0 m/s (dotted line), 13.8 m/s (solid line) and 20.5 m/s (dashed line). The error bars indicate the standard error of the mean.

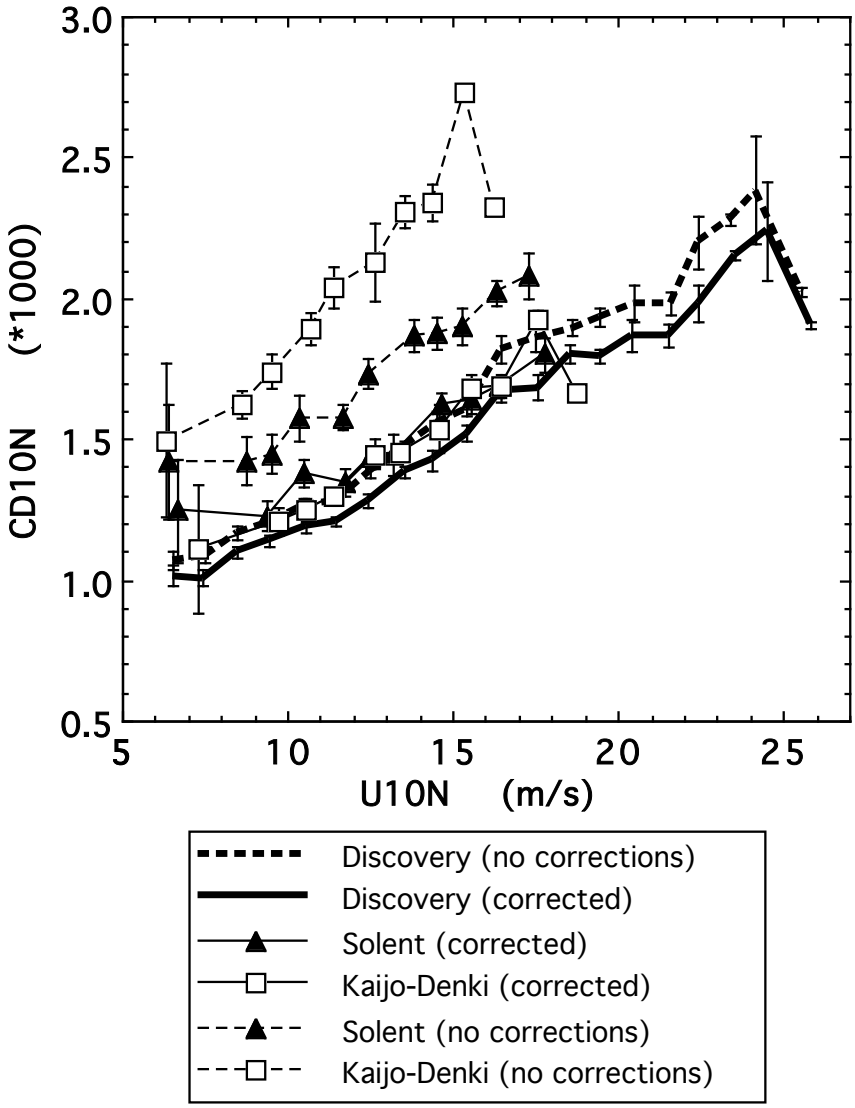

Figure 6.10 Mean C_{D10N} to U_{10N} relationships from the Discovery data before correcting for flow distortion (thick dashed line) and after (thick solid). The mean relationships from the two Darwin sonic anemometers are also shown both before (thin dashed) and after (thin solid) the application of flow distortion corrections. Error bars indicate the standard error of the mean.

7 THE MEAN WIND STRESS TO WIND SPEED RELATIONSHIP OVER THE OPEN OCEANS.

7.1 Introduction

In this section, the mean drag coefficient to wind speed relationship will be determined from the Discovery Southern Ocean data (Section 7.2). The relationship is compared to the results from previous open ocean wind stress studies for low wind speed conditions (Section 7.3) and moderate to high wind speed conditions (Section 7.4) separately.

7.2 The drag coefficient to wind speed relationship.

7.2.a Data selection.

In the last section, the air flow around the research ships Charles Darwin and Discovery was studied using a CFD model. The effects of flow distortion were quantified for flow over the bows of the ships, and were used to obtain the corrected C_{D10N} and U_{10N} estimates. Data selection was restricted to periods when the relative wind direction was within 10 of the ship's bow, since it was shown that the effects of flow distortion may change significantly (Section 5.2.b and Section 6.4.a) outside this range. In the case of the Darwin this limited the number of acceptable wind stress estimates to 73, obtained for wind speeds between 6 and 17 m/s. For the Discovery, 1052 acceptable estimates of wind stress were obtained during wind speeds which ranged from near-calm to 26 m/s. In addition, it was shown in Section 6 that the effects of air flow distortion at the anemometer site on the Discovery were very small in comparison to the distortion effects estimated for the Charles Darwin anemometer sites. For these reasons, the mean C_{D10N} to U_{10N} relationship in this study will be derived from the Discovery data only.

The flow distortion corrections, derived from the CFD model run with a wind speed of 14 m/s, have been shown to apply to all data obtained above 6 m/s, but it is possible that at some lower wind speed the pattern of flow around the ship may change. However, since the wind speed at which this change may happen is not known the air flow distortion corrections have been applied to all data.

7.2.b The mean drag coefficient relationship.

Figure 7.1 shows the individual C_{D10N} values from the Discovery data. At low wind speeds the C_{D10N} estimates diverge according to the stability conditions: for a given wind speed, drag coefficients obtained during stable conditions are much lower than those obtained during near-neutral ($|z/L| < 0.1$) or unstable conditions. As discussed in Section 2.3.c, data obtained at wind speeds below about 2 m/s may not be valid since the anemometer may be above the surface layer. This minimum wind speed is appropriate for neutral conditions: under stable conditions the limit will occur at some higher wind speed. For this reason, data obtained under stable conditions will not be used to derive the mean C_{D10N} to U_{10N} relationship for wind speeds below 6 m/s.

The drag coefficient values reach a minimum at around 6 m/s. The 45 C_{D10N} estimates, obtained during periods where $z/L < 0.1$, could be represented by;

$$1000\, C_{D10N} = -0.4 + \frac{7.7}{U_{10N}} + \frac{1}{U_{10N}^2} \qquad 2 \le U_{10N} < 6 \text{ m/s} \qquad (7.1)$$

where the correlation coefficient, r, was 0.59. These low wind speed results will be discussed in Section 7.3.

The 963 data obtained during wind speeds of 6 m/s or more were fit by a one-way regression;

$$1000\, C_{D10N} = 0.53 + 0.064\, U_{10N} \qquad 6 \le U_{10N} \le 26 \text{ m/s} \qquad (7.2)$$

The correlation coefficient was 0.78, and the standard errors of the intercept and slope of the fit were 0.007 and 0.0016 respectively.

The mean C_{D10N} to U_{10N} relationship could be subject to systematic errors caused by anemometer calibration errors or inaccuracies in the corrections applied to the data to compensate for the effects of flow distortion. An anemometer calibration offset of -2.5%, for example, would cause the drag coefficient to be overestimated by 3 to 4% for a given wind speed (Section 2.3.a). However, the accuracy of the Solent sonic is specified as 1.5%, which would suggest a limit to the bias of the drag coefficient of about 2%. The CFD model of the Discovery suggests that airflow distortion has very little effect on the measured wind speed, but that the flow is displaced vertically by a significant amount. Inaccuracies in the model results (Table 6.2) of 0.3% for the wind speed error and 0.3 m for the vertical displacement would lead to biases in the drag coefficient relationship of about 1% and 2% respectively. Hence, if all sources of bias act in the same sense, the mean C_{D10N} values could be biased by up to 5% for a given wind speed.

One further source of error in the mean relationship is the neglect of wind driven surface currents (Section 2.3.a). This causes the wind speed (relative to the water surface) to be overestimated on average by around 2% (Section 4.8), and, for a given U_{10N}, the C_{D10N} estimate will be underestimated by about 7%. However, as previously discussed, it is common practise to refer the wind speed measurement to the ground rather than to the water surface, effectively parameterising the surface drift into the drag coefficient (Smith et al., 1992). This practise has been followed in this study, allowing the direct comparison of the results from the Discovery data with those of previous studies (Section 7.4).

The individual friction velocity and 10 m neutral wind speed values are shown in Figure 7.2, along with the relationships of Eqns. (7.1) and (7.2). It can be seen that the scatter of the friction velocity values is fairly constant over the entire wind speed range. For wind speeds over 6 m/s, the friction velocity values are all within about 0.08 m/s of the mean.

7.3 Low wind speed drag coefficient relationships.

Figure 7.3 shows the low wind speed C_{D10N} to U_{10N} relationship of Eqn. (7.2), along with those suggested by other authors which are discussed below. Many theories have been proposed to explain the different low wind speed C_{D10N} to U_{10N} relationships found from the various data sets (for example, Wu, 1994). The more simple of the theories assume that, at the lowest speeds, the flow is smooth and that the sea surface can be represented by an aerodynamically smooth solid surface (for example, Smith, 1988). This results in predicted C_{D10N} values which reach a minimum at wind speeds of about 3 m/s, and which increase slowly with decreasing wind speeds below that point. Others, such as Wu (1969) offer a theoretical description of the apparently "rough" flow observed in the experimental studies. However, obtaining reliable wind speed and stress measurements is often complicated by the presence of free convection, since unstable conditions predominate over the oceans at low wind speeds. As conditions become increasingly unstable, the turbulence ceases to be primarily dynamically forced and buoyant forcing becomes dominant. Under these conditions the heat transfer coefficients used in the bulk formulae may be underestimated (Dupuis et al, 1997; Bradley et al., 1991). In the limit of $z/L \rightarrow -\infty$, the friction velocity ceases to be a scaling parameter and Monin-Obukhov scaling is no longer applicable. These points are illustrated below.

The relationship suggested by Dupuis et al. (1997);

$$1000\, C_{D10N} = 0.668 + \frac{11.7}{U_{10N}^2} \qquad U_{10N} \le 5.5 \text{ m/s} \qquad (7.3)$$

was based on data from a ship-borne sonic anemometer, mounted at a height of about 16m. This relationship also agreed well with data obtained by Greenhut and Khalsa (1995) from dissipation measurement made from an aircraft flying at altitudes of 25 to 46 m over the western Pacific. It can be seen that this relationship is very similar to those based on the Discovery Southern Ocean data, i.e. Eqn. (7.1) and the relationship of Yelland and Taylor (1996). These relationships are also a reasonable fit to the near-neutral ($|z/L| < 0.05$) data obtained by Geernaert et al. (1988) who used

a dissipation system mounted at a height of 22 m on a tower located 2 km off the coast of California.

Trenberth et al. (1989) suggested a relationship for low wind speeds by extending the relationship of Large and Pond (1981);

$$1000\, C_{D10N} = 1.14 \qquad 4 \le U_{10N} \le 10 \ \text{m/s} \qquad (7.4)$$

down to wind speeds of 3 m/s, and, for wind speeds below this, applied a fit to the data obtained by Schacher et al. (1981) and Dittmer (1977);

$$1000\, C_{D10N} = 0.62 + \frac{1.56}{U_{10N}} \qquad U_{10N} \le 3 \ \text{m/s} \qquad (7.5)$$

The data of Large and Pond were obtained using propeller anemometers mounted on the Bedford Institute spar buoy and on the foremast of the CCGS Quadra at heights of 12 and 22 m respectively. The data of Schacher et al. were obtained using hot film and hot wire anemometers, mounted on various research vessels at heights of between 4 and 24 m, and those of Dittmer were obtained at heights of less than 6 m. Eqn. (7.5) is also a good fit to the data obtained by Bradley et al. (1991) using a sonic anemometer mounted on a ship's bow boom at a height of 6.5 m. Preliminary results from a sonic anemometer mounted on a buoy at a height of 3 m are also shown (Taylor et al. 1994): these drag coefficient values are not corrected to neutral stability, and, since unstable conditions predominated, the neutral drag coefficients would be somewhat lower than those shown.

The relationships from the experimental studies seem to fall into two distinct groups. The first includes those relationships derived from measurements made at heights of 15 m or more. These may all be represented by a C_{D10N} which increases rapidly as U_{10N} decreases below about 6 m/s. The second group includes studies where measurements were made at heights significantly less than 10 m (assuming that the low wind speed data from Schacher et al. was obtained from their lower measurement heights). These also result in C_{D10n} values which reach a minimum at around 6 m/s or less, but the increase of C_{D10n} with decreasing U_{10n} is much less rapid.

It is possible that the behaviour of the measured C_{D10N} at low wind speeds depends on the measurement height itself. Stability conditions over the ocean tend, on average, to become more unstable as the wind speed decreases (Figure 7.4). As shown by Smith (1988), the magnitude of the stability corrections used in the calculation of the neutral drag coefficient increases rapidly as the wind speed decreases and as z/L becomes more negative, i.e. as the magnitude of the Obukhov length becomes smaller. However, the calculation of the Obukhov length depends on the choice of bulk formulae for the transfer coefficients of heat (Section 2.2.a). These formulae become less valid as z/L becomes more negative and, as the condition of free convection is approached, the buoyancy fluxes are increasingly underestimated (Fairall et al., 1996), which in turn leads to an overestimate of the Obukhov length. Hence, at some value of $z/L < 0$, the stability corrections will be underestimated, resulting in an overestimate of C_{D10n}. For a given Obukhov length, the overestimate of C_{D10N} will be larger at greater measurement heights. This is illustrated in Figure 7.5. For the sake of argument, the measured Obukhov length, L, is assumed to be 20% larger than the real value of the Obukhov length. The dimensionless dissipation function, Φ_ε, is then calculated for a measurement height of 20m, using both the measured and real values of L. The ratio of the resulting values for Φ_ε are shown for different values of z/L. This process is repeated for the same Obukhov lengths, but assuming a measurement height of 5 m. It can be seen that the effect of overestimating the Obukhov length has little effect on the dissipation function for a 5 m measurement height, whereas for a 20 m measurement height the friction velocity would be significantly overestimated by comparison.

The magnitude of the possible overestimate of the Obukhov length is not known, but it would have to be extremely large if it was the sole cause of the discrepancies between the different C_{D10N} to U_{10N} relationships. For example, in order to explain the differences seen in the drag coefficient relationships from the Discovery data and those obtained at lower measurement heights, the Obukhov length would have to be overestimated by 100% or more for $z/L \approx -1$, and by even

larger factors for less unstable conditions. In addition, elevated values of C_{D10N} occur at low wind speeds even under (apparently) near-neutral conditions, as shown by the Discovery data (Figure 7.1) and the data of Geernaert et al. (Figure 7.3).

Hence, if the elevated C_{D10N} estimates obtained from measurements at greater heights are thought to be erroneous, a further explanation may be needed. This may be provided simply by considering the scatter of the observations. Following Wyngaard (1973), Geernaert et al. (1988) suggest that the uncertainty, p, in the dissipation-derived friction velocity estimate can be given by;

$$p = 2\left(\frac{z}{tU}\right)^{0.5} \qquad (7.6)$$

where t is the sampling period in seconds. A 10 minute sample, made at a height of 20 m and for a wind speed of 3 m/s, leads to a 20% uncertainty in the friction velocity estimate. However, as shown in Figure 7.2, the scatter on the friction velocity estimates appears to be constant over the whole wind speed range, and is rather larger than 20% at the lowest wind speeds. The low wind speed friction velocities are examined in more detail in Figure 7.6. The C_{D10N} to U_{10N} relationships of Eqns. (7.1) and (7.2) are shown, as is that of Smith (1988). It can be seen that almost all the friction velocity values for wind speeds between 3 and 10 m/s are within 0.08 m/s of the Smith (1988) relationship. This illustrates that, at the lowest wind speeds, the form of the C_{D10N} to U_{10N} relationship is very sensitive to small biases in the u_* and U_{10N} estimates. At these wind speeds a u_* to U_{10N} relationship is more meaningful since the magnitude of the wind stress is more clearly shown.

None-zero values of the friction velocity at “zero” wind speeds are reported in all the studies discussed above. The estimates of this “minimum friction velocity” value are largest, at about 0.1 m/s, from the studies which employed the greatest measurement heights (for example, Dupuis et al. and this study). This may correspond to the increased effects of free convection at greater heights. However, there is also increased uncertainty in the estimate of the U_{10N} value under such conditions where Monin-Obukhov scaling may not be applicable.

The above arguments are based on drag coefficients obtained using the dissipation technique. However, similar problems occur with the eddy correlation method at low wind speeds. Mahrt et al. (1996) used this method to analyse data obtained from a sonic anemometer mounted 10m above sea level on a tower located in shallow water off the coast of Denmark. In their study, it was found that the neutral drag coefficient could be affected by; the sampling period, non-stationary conditions, the method of averaging used to obtain the mean wind speed, the application of corrections for anemometer "tilt", and the presence of weak surface currents. They also found that data obtained under unstable conditions resulted in elevated estimates of C_{D10N}. The neutral drag coefficient values at the lowest wind speeds were generally reduced from their original values when allowance was made for these problems. Even so, Mahrt et al. concluded that the uncertainty in their measurements precluded any attempt to distinguish between the "smooth" and "rough" flow regimes suggested by different theories (e.g. Wu, 1994). They also postulate that, at low wind speeds, existing similarity theory "is inadequate" and that the calculation of the Obukhov length, and hence the reduction of the drag coefficient to the neutral value, is subject to "large errors at weak wind speeds".

7.4 The drag coefficient under moderate and high wind speeds.

There have been innumerable studies of the wind stress to wind speed relationship over open oceans, coastal waters and lakes. Many of these are discussed by Geernaert (1990). However, only open ocean studies which obtained data at high wind speeds (>10 m/s) will be considered in this section. These are summarised in Table 7.1 and illustrated in Figure 7.7. For clarity, the relationships from the study by Anderson (1993) are not included in the figure since they are very similar to those of Smith (1980).

It has been shown that the estimate of the drag coefficient can be significantly affected both by the imbalance term in the TKE budget (Section 5) and by distortion of the air flow over the measurement platform (Section 6). The possible impact of

these two sources of error on the results from the previous studies will be discussed qualitatively below. Quantified estimates of the errors can not be made, since the necessary information on the distribution of the data with respect to the relative wind direction, the wind speed and the stability conditions is not available.

Study	$1000 * C_{D10N} =$	r	U_{10N} (m/s)	no. data	Anemometer and method.
this study	$0.53 + 0.064\ U_{10N}$	0.78	6-26	963	Solent sonic Dissipation
YT96	$0.60 + 0.070\ U_{10N}$	0.74	6-26	2298	Solent Sonic Dissipation
Anderson (1993)	$0.49 + 0.071\ U_{10N}$ $0.59 + 0.065\ U_{10N}$	0.91 0.83	4.5-18 10-18	84 61	Gill propeller Dissipation
Large and Pond (1981, 1982)	$0.49 + 0.065\ U_{10N}$ 1.14	0.74	10 - 26 4 - 10	973 618	modified Gill prop. Dissipn.
Smith (1980)	$0.61 + 0.063\ U_{10N}$	0.70	6-22	63	Thrust. Eddy correlation

Table 7.1. Drag coefficient relationships (obtained by one-way regression) obtained from studies over the open ocean.

The mean C_{D10N} to U_{10N} relationships from this study and from YT96 (Yelland and Taylor, 1996) were both based on data obtained from the Discovery Southern Ocean cruises. The relationships differ since YT96 accepted data over a much wider range of relative wind directions and did not make any allowances for the effects of airflow distortion. In addition, the imbalance term used by YT96 effectively over-corrected the slightly unstable data which predominated at the higher wind speeds. For these reasons, the relationship proposed in this study supersedes that of YT96, which will not be discussed further.

Smith (1980) employed the eddy correlation method to obtain wind stress data from an anemometer mounted on the BIO tower. Consideration of the imbalance term is therefore irrelevant, since it is only applicable to the dissipation method. Flow distortion at the anemometer site was small since the tower was a very stable moored spar buoy designed to present minimum blockage of the flow. For these reasons, it is thought that the results from this study are unlikely to be affected by any significant systematic error.

In contrast, both the imbalance term and the effects of flow distortion are likely to have had a significant effect on the studies of Anderson (1993) and Large and Pond (1981, 1982). In these studies, a balance between dissipation and production of TKE was assumed and no corrections were made for flow distortion.

Anderson (1993) obtained wind stress data using a propeller anemometer mounted on a mast in the bows of the CSS Dawson. The CFD model of the air flow around this ship (Section 6.4.a) showed that, for bow-on winds, the acceleration of the flow at the anemometer site was insignificant, but that it had been displaced vertically by 0.4 m (or 3% of the instrument height). This would suggest that the drag coefficient results would be overestimated by a few percent. However, the results of Anderson's study include data obtained for relative wind directions within 45º of the bow. The wind tunnel study of the ship (Thiebaux, 1990) shows that over most of this range the measured wind speeds would be overestimated by up to 4% (Figure 6.1.a), which would imply an underestimate of the C_{D10N} values of up to 12% for a given wind speed. To some extent , this would be compensated for by the vertical displacement of the flow, the magnitude of which is not known. In addition, the assumption of a balance between dissipation and production terms in the TKE budget would have resulted in an underestimate of the C_{D10N} values on average: this would, however, be small compared to the effects of flow distortion, since the majority of the data were obtained when $|z/L| < 0.1$. In short, the effects of flow distortion and the imbalance term may have cancelled out for flow directly over the

bows of the Dawson, but it is likely that, for other relative wind directions, the data would be significantly affected by flow distortion.

Large and Pond (1982) described data obtained from an anemometer mounted on a bow mast on the CSS Parizeau. The effects of flow distortion would be the same for these data as for those of Anderson (1993), since the Parizeau is the sister ship to the Dawson. The drag coefficient estimates obtained from the Parizeau experiment were in reasonable agreement with the relationship proposed by Large and Pond (1981) and also with that of Smith (1980).

The earlier study by Large and Pond (1981) employed data obtained from the BIO tower and from the ships F.S. Meteor and the weather ship Quadra. A modified Gill propeller anemometer was located on the BIO tower alongside the instrumentation used by Smith (1980). The anemometer consisted of two propellers, one horizontal and one angled at 60º from the horizontal, in order to obtain stress estimates using the eddy correlation method. The data were "tilt" corrected by rotating the axes to obtain zero mean vertical and cross-stream wind components. Large and Pond estimated that errors in this procedure could amount to a possible 10% error in the mean drag coefficient results. A 10% mean error was also estimated for the results obtained from the ship-borne instrumentation, due to the assumptions implicit in the use of the dissipation method, the estimation of z/L and the measurement of the ship velocity. In order to minimise the effects of flow distortion, the data obtained from the ships was restricted to particular relative wind directions. The range of acceptable wind directions was determined by comparing the data from the Quadra with that from the BIO tower, and the data from the Meteor with near-by buoy data. However, the range of relative wind directions used were large, spanning 135º for the Quadra and 50º for the anemometer on the bow boom of the Meteor, which would suggest that the effects of flow distortion would cause a significant amount of scatter in the results. As in the study of Anderson (1993), a balance between dissipation and production of TKE was also assumed by Large and

Pond, which would result in a relatively small underestimate of the mean drag coefficient.

7.5 Conclusion.

The data from the Discovery Southern Ocean cruises resulted in a drag coefficient to wind speed relationship which could be represented by Eqn. (7.1) for wind speeds between 2 and 6 m/s. It is thought that the increase of C_{D10N} with decreasing wind speeds could be due to the effects of free convection. The behaviour of the wind stress under these conditions needs further investigation.

At moderate and high wind speeds, the Discovery data were well represented by a linear C_{D10N} to U_{10N} relationship;

$$1000\, C_{D10N} = 0.53 + 0.064\, U_{10N} \qquad 6 \le U_{10N} \le 26 \ \ m/s$$

which was very similar to those proposed by Smith (1980) and Large and Pond (1981). It is not surprising that the Large and Pond relationship was similar to that of Smith, since the initial ship data from the Quadra were, in practice, selected by comparison with the eddy correlation data from the BIO tower. However, the results from this study can be viewed as independent verification of the open-ocean C_{D10N} to U_{10N} relationship first proposed by Smith. Furthermore, the present study is based on significantly more data and extends the relationship to higher wind speeds than the Smith (1980) formula.

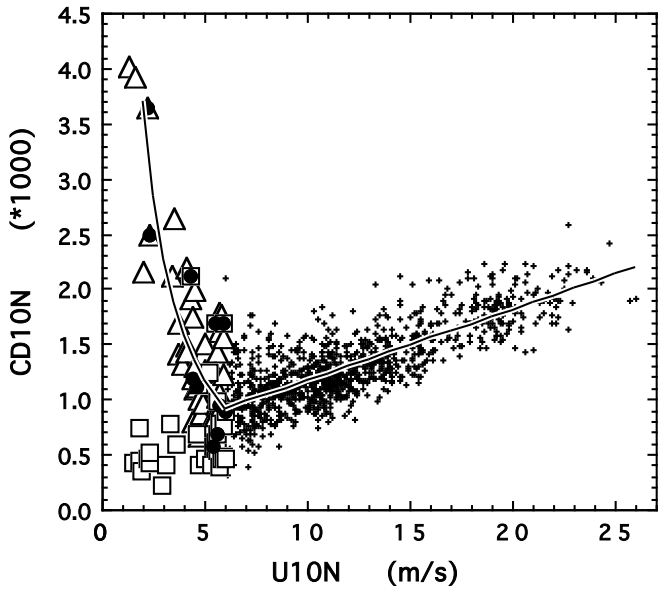

Figure 7.1 Drag coefficient results from the Discovery Southern Ocean cruises. Data obtained at wind speeds of less than 6 m/s are grouped by atmospheric stability: stable data are indicated by the open squares, unstable data by the open triangles and near-neutral ($|z/L| < 0.1$) data by the black circles. Eqns. (7.1) and (7.2) are indicated by the solid line.

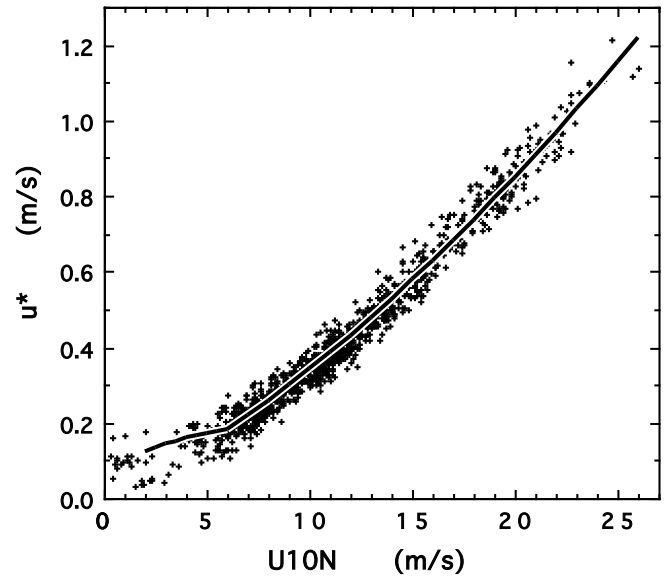

Figure 7.2 Friction velocity values from the Discovery Southern Ocean cruises. Eqns. (7.1) and (7.2) are indicated by the solid lines.

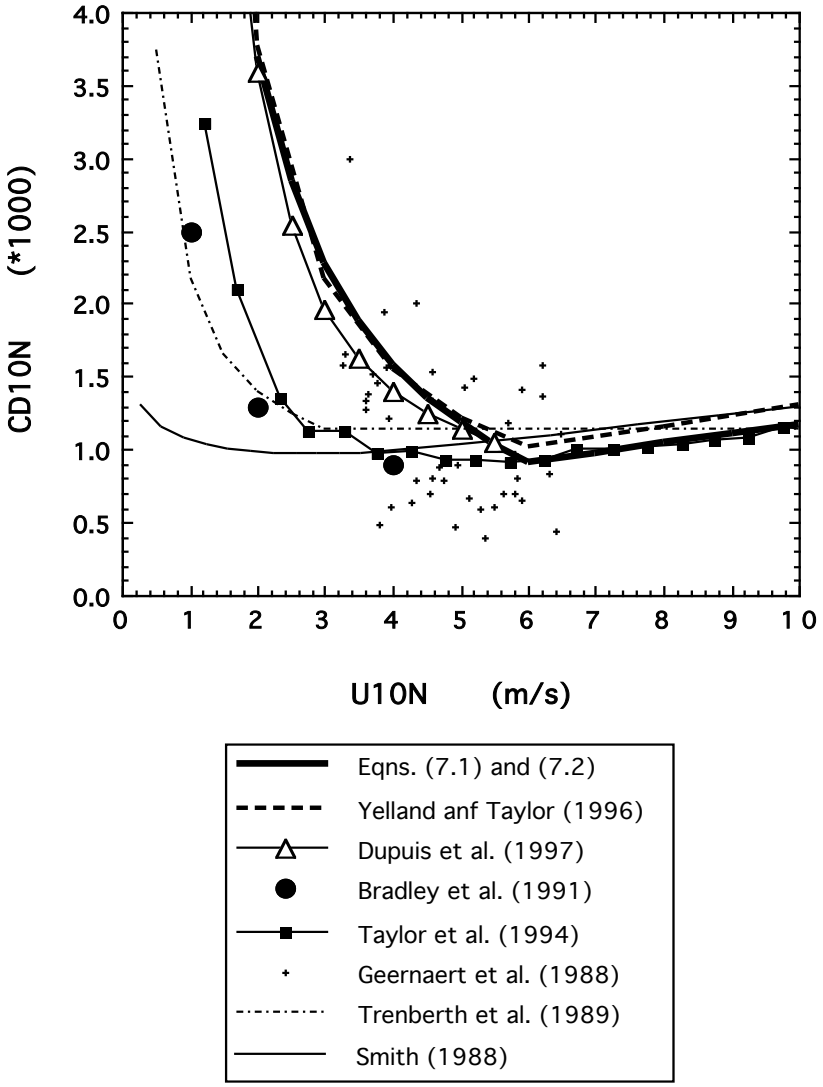

Figure 7.3 Low wind speed C_{D10n} to U_{10n} relationships from various studies as indicated in the key and described in the text.

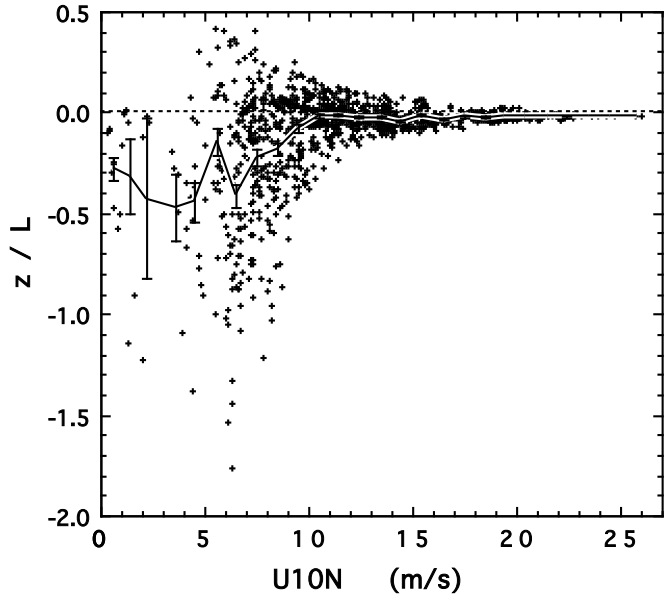

Figure 7.4 Variation of atmospheric stability with wind speed for the Discovery data. The solid line indicates the mean value for a given wind speed and the error bars give the standard deviation of the mean. Data obtained under stable conditions is excluded from the average for wind speeds below 6 m/s.

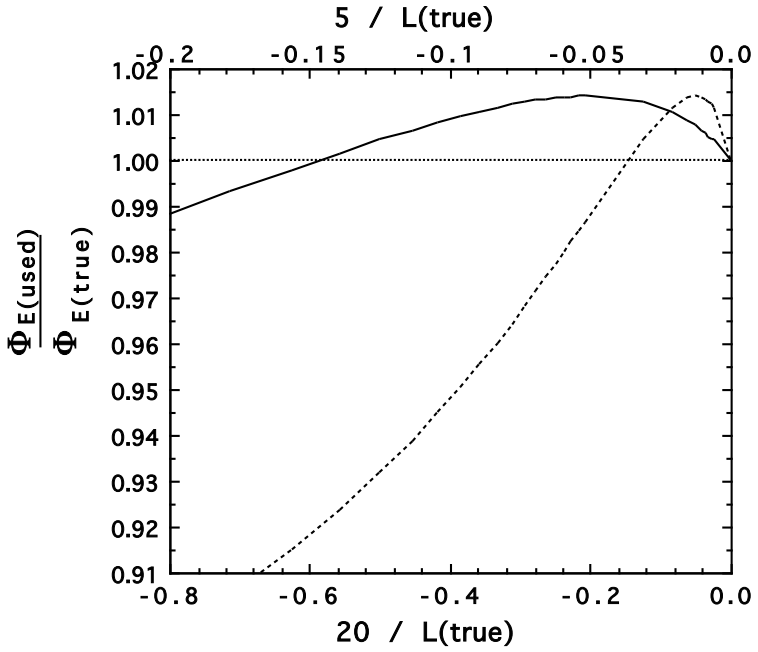

Figure 7.5 Ratio of dimensionless dissipation functions assuming L overestimated by 20% ($\Phi_{E(used)}$) and with the correct value of L ($\Phi_{E(true)}$), for measurement heights of 5m (solid line) and 20m (dashed line).

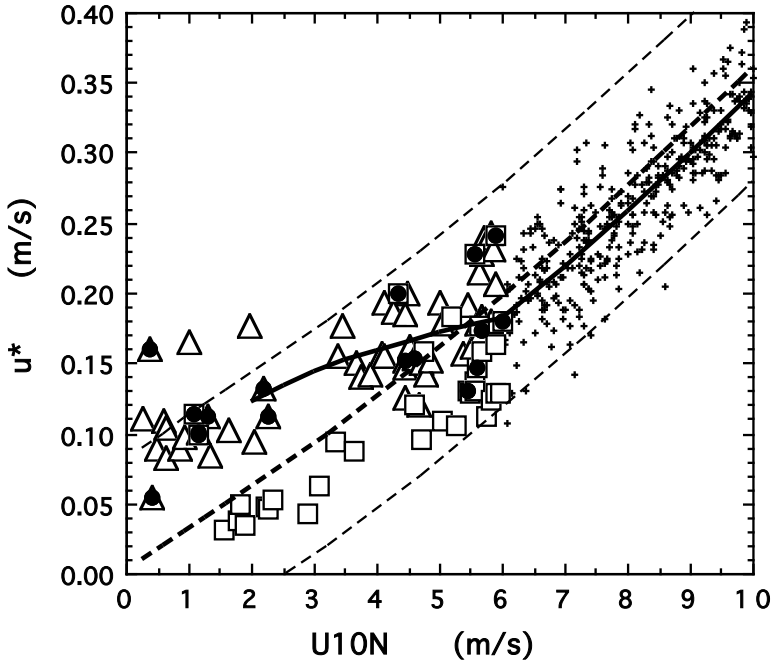

Figure 7.6 Friction velocity estimates from the Discovery data. For wind speeds less than 6 m/s, stable data are indicated by the open squares, unstable data by open triangles and near-neutral ($|z/L| < 0.1$) data by the black circles. The relationship proposed by Smith (1988) is indicated by the heavy dashed line: the faint dashed lines show the same relationship $\pm$0.08 m/s. Eqns. (7.1) and (7.2) are shown by the solid line.

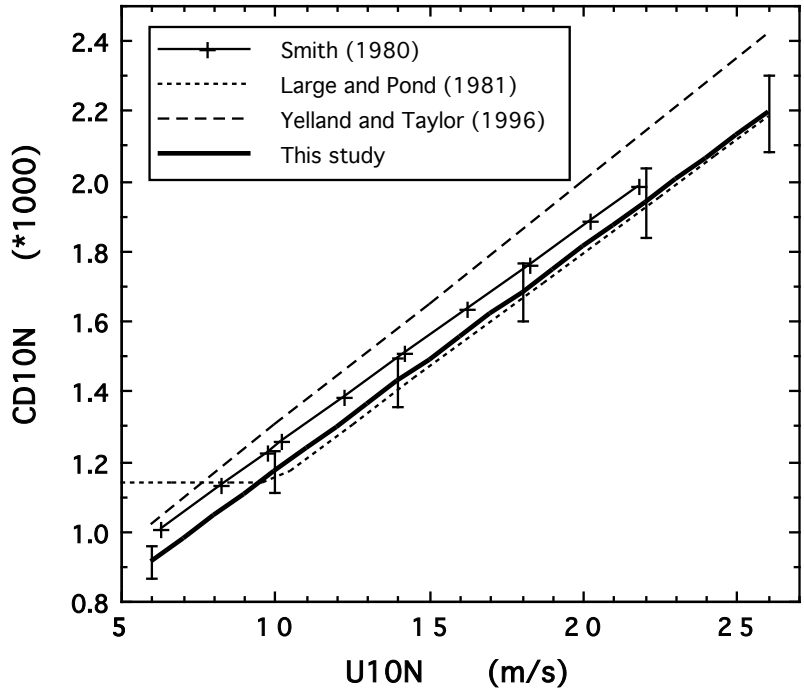

Figure 7.7 Neutral drag coefficient to wind speed relationships proposed for moderate to high wind speed conditions over the open oceans. The error bars indicate the total of the possible biases on the relationship from this study.

8 THE INFLUENCE OF SEA STATE ON THE WIND STRESS.

8.1 Introduction.

This Section examines the wind stress anomalies, or deviations from a mean C_{D10N} to U_{10N} relationship, which have been attributed by previous authors to changes in the sea state or wave conditions. Previous wave-age dependent parameterisations for the wind stress are briefly reviewed in Section 8.2. The mean C_{D10N} to U_{10N} relationship from the Discovery Southern Ocean cruises is compared to that predicted by the Charnock formula for a fully developed sea in Section 8.3, and in Section 8.4 an estimate is made of the effect of an under-developed sea on the drag coefficient. In Section 8.5, the relationship between sea state and the scatter in the drag coefficient data is examined. Section 8.6 discusses the enhanced stress estimates which have been reported in other open-ocean studies and attributed to the sea state.

8.2 Previous wind stress - wave age relationships.

The effect of the sea state on the wind stress has long been a subject for both experimental and theoretical study. Wind stress is related to wind speed via the drag coefficient (Eqn. 2.3) or the roughness length (Eqn. 2.5). These are equivalent parameterisations of the roughness of the sea surface, and are related by Eqn (2.6). From dimensional arguments, Charnock (1955) suggested that the roughness length, z_0, and the friction velocity, u_*, could be related by;

$$\frac{g z_0}{u_*^2} = \alpha \qquad (8.1)$$

where g is the acceleration due to gravity and α is the dimensionless "Charnock constant", sometimes called the dimensionless roughness length. This formulation predicted an increase of wind stress with increasing wind speed.

Smith (1988) suggested that a value of 0.011 for the Charnock constant was as good a fit to the Smith (1980) open ocean data as a linear drag coefficient to wind speed relationship. However, other researchers have found different values for the constant depending on the measurement location. For example, in shallow water or coastal sites a constant of 0.018 has been suggested (Wu, 1980), and measurements made over lakes have suggested higher values still (Geernaert, 1990; Nordeng, 1991). Donelan et al. (1993) summarises some of the many attempts to relate the different estimates of the Charnock constant to some measurable property of the sea state, often via a "wave age" parameter. This is usually defined as C_p / u_* or C_p / U_{10N} where C_p is the phase speed of the dominant wave at the peak of the wave spectrum. In summary, the majority of researchers claim that the roughness length, and hence the wind stress, increases with decreasing wave ages, i.e. that for a given wind speed the drag coefficient will be enhanced by the presence of young or under-developed waves. A comprehensive review of previous work in this area is not attempted in this study. Attention is given to the results from studies which are applicable to, or have been widely applied to, open ocean conditions.

Significant effects of the sea state on the measured wind stress were initially reported from the open ocean studies of Large and Pond (1981) and Denman and Miyake (1973). In both studies, coherent anomalies of the order of 20% of the mean drag coefficient were seen to persist for periods of a few hours, and were attributed to changes in the sea state. However, empirical relationships between the sea state and wind stress have not been determined from such open-ocean studies.

One of the first empirical relationships was suggested by Donelan (1982) who obtained eddy correlation measurements of the wind stress from a platform in 12 m of water in Lake Ontario. Data from the HEXOS experiment, carried out from a platform in 18 m of water in the North Sea, resulted in a wave-age dependent stress formulation (Smith et al., 1992) which was similar to that found by Donelan (1990) in a later Lake Ontario experiment. These relationships predict an increase in the drag

coefficient of up to 100% for shallow water, young wave environments compared to long-fetch deep water conditions (Kent et al., 1997).

However, Figure 8.1 shows that, for a fully developed sea, the Smith (1992) HEXOS relationship;

$$\frac{gz_o}{u_*^2} = 0.48\left(\frac{C_p}{u_*}\right)^{-1} \qquad (8.2)$$

overestimates the drag coefficient by 20% for wind speeds of around 6 m/s and by 15 % for the highest wind speeds compared to typical open ocean C_{D10N} to U_{10N} relationships. Despite this, the HEXOS formula has been applied to open ocean conditions by, for example, Gulev (1995) who used wind and wave data from a climatology to obtain wind stress estimates which were up to 25% larger than those computed from an unspecified "traditional" method. Similarly, wave-age dependent stress formulations are sometimes incorporated into coupled models: the wave-dependent stress relationship employed in the wind-wave model of Janssen (1996) results in C_{D10N} estimates which are 40% larger on average than those found in this study.

8.3 Comparison of open ocean data with the Charnock relationship.

Figure 8.2 shows the mean C_{D10N} to U_{10N} relationship from the Discovery data, along with those resulting from the assumption of the Charnock relationship (Eqn. 8.1). It can be seen that, at the highest wind speeds, the Discovery data are fit by a Charnock relationship with a constant of 0.013, whereas the lower wind speeds are fit by a constant of 0.007. A mean constant of 0.010 could be approximated by the linear relationship;

$$1000\, C_{D10N} = 0.75 + 0.050\, U_{10N} \qquad (8.3)$$

which is significantly different from the fit to the data Eqn. (7.2);

$$1000\, C_{D10N} = 0.53 + 0.064\, U_{10N} \qquad 6 \le U_{10N} \le 26 \ \ m/s$$

given that the standard deviations of the intercept and slope of this fit are 0.007 and 0.0016 respectively. However, if Eqn. (8.1) is applicable to a fully developed sea then the steeper slope of Eqn. (7.2) could suggest that at the higher wind speeds the waves are underdeveloped and that a wave age dependent formula of the form of Eqn (8.2) would be more appropriate.

8.4 An estimate of the expected wave age effect in the open ocean.

The Discovery data were collected over the open ocean, where depth and fetch did not limit the wave development. However, the wind speed varied with time and hence the sea-state could be considered to be duration-limited (Tucker, 1991). Estimating the duration is not straightforward, since weather systems persist over periods of days. The arrival of a front, for example, is accompanied by waves which have been influenced by the winds associated with the front for an unknown length of time. The significant wave height estimates, H_s, from the SBWR data (Section 4.6) were compared to those predicted for fully developed waves, H_{sB}. This was estimated from the wind speed using the relationship suggested by Bouws (1988);

$$H_{sB} = 0.0246\, U_{10N}^2 \qquad (8.4)$$

which was based on the Pierson-Moscowitz wave spectrum. The variation of the ratio H_s/H_{sB} with wind speed is shown in Figure 8.3. Also shown is the ratio H_{sD}/H_{sB}, where H_{sD} is the significant wave height predicted for wave development under duration-limited conditions (Tucker, 1991);

$$H_{sD} = 0.0146\, D^{5/7} U^{9/7} \qquad (8.5)$$

and D is the duration in hours.

In the mean, for wind speeds of 12 m/s or less the waves are fully developed: values of the ratio greater than one indicate the presence of swell. Above 15 m/s, the mean H_s/H_{sB} indicates that the measured wave heights correspond to those expected

for a wind speed duration of 30 hours. Individual data suggest duration times of 15 hours or less. It must be noted that the SBWR estimated H_s will be increased when swell is present, and that the true estimate of the duration would be decreased under these conditions.

The size of the drag coefficient anomaly which would be predicted for these conditions was then estimated using the HEXOS formula (Eqn. 8.2). The C_{D10N} values predicted by the HEXOS formula for fully developed conditions were 15 to 20% larger than those from the Discovery (Section 8.2). This difference was removed by reducing the constant in Eqn. (8.2), hence;

$$\frac{gz_o}{u_*^2} = 0.26\left(\frac{C_p}{u_*}\right)^{-1} \qquad (8.6)$$

Estimates of C_p / u_* were obtained by assuming a wind duration of 30 hours. This assumption, with Eqn (8.6), resulted in a mean C_{D10N} to U_{10N} relationship very similar to that from the Discovery data. Eqn. (8.6) was then used to predict the relationships which would result from an infinite wind duration, and for a duration of 15 hours. These are shown in Figure 8.4. If the Discovery mean relationship represents an average duration of 30 hours, it can be seen that duration periods longer or shorter than this should result in C_{D10N} anomalies of the order of 10% at the higher wind speeds. Larger anomalies may occur if, as thought, the duration has been overestimated due to the presence of swell waves increasing the estimate of H_s. In addition, the C_{D10N} anomalies caused by the duration limited wave development should, by definition, persist for periods of at least a few hours.

8.5 The effect of sea state on the RRS Discovery wind stress data.

8.5.a The scatter in the C_{D10N} estimates from Discovery data.

This section examines the scatter in the wind stress to wind speed relationship obtained during the Discovery cruises. Only data obtained at wind speeds of 6 m/s or more will be considered, since data obtained at lower wind speeds were very

scattered and may have been affected by free convection (Section 7.3). The friction velocity estimates were scattered about a mean u_* to U_{10N} relationship (Section 7.2) with a standard deviation of almost 9%: equivalently, the scatter of the drag coefficients about the mean relationship was 18%. This is consistent with the r.m.s. errors of 3% for wind speed and 6% for u_* estimated from instrument comparisons on the RRS Darwin by Yelland et al. (1994). It is therefore thought that the scatter in the Discovery data can be completely accounted for by random experimental errors. However, the results from the Discovery cruises were examined for systematic deviations from the mean C_{D10N} to U_{10N} relationship which could be attributed to changes in the sea state. To this end, the percentage C_{D10N} "anomalies", ΔC_D, were calculated from;

$$\Delta C_D = 100 \frac{(C_{D10N} - C_{DFIT})}{C_{DFIT}} \qquad (8.7)$$

where C_{DFIT} is calculated from the measured U_{10N} using the mean relationship of Eqn. (7.2).

8.5.b Dependence of ΔC_D on wave development.

The variation of ΔC_D with the ratio H_s/H_{sB} is shown in Figure 8.5.a. It can be seen that, in the mean, there is no significant dependence of ΔC_D on the sea state. This was confirmed by separation of the data into different classes according to the value of the ratio H_s / H_{sB}. The mean C_{D10N} to U_{10N} relationships of these classes did not show any systematic difference (Figure 8.5.b). The SBWR was the only source of wave information available, but the sea-state estimates obtained were not satisfactory since the measurements could be dominated by the presence of swell waves. It was thought that a more useful indication of the sea state could be obtained simply from the wind history, by making the assumption that for increasing wind speeds or changes in the wind direction the seas would generally be under-developed.

8.5.c Dependence of ΔC_D *on wind history.*

Figure 8.6.a shows ΔC_D against the rate of change of the wind speed, $\Delta U_{10N} / \Delta t$, where ΔU_{10N} and Δt are simply the differences in wind speed and time (in seconds) between one wind stress determination and the next. In this case, the data have been selected for time differences of one hour or less as well as for wind speeds greater than 6 m/s. As before, the individual data show large scatter and the ΔC_D values show no dependence on the rate of change of the wind speed for steady or increasing winds. However, for decreasing winds there appears to be a mean positive ΔC_D, i.e. an increased mean stress. Although the mean signal is small compared to the scatter in the data, it produces a systematic difference in the mean C_{D10N} to U_{10N} relationship of between 5% and 10% over most of the wind speed range, as shown in Figure 8.6.b. In this Figure, the data were classed as "steady" if the wind speed did not change on average by more than 0.5 m/s in a 15 minute period. Examination showed that the data with positive ΔC_D values associated with rapidly decreasing wind speeds did not occur consecutively and were widely scattered throughout the data set: they could not be confidently associated with any particular event, such as the passage of a front. It is likely that the apparent dependence of ΔC_D on $\Delta U_{10N} / \Delta t$ is not significant. However, given the weight of opinion behind the arguments for significant effects of sea state on wind stress, further investigation of these C_{D10N} "anomalies" seemed justified.

The change in true wind direction, $\Delta D_{true} / \Delta t$, was found in the same fashion as $\Delta U_{10N} / \Delta t$. Figure 8.7.a shows that rapid changes in wind speed were generally accompanied by changes in the wind direction. The data were separated according to whether the wind direction was steady, backing or veering. The changes in wind direction were small, with a difference of $\Delta D_{true} / \Delta t = 0.01$ corresponding to a shift of less than 10º in 15 minutes and with maximum differences of less than 20º in 15 minutes. However, Figure 8.7.b shows that the mean C_{D10N} may be increased by up to 5% for positive changes in the true wind direction. Since the ship's navigation

officers do not respond instantly to a change in true wind direction, it is to be expected that such changes would result in a change in the relative wind direction, as shown in Figure 8.8.a. Data selection was restricted to a narrow range of relative wind directions in order to minimise the effect of changing flow distortion with relative wind direction. However, Figure 8.8.b demonstrates that even a 10º difference in relative wind direction has a small, but significant, effect on the mean C_{D10N} to U_{10N} relationship: hence any increase in the mean C_{D10N} with a positive change in true wind direction is most probably due to a change in the effects of flow distortion with relative wind direction. However, no equivalent explanation was found for the small increase in the mean C_{D10N} estimates associated with decreasing wind speeds (Figure 8.6), since there was no statistical link between decreasing winds and relative wind direction (Figure 8.9).

8.5.d The persistence of the C_{D10N} "anomalies".

Section 8.5.c investigated the relationships between ΔC_D and changes in the wind speed or direction between one C_{D10N} estimate and the next. However, for the sake of argument, a change in wind speed could cause a C_{D10N} "anomaly" which persists for some later time during which the wind speed had become steady. Examination of the data found no such persistent anomalies. However, since the anomalies were expected to be of the order of 10% (Section 8.4) it was thought that they may be masked by the relatively large scatter in the results (Section 8.5.a). In order to investigate this, the data were smoothed using a running 2 hour "top-hat" filter, which reduced the standard deviation of the ΔC_D estimates from 18% to 7%. Only a limited amount of continuous data were available since the original data set had gaps of a day or more between some samples. Some small anomalies were seen to persist for an hour or so in the smoothed data, but could not be associated with either sea state or wind history.

By far the largest and most persistent anomaly occurred during a storm where the wind speed reached a maximum of more than 23 m/s during the night of day 379

(13th January 1993). The time series of smoothed data obtained during this storm are shown in Figure 8.10. The logging of the data from the anemometer failed at the peak of the storm and did not resume functioning until 6 hours later. However, it can be seen that while the wind speed increased from 18 to over 23 m/s, the ΔC_D estimates were very small, whereas during the 12 hours during which the wind decreased to 15 m/s, the ΔC_D estimates averaged between 5 and 10% . While the wind speed was increasing, the true wind direction was fairly steady at 275º, but had shifted by about 20º by the time the logging system had resumed working. However, it can be seen that the enhancement of the C_{D10N} estimates correlates much more closely with the relative wind direction than with the changes in the wind speed or true wind direction.

8.5.e Conclusion.

A systematic differences from the mean C_{D10N} to U_{10N} relationship seemed to occur during periods when the wind speed decreased rapidly (Section 8.5.c). No statistical link could be found between decreasing wind speeds and relative wind direction (Figure 8.9), i.e. with changes in the flow distortion effects. In contrast, the largest and most persistent anomaly seen in the smoothed data was clearly caused by changes in the relative wind direction of less than 5º. Hence at least some part of the systematic difference in the C_{D10N} estimates is not attributable to the decrease in the wind speed. It is therefore thought that the systematic difference seen in Figure 8.6 is not significant.

In conclusion, this examination of the data from the Discovery cruises revealed no anomalies in the C_{D10N} estimates that could be attributed to sea state conditions or changes in the wind speed or direction. It is thought that if the drag coefficient is dependent on wave age in some fashion then the effects must be very small and/or short lived in comparison to those predicted by the HEXOS-type formula of Eqn (8.6).

8.6. Discussion.

8.6.a Previous examples of wave age effects over the open ocean.

The lack of observed drag coefficient anomalies in the Discovery data contrasts with the large anomalies found over the open ocean in previous studies, as described by Large and Pond (1981) and by Denman and Miyake (1973). In the latter study, a ship-borne anemometer was used to obtain the wind speed and stress measurements, and data were accepted from a range of relative wind directions spanning 180º. Estimates of the flow distortion were not available and no corrections were made to the measurements for non-neutral atmospheric stability. The results were so scattered that the authors concluded that the drag coefficient did not depend on the wind speed, which ranged from 4 to 17 m/s, or on atmospheric stability. The observed dependence of the drag coefficient on the sea state was probably due to either the assumption of a constant drag coefficient, or to a change in the flow distortion with relative wind direction, or to the lack of stability corrections, or any combination of these. In contrast, the results from the Large and Pond experiment were both more numerous and of higher quality. These authors also reported an increase in the dissipation-derived drag coefficient estimates after the passage of a storm. The estimates were obtained from an anemometer mounted on the BIO mast, so although there was a large coincident shift in the wind direction the effects of flow distortion are unlikely to be significant. However, the anomaly was observed during wind speeds of around 5 m/s and for rather stable conditions ($z/L \geq 0.2$): the doubtful accuracy of the dissipation method under such conditions has been discussed in Section 7.3.

More recently, Donelan et al. (1997) obtained wind stress data in deep water off the coast of Virginia. A K-Gill anemometer-vane was mounted on the foremast of a small twin-hull ship, and was used to measure the wind stress using both the dissipation and the eddy correlation methods. Ship motion and directional wave spectra were measured. These authors suggest that their results show an increase in

the wind stress when swell is present and is travelling either across, or counter to, the direction of the wind wave field. In addition, they suggest that the inertial dissipation method underestimates these anomalies in comparison with the eddy correlation method. The results from this study were made available in Table 1 of the paper. The authors also kindly provided us with the relative wind direction information which was not included in their Table. Figures 8.11 reproduces Figure 7 of Donelan et al.. It can be seen that, as reported, enhanced stress measurements are seen for counter and cross swell cases. The enhancement is smaller for the dissipation-derived estimates under low wind speeds. However, it is important to note that the data were collected during several distinct periods which had different atmospheric conditions and average relative wind direction, as well as different sea states.

Figure 8.12 shows the variation of z/L with wind speed for the four different sea state classes. It can be seen that for the pure wind sea cases, the data were obtained under relatively near-neutral conditions, whereas the counter- and cross-swell cases were obtained under more unstable conditions. Donelan et al. argue that, for low wind speeds (less than 6 m/s) and counter-swell conditions, the dissipation method is inadequate since it does not produce the same elevation in the u_* estimates as found by the eddy correlation method. This argument seems flawed on two counts. The first is that Donelan et al. assumed a balance between production and dissipation in the TKE budget, hence their estimates of the dissipation-derived friction velocities would be underestimated, especially at the lower wind speeds. Secondly, both methods are likely to produce high estimates at low wind speeds not because of the sea state but because the conditions were very unstable, with $-10 < z/L < -4$. Under such conditions free convection will affect the results from either method (Section 7.3).

Figure 8.13 shows the relative wind directions at which the data were obtained. The pure wind sea cases were all obtained when the wind was blowing either directly over the bows or to port of the bows, whereas the majority of the

counter- and cross-swell cases were obtained when the wind was to starboard of the bows. Figures 8.14.a and b show the eddy correlation- and dissipation-derived u_* estimates, separated into classes by relative wind direction rather than sea state (c.f. Figure 8.11). It can be seen that the correlation of enhanced stress with relative wind direction is almost as good as the correlation with sea state.

It is therefore thought that the criticism of the dissipation technique was unjustified and that the sea-state correlation proposed by Donelan et al. is spurious, i.e. that the enhanced stress estimates could have been due to a change in the distortion of the flow reaching the anemometer. It is likely that the effects of flow distortion were significant, since the friction velocity estimates were significantly larger than expected from other open ocean studies. It is not possible to judge whether flow to the anemometer was accelerated or decelerated, but it would almost certainly have been displaced upwards.

8.6.b Implications of the Discovery results.

This study shows that the wind stress over the open ocean can be well represented by a simple C_{D10N} to U_{10N} relationship, and that the effects of sea state on this relationship are insignificant. The scatter in the Discovery drag coefficient estimates could not be related to the sea state and could be explained entirely by experimental noise. The open ocean sea-state effects described by previous authors are thought to have been due to the effects of flow distortion, the neglect of the imbalance term in the TKE budget or to other experimental causes. The effects of flow distortion seem to be of particular importance, since the impact on the drag coefficient estimate is both large and very sensitive to changes in the relative wind direction.

The lack of any significant effect of the sea state on the wind stress could be due either to 1) an absence of young waves due to the persistence of weather systems (Section 8.5a), or 2) the presence of swell waves. The mechanism by which the presence of swell waves could suppress the characteristics of young wind seas is not

known. However, apart from the studies discussed in Section 8.6.a, no evidence for a wave-age dependence of the wind stress has been reported for cases where swell waves are present. For example, Dobson et al. (1994) were unable to verify the HEXOS formula in open ocean conditions. Indeed, Smith et al. (1996), in their review of the HEXOS programme, state that the application of the HEXOS formula should be restricted to sites with a water depth of 18 m, or to wind speeds below 13 m/s. However, the results from this study suggest that the formula is not applicable in the open ocean even at the lower wind speeds. Again, this may be due to the prevalence of swell waves in the open ocean: Smith et al. (1996) state that the dependence of the wind stress on the wave age was only apparent for single-peaked wave spectra.

In addition to the lack of support for a wave-age dependency of the open ocean wind stress, the validity of wave-age relationships derived from coastal and lake experiments is also now being questioned. For example, Oost (1997) re-examined the HEXOS data and found that the reported wave-age dependence of the wind stress (Smith et al., 1992) was caused by long wave-length waves shoaling into the shallow water depth, rather than by the presence of under-developed waves. In addition, the slope of the revised mean C_{D10N} to U_{10N} relationship was significantly less than that originally proposed, although the predicted C_{D10N} values were still larger than those from open ocean relationships by about 20%.

The use of a wave-age dependent parameterisation of the wind stress is not recommended for open ocean conditions since this would result in a considerable over-estimate of the stress. A linear C_{D10N} to U_{10N} relationship such as that given in this study (Section 7.2.b) should be used.

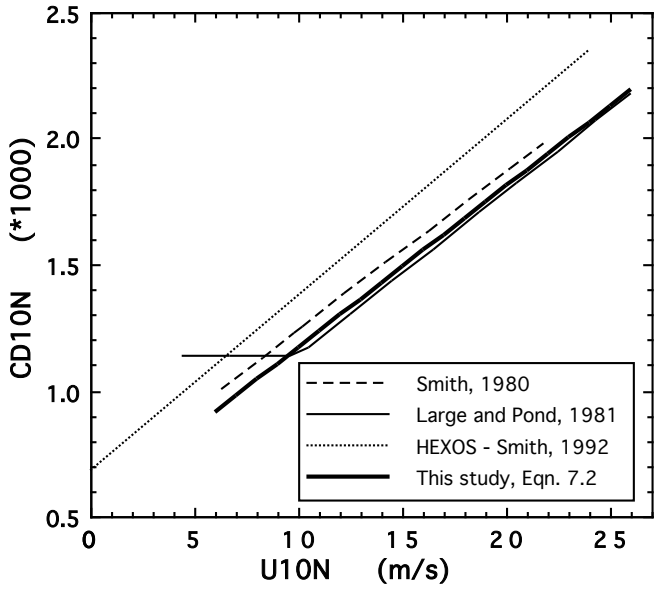

Figure 8.1 The HEXOS relationship for a fully developed sea (dotted line) compared to the open-ocean relationships suggested by this study (thick solid), Large and Pond (1981) (thin solid) and Smith (1980) (dashed).

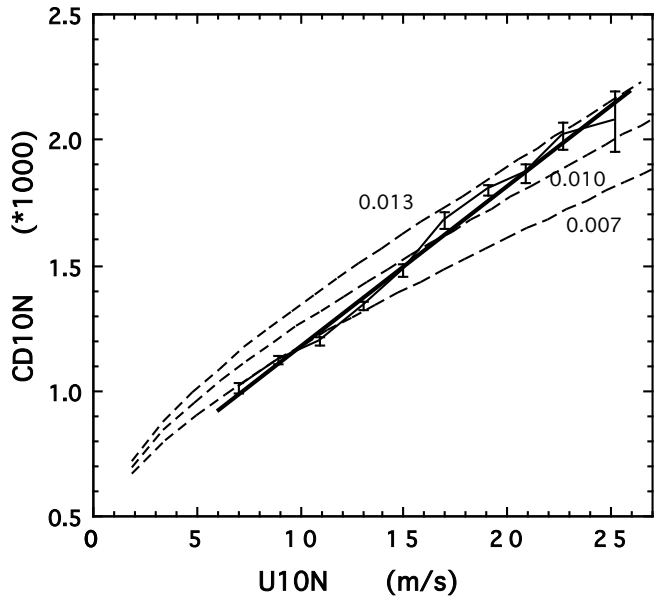

Figure 8.2 The mean C_{D10N} results from the Discovery data (thin solid), where the error bars indicate the standard deviation of the mean. The fit to the data (Eqn. 7.2) is shown by the thick solid line. The dashed lines represent the Charnock relationships with the values of the constants as indicated.

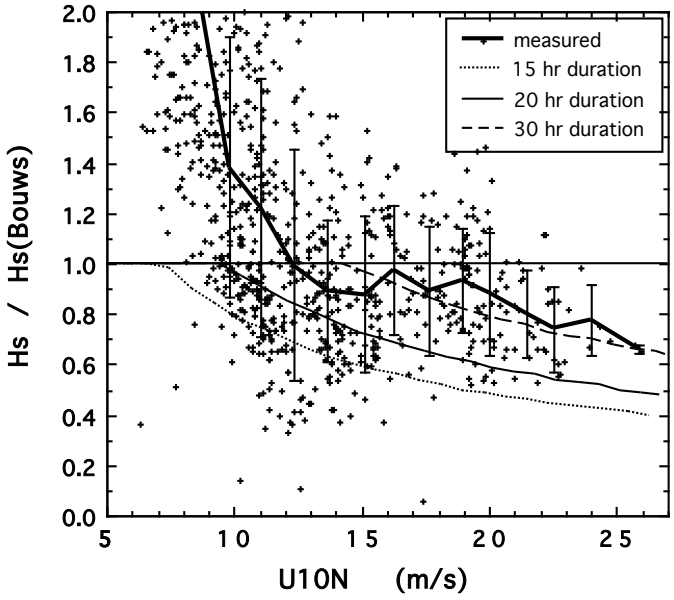

Figure 8.3. Wave development with wind speed. The thick solid line indicates the ratio of the measured significant wave height to that expected for a fully developed sea (from Bouws, 1988). The thin lines represent the ratio of significant wave heights for different wind durations to that for a fully developed sea.

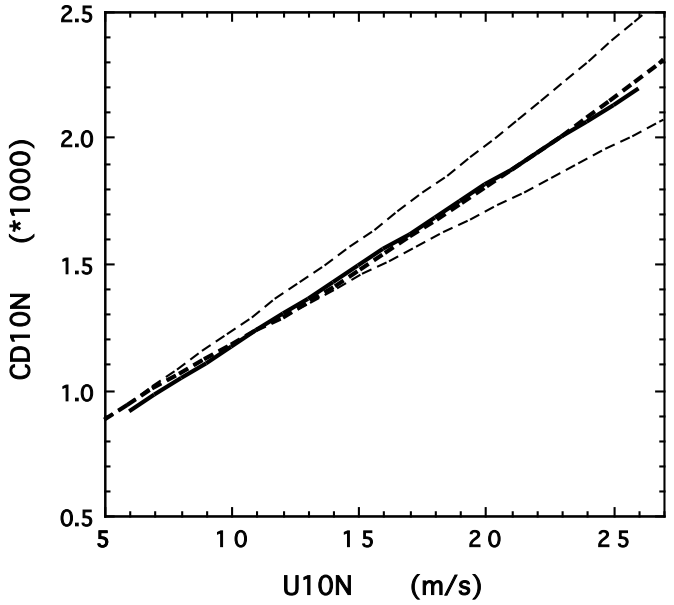

Figure 8.4. The mean Discovery C_{D10N} to U_{10N} relationship of Eqn. 7.2 (solid line) and the relationship from the adjusted HEXOS formula of Eqn. (8.6), assuming a wind duration of 30 hours (thick dashed line). The thin dashed lines represent an unlimited or infinite wind duration (lower) and a duration of 15 hours (upper).

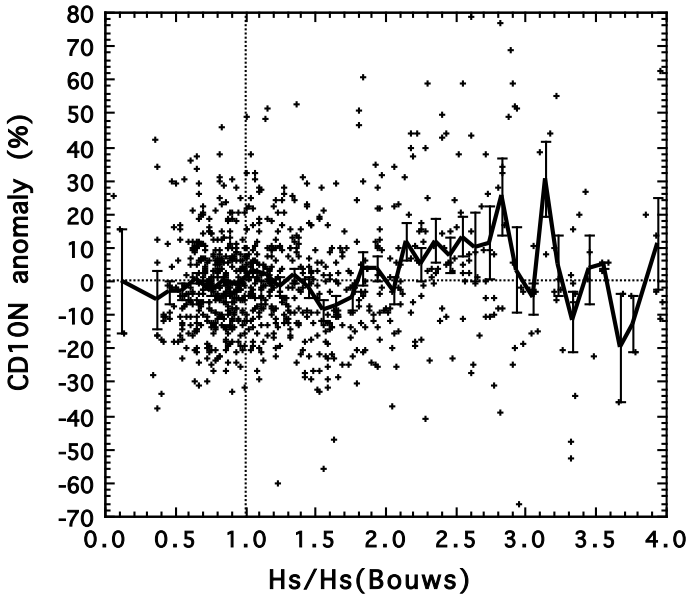

Figure 8.5.a Variation of the drag coefficient "anomaly" with wave development, given by the ratio of the measured H_s to that expected for a fully developed sea.

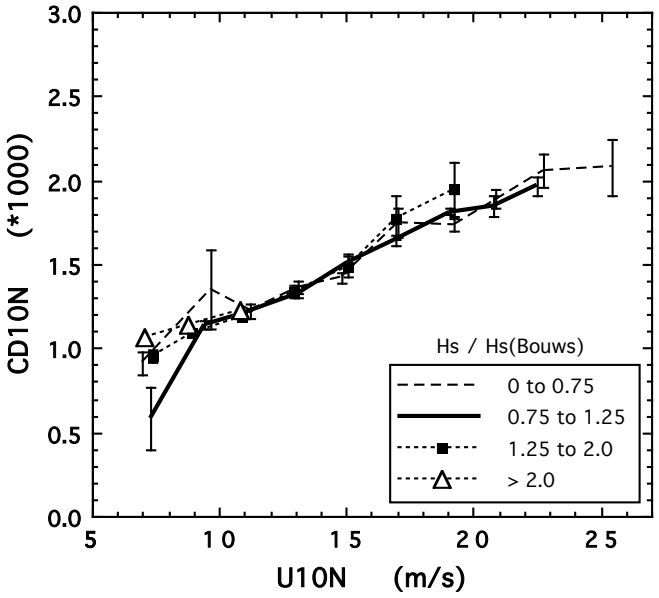

Figure 8.5.b The mean C_{D10N} to U_{10N} relationships for the data classed by wave development as indicated in the key. Underdeveloped waves are represented by a ratio of less than 1.

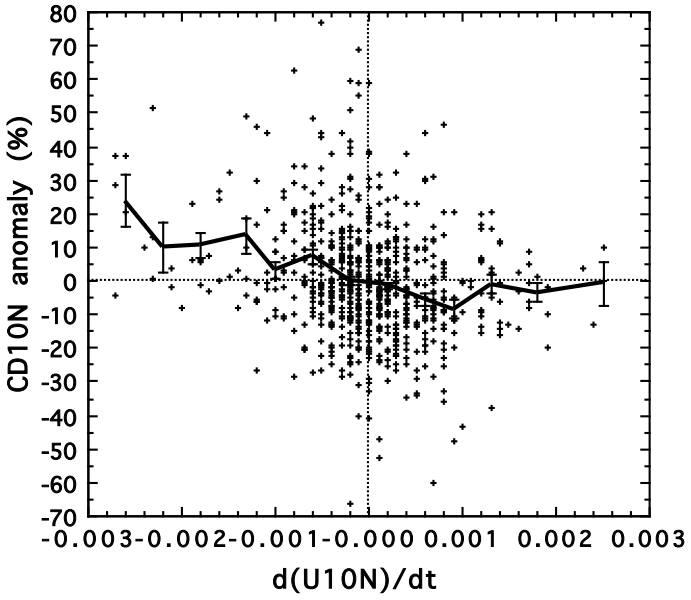

Figure 8.6.a. Variation of ΔC_D with the rate of change of the wind speed, $\Delta U_{10N} / \Delta t$, where a value of -0.003 represents a decrease of 2.7 m/s in 15 minutes.

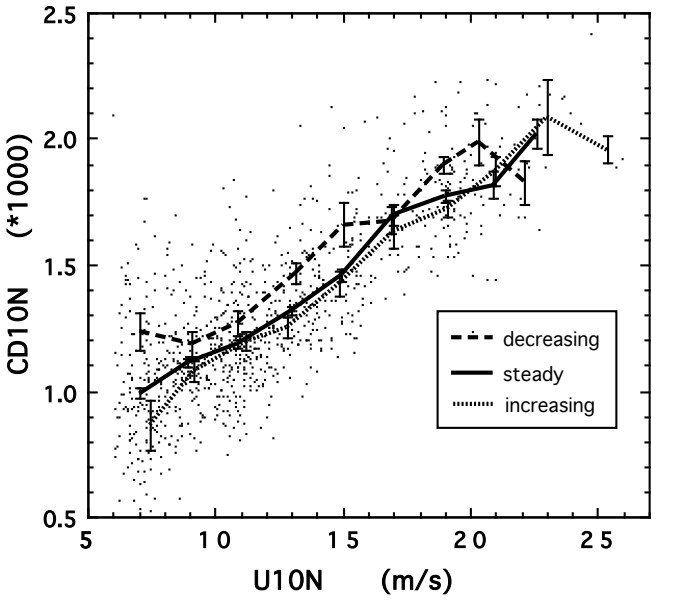

Figure 8.6.b. The mean C_{D10N} to U_{10N} relationships for periods where the wind was decreasing (dashed line), steady (solid) or increasing (dotted).

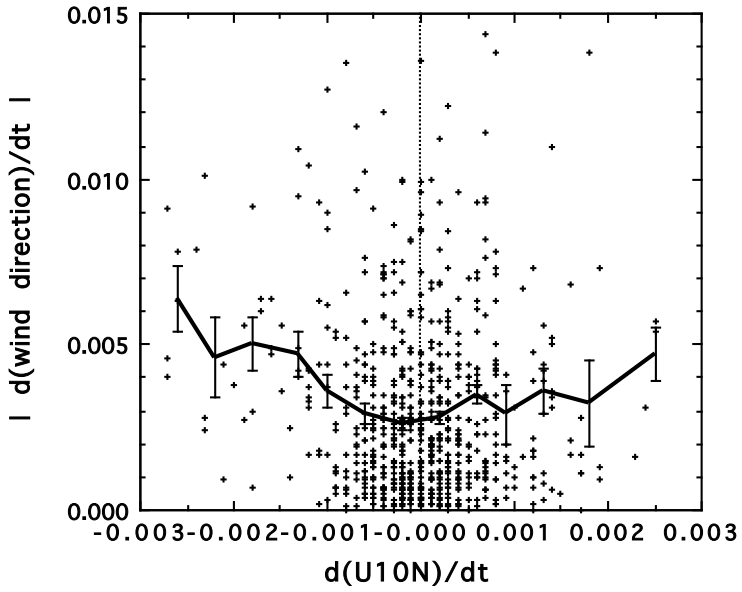

Figure 8.7.a. The variation of the magnitude of the change in the true wind direction with the change in wind speed. A direction change of 0.015 is equivalent to a 13.5º shift in 15 minutes.

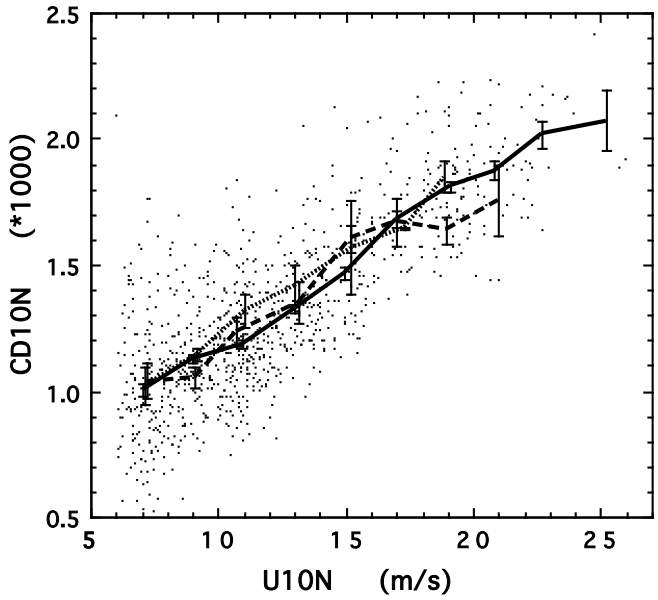

Figure 8.7.b. The mean C_{D10N} to U_{10N} relationships after separation of the data according to the change in the wind direction. A positive change is indicated by the dotted line and a negative change by the dashed line. Cases where the wind direction was steady (i.e. changed by less than 5º in 15 minutes) are shown by the solid line.

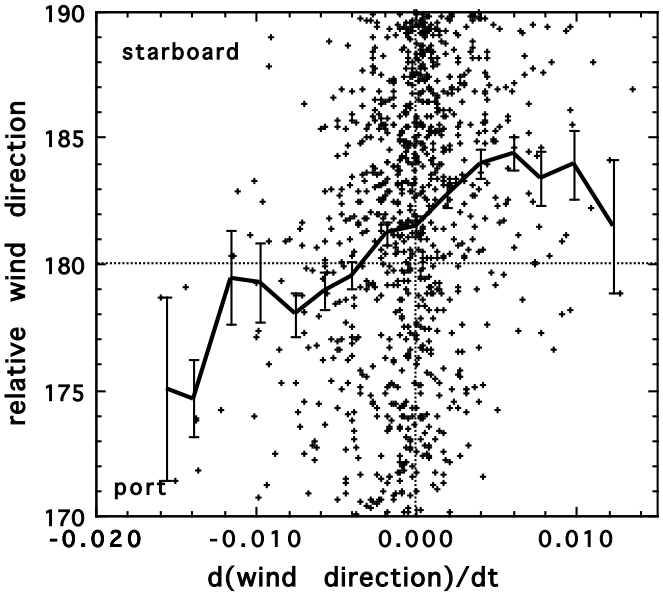

Figure 8.8.a. The variation of the relative wind direction with a change in the true wind direction. A wind blowing directly over the bows of the ship is represented by a relative direction of 180º.

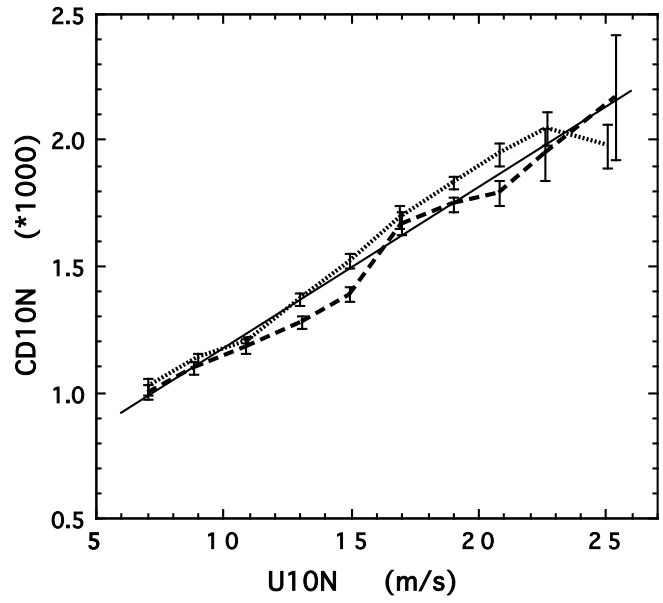

Figure 8.8.b. The dependence of the mean drag coefficient on relative wind direction. Winds blowing to port of the ship's bow are represented by the dashed line, and winds to starboard by the dotted line. The mean relationship (Eqn. 7.2) is indicated by the thin solid line.

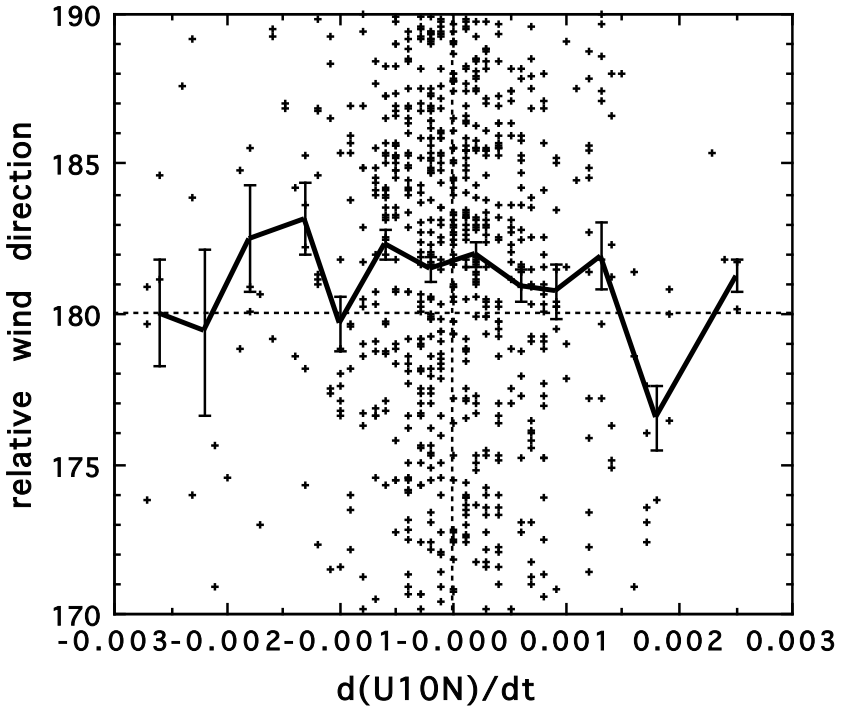

Figure 8.9 The variation of relative wind direction with the rate of change of wind speed.

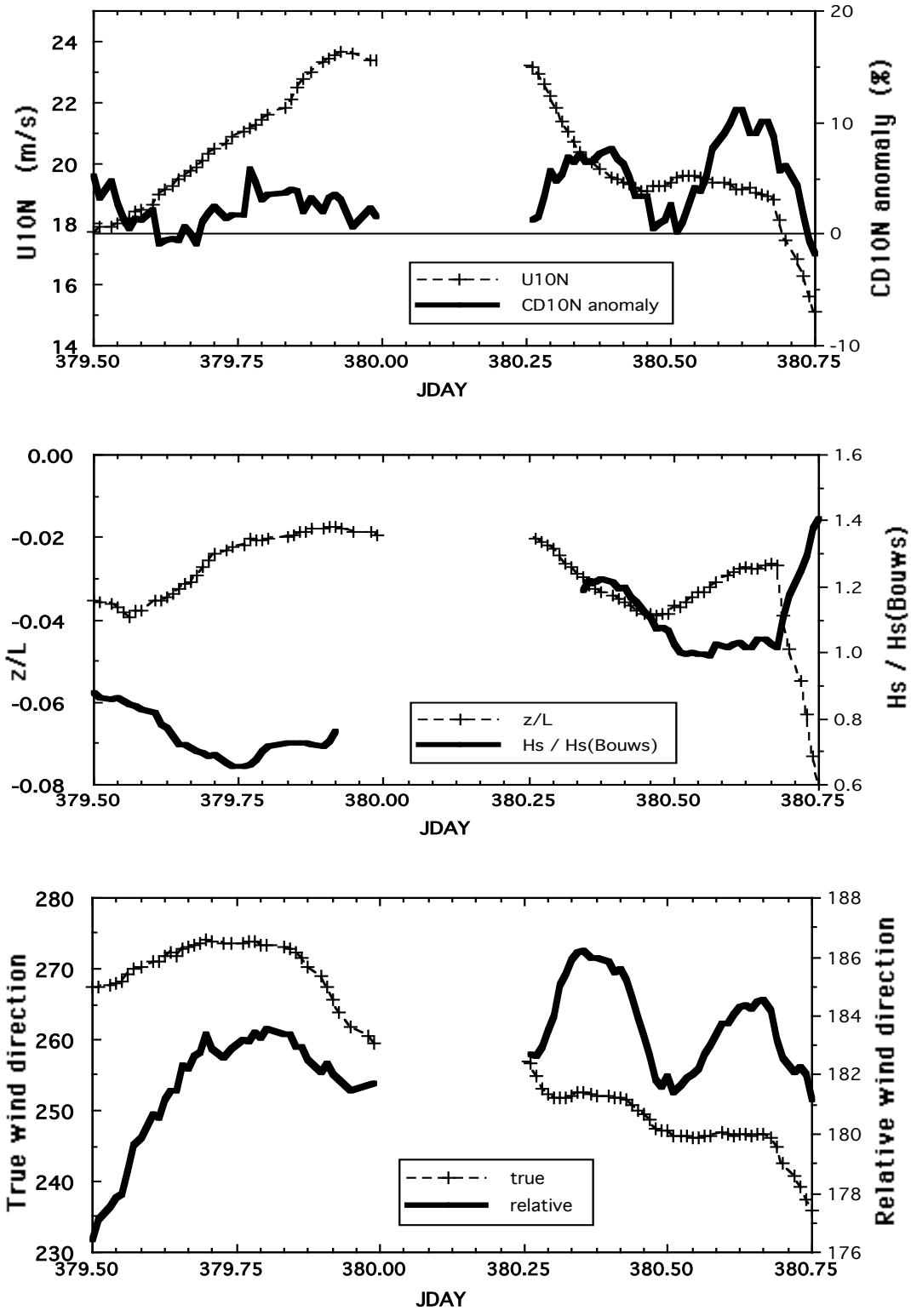

Figure 8.10 Time series of data smoothed with a running 2 hour filter; (top) 10 m wind speed and ΔC_D, (middle) stability parameter and wave development, (bottom) true and relative wind directions.

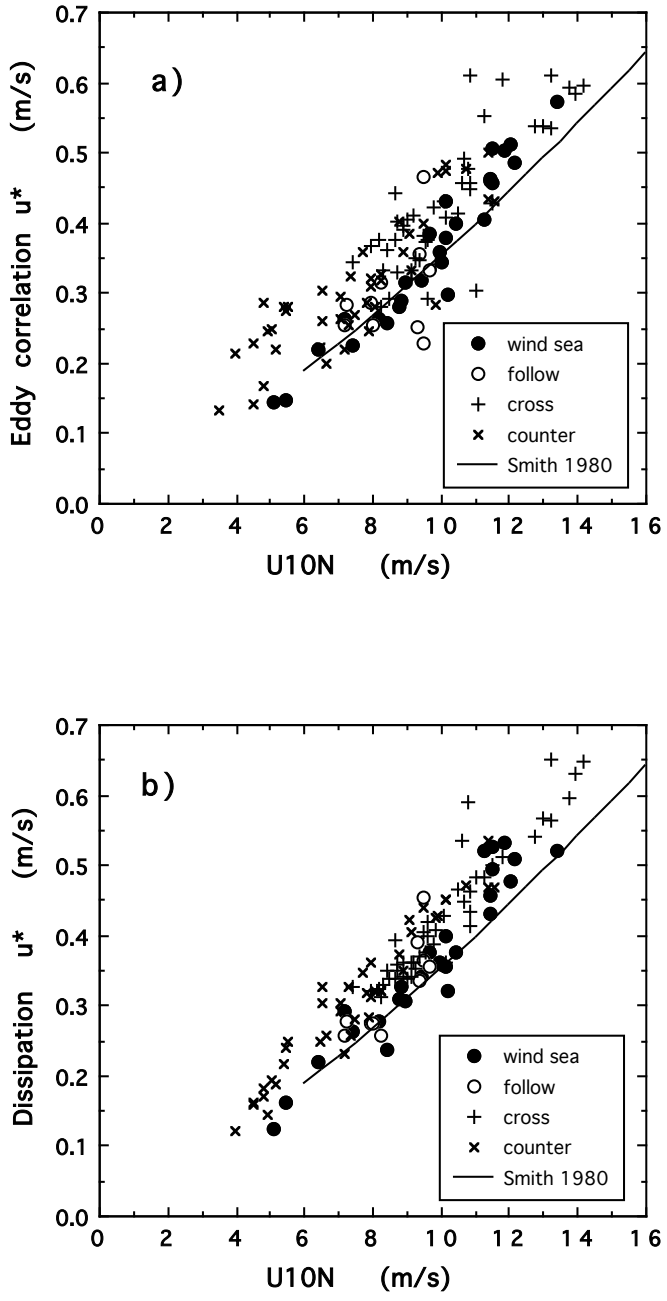

Figure 8.11. Friction velocity data from Donelan et al. (1997), separated into sea-state classes of pure wind sea and mixed wind sea and swell as indicated. Also shown is the relationship of Smith (1980) (solid line). Simultaneous data were obtained by a) the eddy correlation method, and b) the dissipation method.

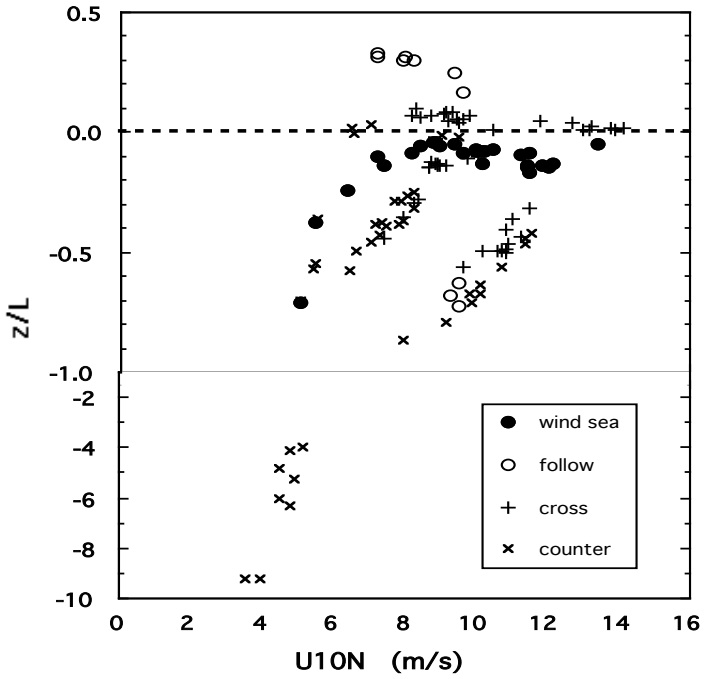

Figure 8.12. Variation of atmospheric stability with wind speed for the different sea state classes. Note change of scale at $z/L = -1$. Data were obtained from Table 1 of Donelan et al. (1997).

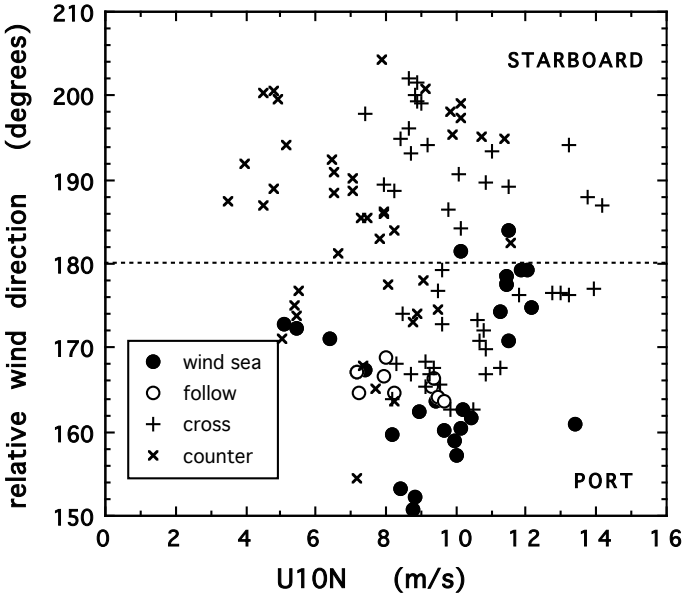

Figure 8.13. The variation of relative wind direction with wind speed for the different sea-state classes. Winds blowing directly over the bows of the ship are represented by a relative direction of 180º.

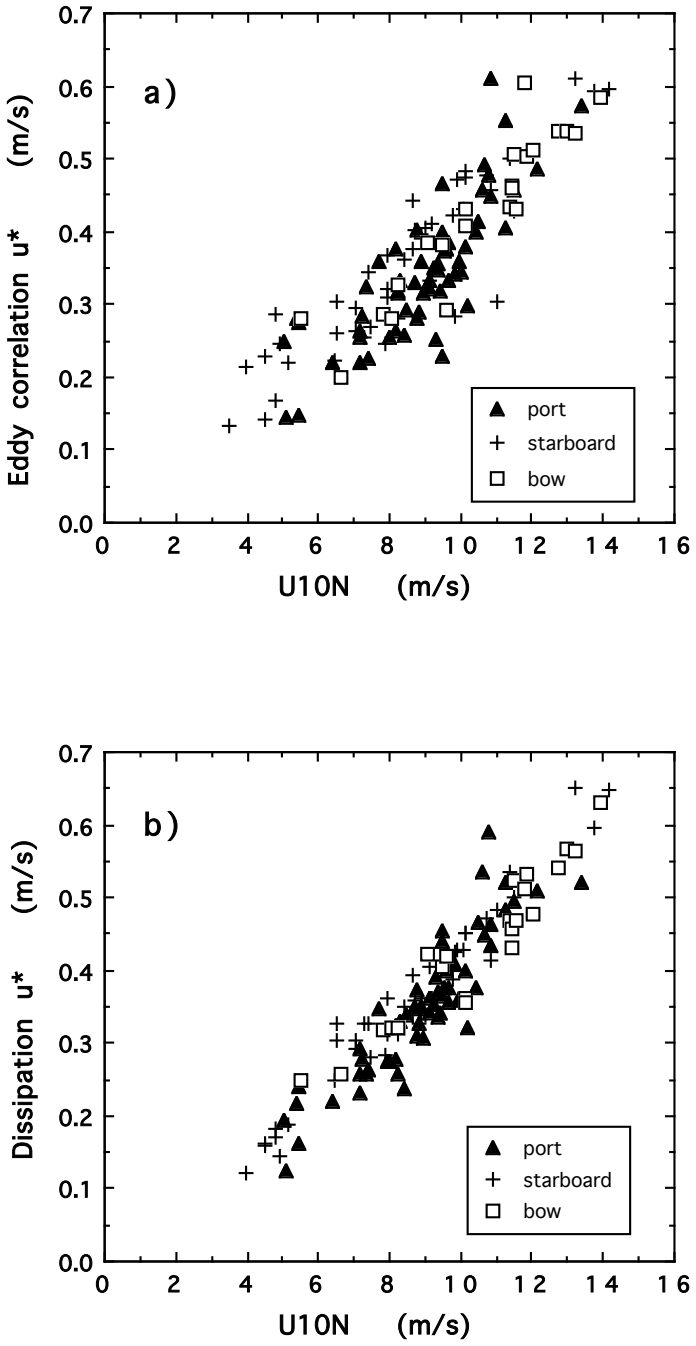

Figure 8.14. As Figure 8.11, except the data of Donelan et al. are separated according to relative wind direction rather than by sea state.

9 SUMMARY AND DISCUSSION

9.1 Data and preliminary results

This study described the collection, analysis and results of a large open-ocean wind stress data set, most of which was obtained during three cruises of the RRS Discovery in the Southern Ocean and the remainder during RRS Charles Darwin cruise 43 in the North Atlantic. During the Darwin cruise, about 140 concurrent estimates of the wind stress were obtained from each of four anemometers (including a prototype Solent sonic) which were located on the foremast platform in the ship's bows. The Discovery cruises produced 2633 wind stress estimates from a Solent sonic anemometer mounted on the ship's foremast platform. In both cases, the data were all obtained when the wind was blowing within 30º of the ships' bows. The Discovery data were obtained under a wide range of conditions; the wind speed ranged from near calm to 26 m/s, and z/L varied from -2 to +4. The large amount of high quality Discovery data allowed a number of significant effects to be seen for the first time.

The data from the four anemometers deployed during the Darwin cruise resulted initially in drag coefficient estimates that varied by up to 30% from one instrument to another. It was thought that these discrepancies were largely due to distortion of the flow of air to the anemometers, caused by the presence of the ship's hull and superstructure. That the effects of flow distortion could have a significant impact on the drag coefficient estimates, obtained using a well-exposed anemometer, was confirmed by the Discovery data. These data showed that small changes (of the order of 10º) in the mean relative wind direction produced significant differences in the mean C_{D10N} to U_{10N} relationship. The investigation of the flow distortion around the ships is discussed further below.

9.2 The imbalance term in the TKE budget.

The magnitude of the effects of flow distortion prompted a re-analysis of the dimensionless dissipation function used in the inertial dissipation method of estimating the wind stress. An earlier analysis (Yelland and Taylor, 1996) had shown that the assumption of a balance between the production and dissipation terms in the turbulent kinetic energy budget did not hold, at least under non-neutral conditions. In the earlier analysis, all the Discovery data obtained for winds within 30º of the ship's bow were used to estimate the magnitude of the imbalance term. This imbalance term, Φ_D, varied with stability, as expected, but was also found to have a dependence on the mean wind speed. However, further examination suggested that there may have been some correlation of the wind speed dependency with relative wind direction, i.e. that the wind speed dependency may have been erroneous. To avoid, or at least minimise, this possibility a subset of data was selected in which the correlation between wind speed and relative wind direction was not significant. In the re-analysis, only data where the relative wind direction was within 10º of the bow were used. The results of the re-analysis suggested that, for unstable conditions, the form of the imbalance term could be represented by;

$$\Phi_D = \frac{z}{L}\left(0.5 - \frac{U_{10N}}{6.5}\right) \qquad z/L < 0$$

For stable conditions it was found that the imbalance was zero if the dimensionless profile function was altered so that;

$$\phi_m = 1 + 6.6\frac{z}{L} \qquad z/L > 0$$

The application of the imbalance term to the Discovery data successfully removed the previously observed differences between the wind stress data obtained during unstable and neutral atmospheric stability conditions. The mean C_{D10N} to U_{10N} relationship was increased by about 5% over most of the wind speed range. The imbalance term was determined by comparison of non-neutral to neutral data. With this in mind, the term represents a mean excess of production over dissipation

of between 5 and 10 % for wind speeds in excess of 12 m/s. For lower wind speeds the imbalance was larger, with a mean excess of 25% for wind speeds of around 7 m/s.

9.3 The effects of flow distortion on the drag coefficient.

The effects of air-flow distortion on the drag coefficient estimates was quantified with the aid of a computational fluid dynamics (CFD) model. Since it is believed to be the first time that a fully 3-dimensional model has been used in this fashion, the model was first validated by simulating the flow over two Canadian research ships which had previously been tested in a wind tunnel. Use of the model results of the flow over the Charles Darwin provided further validation. After correcting the results from each instrument to allow for deceleration and vertical displacement of the flow, the discrepancy in the C_{D10N} estimates was reduced from up to 30% to less than 5%. Furthermore, the initial C_{D10N} to U_{10N} relationships from the Darwin were up to 60% larger than would be expected for open ocean data, such as that from the Discovery. After correcting for flow distortion, this difference was reduced to 5%. For the Darwin, the effect of the flow distortion on the wind speed estimate was much more severe than on the estimate of the friction velocity. This suggests that to obtain wind speed estimates from a large platform (such as a merchant ship), the most accurate result may be obtained by using the dissipation method to measure the stress and to obtain the wind speed via a C_{D10N} to U_{10N} relationship.

The CFD model of the Discovery showed that the anemometer site on this ship was much less affected by flow distortion than the anemometer sites on the Darwin. The deceleration of the flow was negligible (0.5%), but the 1 m vertical displacement was significant. These effects resulted in a reduction of the initial drag coefficient estimates by about 5% for a given wind speed.

9.4 The C_{D10N} to U_{10N} relationship and the effects of sea state.

The open ocean wind stress to wind speed relationship was determined from the Discovery data, obtained for relative wind directions within 10º of the ship's bows, after allowance had been made both for the imbalance in the TKE budget and for the effects of flow distortion. The mean C_{D10N} estimates increased with decreasing wind speed for winds below 6 m/s, possibly due to the effects of free convection. Above that wind speed, the data were well described by the relationship;

$$1000\, C_{D10N} = 0.53 + 0.064\, U_{10N} \qquad 6 \le U_{10N} \le 26 \ \ m/s$$

This confirms the open-ocean relationships suggested by Smith (1980) and Large and Pond (1981).

The scatter in the C_{D10N} values was investigated in order to quantify the effects of sea state, or of wind history on the wind stress. Since the sea state was not fetch or depth limited, an estimate was made of the expected drag coefficient anomaly using a modified HEXOS-type formula applied to duration limited sea-states. This predicted anomalies of the order of 10% or more, persisting over periods of at least a few hours. No such anomalies were found. It is thought that the wave age dependent stress formulations, derived from data obtained over shallow water, do not apply to open ocean conditions. Previous reports of evidence for a sea-state dependent stress over the open ocean are probably erroneous and could be attributed to experimental error, the assumption of a balance between dissipation and production in the TKE budget or to the effects of flow distortion. The effects of flow distortion are large and vary rapidly with relative wind direction. In the case of a ship-mounted anemometer, a change in relative wind direction can be caused by the response of the ship to a change in the sea state, such as the arrival of a cross-wind swell. This could cause a drag coefficient "anomaly" to be mistakenly associated with the change in sea state rather than to the change in air-flow distortion.

The results of this study show that wave-age dependent wind stress formulations are redundant for open-ocean conditions. A simple C_{D10N} to U_{10N} relationship should be used to estimate the wind stress from the wind speed.

9.5 Areas for further investigation.

9.5.a The wind speed dependent imbalance term.

One question posed by the results of this study is that of the imbalance between local production and dissipation in the turbulent kinetic energy budget. As described, the form of the imbalance term depends on the wind speed as well as on atmospheric stability. Although this may explain why the previous estimates of the imbalance differ, independent verification of the wind speed dependence is required. This may be provided by the results of a recent experiment on the RV FLIP (Edson, pers. comm) where the imbalance term was seen to be a function of the sea-state, itself dependent on the wind speed.

9.5.b Isotropy

Henjes (1996) examined a portion of the Discovery data used in this study and showed the presence of the 4/3 ratio in the spectral levels predicted by the assumption of local isotropy (Section 2.2.b). The data examined were all obtained for wind speeds of around 10 m/s and significant wave heights of about 6 m, conditions which were fairly typical of the study. Schmitt et al. (1978) suggest that the degree of anisotropy depends on the ratio of the measurement height to the wave height, with significant anisotropy occurring for a height ratio of between 5 to 10. As shown by the results of Henjes, isotropy was found for a height ratio of 3. However, wind speeds of up to 26 m/s were obtained, with significant wave heights of up to 14 m suggesting a height ratio of nearer 1. We intend to examine this high wind speed data to determine at what point, if at all, significant evidence of anisotropy occurs.

9.5.c Distortion of the air flow over the ship.

Validation of the CFD software is continuing. The Darwin and Discovery will be modelled for air flow at different relative wind directions, and both ships have been instrumented with an array of anemometers at various sites around the superstructure. The modelled wind speed errors will be further validated by comparison of relative wind speed errors between one anemometer site and another. Validation of the modelled vertical displacement of the flow will be tested using the stress estimates obtained from a second Solent sonic anemometer located on top of the main mast of the ship. At this site, the displacement is expected to be significantly larger than at the foremast anemometer site. In addition, simulations of low wind speed flow will also be made to investigate at which speed, if at all, the pattern of flow around the ship changes.

References

Anderson, R. J., 1993: A study of wind stress and heat flux over the open ocean by the inertial dissipation method. *J. Phys. Oceanogr.*, **23** (10), 2153 - 2161.

Augstein, E., H. Hoeber and L. Kruegermeyer, 1974: *Fehler bei Temperatur-, Feuchte- und Windmessungen auf Schiffen in tropischen Breiten. Meteor Forschungsergebnisse* B9, 1 - 10.

Birch, K. G. and R. W. Pascal, 1987: A meteorological system for research applications - MultiMet. *Fifth International Conference on Electronics for Ocean Technology*, Heriot-Watt University, Edinburgh, Institute of Electronic and Radio Engineers (IERE Publication No. 72), 7 - 12.

Blanc, T. V., 1986: *Superstructure flow distortion corrections for wind speed and direction measurements made from Tarawa Class (LHA1-LHA5) ships. NRL Report 9005*, Naval Research Laboratory, Washington, D.C., 20pp.

Blanc, T. V., 1987: *Superstructure flow distortion corrections for wind speed and direction measurements made from Virginia Class (CGN38-CGN41) ships. NRL Report 9026*, Naval Research Laboratory, Washington, D.C., 24 pp.

Bouws, E., 1988: Basic definitions and descriptions of ocean waves. *Guide to wave analysis and forecasting*. World Meteorological Organization publication 702, 23-25.

Bradley, E. F., P. A. Coppin and J. S. Godfrey, 1991: Measurements of sensible and latent heat flux in the Western Equatorial Pacific Ocean. *J. Geophys. Res.* **96**, 3375-3389

Brook, R. R., 1977: Effective dynamic response of paired Gill anemometers. *Boundary-Layer Meteorol.*, **11**, 33-37.

Busch, N. E., 1972: On the mechanics of atmospheric turbulence. : *Workshop on Micrometeorology*, D. A. Haugen, Ed., American Meteorological Society, 1 - 65.

Businger, J. A., J. C. Wyngaard, Y. Izumi and E. F. Bradley, 1971: Flux Profile relationships in the atmospheric surface layer. *J. Atmos. Sci.*, **28**, 181 - 189.

Champagne, F. H., C. A. Friehe, J. C. LaRue, and J. C. Wyngaard, 1977: Flux measurements, flux estimation techniques, and fine-scale turbulence measurements in the unstable surface layer over land. *J. Atmos. Sci.*, **34**, 515-530.

Charnock, H., 1955: Wind stress on a water surface. *Quart .J. Roy. Meteor. Soc.*, **81,** 639-640.

Ching, J. K. S., 1976: Ship's influence on wind measurements determined from BOMEX mast and boom data. *J. Appl. Meteorol.*, **15**(1), 102 - 106.

Clayson, C. H., 1994: ADOX Sonic processing system. *Unpublished COTD manuscript (Met. Team. document 94/26).*

Deacon, E. L., 1988: The streamwise Kolmogoroff constant. *Boundary-Layer Meteorol.*, **42**, 9 - 17.

Denman, K. L. and M. Miyake, 1973: Behaviour of the mean wind, the drag coefficient, and the wave field in the open ocean. *J. Geophys. Res.*, **78**, 1917-1931.

Detering, H. W. and D. Etling, 1985: Application of the E-e turbulence closure model to the atmospheric boundary layer. *Boundary-Layer Meteorol.*, **33**, 113-133.

Dittmer, K., 1977,: The hydrodynamic roughness of the sea surface at low wind speeds. *Meteor Forschungsergeb.*, **12**, 10-15.

Dobson, F. W., S. D. Smith and R. J. Anderson, 1994: Measuring the relationship between wind stress and sea state in the open ocean in the presence of swell. *Atmosphere-Ocean*, **32**(1), 237 - 256.

Dobson, F. W., S. D. Smith and R. J. Anderson, 1995: Open-ocean measurements of the wind stress-sea state relationship. *Proceedings, 4th International Workshop on Wave Hindcasting and Forecasting,* Oct. 16-20 1995 Banff, Alberta. Environment Canada, Atmospheric Environment Service, 4905 Dufferin St., Downsview, ON M3H 5T4, Canada: 171-176

Dobson, F.W., 1981: Review of reference height for, and averaging time of, surface wind measurements at sea. *Marine Meteorology and Related Oceanographic Activities 3,* World Meteorological Organisation, Geneva, 64pp.

Donelan, M. A., 1982: The dependence of the aerodynamic drag coefficient on wave parameters. *Proc. First Int. Conf. on Meteorology and Air-Sea Interaction of the Coastal Zone*, the Hague, 381-387

Donelan, M. A., 1990: Air-Sea Interaction. : In *The Sea*, B. Le Mehaute and D. M. Hanes, eds. Wiley-Interscience, New York, 239 - 292.

Donelan, M. A., F. Dobson, S. D. Smith and R. A. Anderson, 1993: On the dependence of sea surface roughness on wave development. *J. Phys. Oceanogr.*, **23**, 2143-2149

Donelan, M. A., W. M. Drennan and K. B. Katsaros, 1997: The air-sea momentum flux in conditions of wind sea and swell., *J. Phys. Oceanogr., accepted for publication.*

Dunckel, M., L. Hasse, L. Krugermeyer, D. Schriever and J. Wucknitz, 1974: Turbulent fluxes of momentum, heat and water vapour in the atmospheric surface layer at sea during ATEX. *Boundary-Layer Meteorol.*, **6**, 81 - 106.

Dupuis, H., 1994: *Wind speed errors for the research ship Le Suroit. (personal communication).*

Dupuis, H., P. K. Taylor, A. Weill and K. Katsaros, 1997: The inertial dissipation method applied to derive turbulent fluxes over the ocean during the SOFIA/ASTEX and SEMAPHORE experiments in low to moderate wind speeds. *Accepted for publication in J. Geophys. Res.*

Dyer, A. J.. and B. B. Hicks, 1982: Kolmogorov constants at the 1976 ITCE. *Q. J. Roy. Met. Soc.*, **96**, 715.

Edson, J. B., C. W. Fairall, P. G. Mestayer and S. E. Larsen, 1991: A Study of the Inertial-Dissipation Method for Computing air-Sea Fluxes. *J. Geophys. Res.*, **96**(C6), 10689-10711.

Fairall, C. W. and J. B. Edson, 1994: Recent measurements of the dimensionless turbulent kinetic energy dissipation function over the ocean. *Second International Conference on Air-Sea Interaction and on the Meteorology and Oceanography of the Coastal Zone.*, Lisbon, Portugal, 22-27 September 1994. American Meteorological Society, 224-225

Fairall, C. W. and S. E. Larsen, 1986: Inertial-Dissipation Methods and Turbulent Fluxes at the Air-Ocean Interface. *Boundary-Layer Meteorol.*, **34**, 287-301.

Fairall, C. W., J. B. Edson, S. E. Larsen and P. G. Mestayer, 1990: Inertial-dissipation air-sea flux measurements: a prototype system using realtime spectral computations. *J. Atmos. & Oceanic Tech.*, **7**, 425 - 453.

Fairall, C. W., E. F. Bradley, D. P. Rogers, J. B. Edson and G. S. Young: Bulk parameterization of air-sea fluxes for Tropical Ocean Global Atmosphere Coupled-Ocean atmosphere Response Experiment. *J. Geophys. Res.*, **101** (C2), 3747-3764.

Frenzen, P. and C. A. Vogel, 1992: The turbulent Kinetic Energy budget in the atmospheric surface layer: a review and an experimental reexamination in the field. *Boundary-Layer Meteorol.*, **60**, 49 - 76.

Frenzen, P. and C. A. Vogel, 1994: On the sensitivity of the ϕ_m function to k: a corrected illustration for the turbulent kinetic energy budget in the ASL. *Boundary-Layer Meteorol.*, **68**, 439-442.

Garratt, J. R., 1992: *The Atmospheric Boundary Layer*, .Cambridge University Press, Cambridge, 316pp.

Geernaert, G. L., 1990: Bulk parameterizations for the wind stress and heat fluxes: In *Surface waves and fluxes. Volume 1 - current theory*. Geernaert, G. L. and W. J. Plant, Eds., .Kluwer Academic Publishers, Dordrecht, Holland, 336 pp.

Geernaert, G. L., K. B. Katsaros and K. Richter, 1986: Variation of the Drag Coefficient and Its Dependence on Sea State. *J. Geophys. Res.*, **91**(C6), 7667-7679.

Geernaert, G. L., K. L. Davidson, S. E. Larsen and T. Mikkelsen, 1988: Wind Stress Measurements During the Tower Ocean Wave and Radar Dependence Experiment. *J. Geophys. Res.*, **93**(C11), 13913-13923.

Godshall, F. A., W. R. Seguin and P. Sabol, 1976: *Analysis of ship surface meteorological data obtained during GATE intercomparison periods.*, NOAA, CEDDA.

Greenhut, G. K. and S. D. S. Khalsa, 1997: Bulk transfer coefficients and dissipation-derived fluxes in low wind speed conditions over the western equatorial Pacific Ocean. *J. Geophys. Res.* **100**(C1), 857-863

Gulev, S. K., 1995: Climatology of wind waves and wave age based wind stress from COADS. *Proc. Third Int. Conf. on Modelling Global Climate Change and Variability.* MPI, Hamburg, Germany, 4-8 September 1995

Henjes, K. 1996: Isotropic and anisotropic correlations in turbulent wind speed data. *Boundary-Layer Meteorol.* Accepted for publication, March 1997

Hicks, B. B. and A. J. Dyer, 1972: The spectral density technique for the determination of eddy fluxes. *Q. J. Roy. Met. Soc.*, **98**, 838 - 844.

Hutchings, J., M. J. Yelland and P. K. Taylor, 1995: A preliminary computational fluid dynamics (CFD) analysis of the airflow over the CSS Hudson. *James Rennell Centre contract report*. Southampton Oceanography Centre, Southampton, UK

Janssen, P. A. E. M., 1996: Personal communication.

Kahma, K. K. and M. Lepparanta, 1981: On errors in wind speed observations on R/V Aranda. *Geophysica*, **17**(1-2), 155-165.

Kaimal, J. C. and D. A. Haugen, 1969: Some errors in the measurement of Reynolds stress. J. Appl. Meteor., **8,** 460-462.

Kent, E. C., P. K. Taylor and P. Challenor, 1997: A Comparison of Ship and Scatterometer-Derived Wind Speed Data in Open ocean and coastal areas. *Submitted to J. Atmospheric Ocean Technology*

Kent, E.C., K. G. Birch, R. W. Pascal and P. K. Taylor, 1992: Evaluation on Cruise 62A of a Magnavox MX 4200 GPS receiver and KVH fluxgate compass to provide ship speed and heading. *Internal Document 2, James Rennell Centre for Ocean Circulation.*

Khalsa, S. j. s. and J. A. Businger, 1977: The drag coefficient as determined by the dissipation method and its relation to intermittent convection in the surface layer. *Boundary-Layer Meteorol.*, **12**, 273-297.

Kidwell, K. B. and W. R. Seguin, 1978: *Comparison of mast and boom wind speed and direction measurements on US GATE B-Scale Ships*. NOAA Tech. Rep. EDS 28, CEDDA, Washington, D.C.

Kraus, E. B. and J. A. Businger, 1994: *Atmospher-ocean interaction*, .Oxford University Press, New York, USA.

Large, W. G. and S. Pond, 1981: Open Ocean Momentum Flux Measurements in Moderate to Strong Winds. *J. Phys. Oceanogr.*, **11**, 324-336.

Large, W. G. and S. Pond, 1982: Sensible and Latent Heat Flux Measurements over the Ocean. *J. Phys. Oceanogr.*, **12**, 464-482.

Large, W. G., 1979: *The turbulent fluxes of momentum and sensible heat over the sea during moderate to strong winds*. , Ph.D. thesis, University of British Columbia, pp. 180.

Launder, B. E. and B. Spalding, 1974: The numerical computation of turbulent flows. *Comp. meth. in Appl. Mech. Eng*. **3**, 269-289.

Lenschow, D. H., J. C. Wyngaard and W. T. Pennell, 1980: Mean-field and second-moment budgets in a baroclinic, convective boundary layer. *J. Atmos. Sci.*, **37**, 1313 - 1326.

Mahrt, L, D. Vickers, J. Howell, J. Højstrup, J. M. Wilczak, J. Edson and J. Hare, 1996: Sea surface drag coefficients in the Risø Air Sea Experiment. *J. Geophys. Res.* **101**(C6), 14327-14335

Marsden, R. F., G. A. McBean and B. A. Proctor, 1993: Momentum and sensible heat fluxes calculated by the dissipation technique during the Ocean Storms Project. *Boundary-Layer Meteorol.*, **63,** 23-38.

McBean, G. A. and J. A. Elliott, 1975: The vertical transports of kinetic energy by turbulence and pressure in the boundary layer, *J. Atmos. Sci*, ***32,*** *753-766*

Moat, B. I. and M. J. Yelland, 1996a: Air flow over the R.R.S Charles Darwin: the disturbance of the flow at the anemometer sites used during cruises CD43 and CD98. *SOC Internal Document 5*. Southampton Oceanography Centre, Southampton, UK

Moat, B. I. and M. J. Yelland, 1996b: Airflow over the R.R.S Discovery: variation of velocity errors with wind speed. *SOC Internal Document 4*. Southampton Oceanography Centre, Southampton, UK

Moat, B. I., Yelland, M. J. and Hutchings, J. 1996. Airflow over the R.R.S. Discovery using the Computational Fluid Dynamics package Vectis, *SOC Internal document 2*, Southampton Oceanography Centre, Southampton, UK.

Neugum, A, 1996: Systematic influences in the determination of stress at sea with the so-called "dissipation" technique. (in German) *Doctoral thesis*, Inst. fur Meereskunde, Universitat Kiel, Germany, 107 pp.

Nordeng, T.E., 1991: On the wave age dependent drag coefficient and roughness length at sea. *J. Geophys. Res.*, **96**, 7167-7174.

OOSDP, 1995: Scientific Design for the Common Module of the Global Ocean Observing System and the Global Climate Observing System: An Ocean Observing System for Climate. Dept. of Oceanography, Texas A&M University, Dr. Worth D. Nowlin, Jr., College Station, Texas, 265.pp.

Oost, W. A., 1997: The KNMI HEXMAX stress data - a revisit. *Submitted to Boundary-Layer Meteorol.*

Oost, W. A., C. W. Fairall, J. B. Edson, S. D. Smith, R. J. Anderson, J. A. B. Wills, K. B. Katsaros and J. DeCosmo, 1994: Flow distortion calculations and their application in HEXMAX. *J. Atmos. & Oceanic Tech.*, **11**(2), 366 - 386.

Paulson, C. A., 1970: The mathematical representation of wind speed and temperature profiles in the unstable atmospheric surface layer. *J. Appl. Meteorol.*, **9**, 857 - 861.

Pitt, E. G., 1981: Spectral analysis of wave data. *Institute of Oceanographic Sciences Internal Document 120*, Southampton Oceanography Centre, Southampton, UK

Queffeulou, P., 1991: Accuracy of wind measurements performed on buoys, ship, and island during the TOSCANE-2 Experiment. *J. Atmos. & Oceanic Tech.*, **8**, 835 - 855.

Ramnstorf, S., 1988: Wind observations from RV Rapuhia. *Physics Section report (Internal Report 88/2)*, Division of Marine & Freshwater Science, DSIR, Wellington, New Zealand, 12 pp.

Romanov, Y. A., I. B. Fedorova, M. S. Chervyakov and G. I. Shapiro, 1983: An improvement in the accuracy of shipboard measurements of wind speed and direction based on aerodynamic tests of a ship model. *Oceanology*, **23**(2), 267 - 270.

Schacher, G. E., K. L. Davidson, T. Houlihan and C. W. Fairall, 1981: Measurements of the rate of dissipation of turbulent kinetic energy, e, over the ocean. *Boundary-Layer Meteorol.*, **20**, 321 - 330.

Schmitt, K. F., C. A. Friehe and C. H. Gibson, 1978: Sea Surface Stress Measurements. *Boundary-Layer Meteorol.*, **15**, 215-228.

Smith, S. D., 1980: Wind Stress and Heat Flux over the Ocean in Gale Force Winds. *J. Phys. Oceanogr.*, **10**, 709-726.

Smith, S. D., 1988: Coefficients for Sea Surface Wind Stress, Heat Flux and Wind Profiles as a Function of Wind Speed and Temperature. *J. Geophys. Res.*, **93**, 15467-15474.

Smith, S. D., K. B. Katsaros, W. B. Oost and P. G. Mestayer, 1996: The impact of the HEXOS programme. *Boundary-Layer Meteorol.*, **78**, 121-141.

Smith, S. D., R. J. Anderson, W. A. Oost, C. Kraan, N. Maat, J. DeCosmo, K. B. Katsaros, K. L. Davidson, K. Bumke, L. Hasse and H. M. Chadwick, 1992: Sea surface wind stress and drag coefficients: the HEXOS results. *Boundary-Layer Meteorol.*, **60**, 109-142.

Stull, R. B., 1988: *An Introduction to Boundary Layer Meteorology*, .Kluwer Academic Publishers, Dordrecht, Holland, 666 pp.

Surry, D., R. T. Edey and I. S. Murley, 1989: *Speed and direction correction factors for ship borne anemometers. Engineering Science Research Report BLWT-SS9-89*, Univ. of Western Ontario, London, Ontario, 83 pp.

Taylor, P. K., 1995: A program to calculate fluxes using the bulk formulae - Bform., *unpublished manuscript*

Taylor, P. K., M. J. Yelland, K. G. Birch, C. H.. Clayson and R. W. Pascal, 1994: Field Measurements of Wind and Wind Stress: the Sonic Buoy. *MAFF Conf. of River and Coastal Engineers*, Loughborough, Flood and Coastal Defence Division, MAFF, 1.1.1-1.1.20

Taylor, P.K., E. Kent, M.J. Yelland and B. Moat, 1995: The Accuracy of wind observations from ships. *Proceedings of the International COADS Winds Workshop*, Kiel, Germany, 31st May - 2nd June 1994. Berichte aus dem Institut F¨ur Meereskunde an der Christian-Albrechts-Univerität, Nr. 265, 301 pp.

Thiebaux, M.L. 1990: Wind Tunnel Experiments to Determine Correction Functions for Shipboard Anemometers. Canadian Contractor Report of Hydrography and Ocean Sciences No. 36, Bedford Inst. Oceanography, Halifax, Nova Scotia, 57pp.

Tillman, J. E., L. Landberg and S. E. Larsen, 1994: The boundary layers of Mars: Fluxes , stability, turbulent spectra and growth of the mixed layer. *J. Atmos. Sci.*, **51**, 1709 - 1727.

Trenberth, K. E., G. L. Large and J. G. Olson, 1989: The effective drag coefficient for evaluating wind stress over the oceans. *J. Climate*, **2**, 1507-1516

Tucker, M. J., 1991: Waves in ocean engineering. Ellis Horwood Ltd., Chichester, U.K., 431 pp.

Weiler, H. S. and R. W. Burling, 1967: Direct Measurements of Stress and Spectra of Turbulence in the Boundary Layer Over the Sea. *J. Atmos. Sci.*, **24**, 653-664.

Weller, R. A., D. L. Rudnick, R. E. Payne, J. P. Dean, N. J. Pennington and R. P. Task, 1990: Measuring near surface meteorology over the ocean from an array of oceanographic moorings in the sub-tropical convergence zone. *J. Atmos. & Oceanic Tech.*, **7**(85 - 103).

Wieringa, J., 1980: A revaluation of the Kansas mast influence on the measurement of stress and cup overspeeding. *Boundary-Layer Meteorol.*, **18**, 411-430.

Willis, G. E. and J. W. Deardorff, 1976: On the use of Taylor's translation hypothesis for diffusion in the mixed layer. *Quart. J. Roy. Meteor. Soc.*, 102, 817-822.

Wu, J., 1969: Froude number scaling of wind-stress coefficients. *J. Atmos. Sci.*, **26**, 408-413

Wu, J., 1980: Wind stress coefficients over the sea surface near neutral conditions - a revisit. *J. Phys. Oceanogr.*, **10**, 727-740.

Wu, J., 1994: The sea surface is aerodynamically rough even under light winds. *Boundary-Layer Meteorol.*, **69**, 149-158

Wucknitz, J., 1979: The influence of anisotropy on stress estimation by the indirect dissipation method. *Boundary-Layer Meteorol.*, **17**, 119-131

Wucknitz, J., 1980: Flow distortion by supporting structures. *Air-Sea Interaction.* Eds. F. Dobson, L. Hasse and R. Davis. 605-626.

Wyngaard, J. C. and O. R. Cote, 1971: The budgets of turbulent kinetic energy and temperature variances in the atmospheric surface layer. *J. Atmos. Sci.*, **28**, 190 - 201.

Wyngaard, J. C., 1973: On surface layer turbulence : *Workshop on Micrometeorology*, D. A. Haugen, Ed., American Meteorological Society, 136

Yelland, M. J. and P. K. Taylor, 1996: Wind stress measurements from the Open Ocean. *J. Phys. Oceanogr.*, **26**, 541-558.

Yelland, M. J., B. I. Moat, P. K. Taylor, R. W. Pascal, J. Hutchings and V. C. Cornell, 1996: Wind stress measurements from the open ocean corrected for air-flow distortion by the ship. *Submitted to J. Phys. Oceanogr.*

Yelland, M. J., P. K. Taylor, I. E. Consterdine and M. H. Smith, 1994: The use of the inertial dissipation technique for shipboard wind stress determination. *J. Atmos. & Oceanic Tech.*, **11**(4 (part 2)), 1093 - 1108.

Yelland, M. J., Taylor, P. K., Birch, K. G., Pascal, R. W. and Williams, A. L., 1991: Evaluation of a Solent Sonic Anemometer on RRS Charles Darwin Cruise 43. *Report 288, Institute of Oceanographic Sciences, Wormley, Surrey, UK, 55 pp.*